VERSLAGEN EN VERHANDELINGEN

TRANSACTIONS

NATIONAAL LUCHTVAARTLABORATORIUM

NATIONAL AERONAUTICAL RESEARCH INSTITUTE

AMSTERDAM

XX — 1955

CONTENTS.

Thirty-sixth Annual Report

of the

National Aeronautical Research Institute

N.L.L.

1955

A. Board and Organization.

On 31 December 1955 the Board consisted of the following members:

Prof. Dr. Ir. H. J. van der Maas, President,	Technical University, Delft Ministry of Education, Arts and Sciences.
J. W. F. Backer, Vice-President	Dir. Gen., Dept. of Civil Aviation Ministry of Transport and "Waterstaat".
Dr. L. Neher	Ministry of Transport and "Waterstaat".
Prof. Ir. D. Dresden	President National Council for Industrial Research T. N. O.
Col. Ir. C. W. A. Oyens	Dep. Director of Ordnance and Supplies, Royal Netherlands Air Force.
Captain (E) Royal Neth. Navy E. C. Leertouwer	Director Air Material Division, Royal Netherlands Navy.
Dr. J. W. de Stoppelaar	Director of Economic Affairs, Ministry of Overseas Territories.
Drs. H. P. Jongsma	Director for Financial Participations, Ministry of Economic Affairs.
Mr. O. W. Vos	Dep. Director for Financial Participations, Ministry of Finance.
P. A. van de Velde	Advisor Aviolanda Aircraft Company Inc.
Ir. H. C. van Meerten	Chief Designer and Ass. Manager, Royal Netherlands Aircraft Factories Fokker.
C. Wijdooge	Head Techn. Sales Dept., Royal Dutch Airlines, K. L. M.
Prof. Dr. W. J. D. van Dijck	Scient. Advisor Royal Dutch Shell, for the Royal Dutch Aeronautical Association.

The executive committee consisted of president and vice-president. Mr. G. C. Klapwijk continued to be Secretary-treasurer of the Board. Lt. Col. A. H. Geudeker joined the Bureau of the Board as principal technical officer. Prof. Dr. A. van der Neut and Prof. Dr. R. Timman were Scientific Advisors to the Laboratory appointed by the Board.

Parliament approved the Bill involving modification of the subsidizing policy in the Charter of the Institute, which Bill has been gazetted in the "Staatsblad nr. 105", dd. 29 March, 1955.

The Advisory Scientific Committee has been superseded by a joint Scientific Committee N.L.L.-N.I.V. in consideration of the common needs for scientific advices of both the Institute and the Netherlands Aircraft Development Board (N. I.V.).

Prof. Dr. Ir. W. T. Koiter has been appointed Chairman of the Committee, Prof. Dr. Ir. W. F. Brandsma, Maj. Gen. Prof. Dr. G. Otten and Prof. Dr. L. J. F. Broer have been appointed members.

Five subcommittees have been set up, for Strength and Materials, Theoretical Aerodynamics, Applied Aerodynamics, Aero-elasticity and Flight-Testing.

As the Advisory Group for Aeronautical Research and Development (AGARD) has been definitely established within NATO in 1954, delegates of the various countries had to be appointed again under the new rules. By the Minister of War and of the Navy the President of the Board and the Director of the Institute have been appointed National Delegates, whereas two members of the Staff have been appointed Panel Members.

February 1955 the Institute concluded an agreement with the Association Internationale des Constructeurs de Matériel Aéronautiques (AICMA) regarding the use of the NLL-transonic windtunnel for the aircraft constructors of the Western European continent.

B. The Laboratory.

1 *General.*

1.1 *Staff.*

The management consisted of:

Director:	Prof. Dr. C. Zwikker
Dep. Director:	Ir. A. Boelen
Section Aerodynamics (A):	Ir. N. Feis
Section Combustion (C):	Ir. A. J. Marx Drs. W. J. Basting
Section Flutter and Theoretical Aerodynamics (F):	Dr. Ir. A. I. van de Vooren
Section Gasdynamics (G):	Dr. S. F. Erdmann
Section Helicopters (H):	Ir. A. J. Marx Ir. L. R. Lucassen
Section Materials and Structures (M and S):	Dr. Ir. F. J. Plantema
Windtunnel Construction Bureau (N):	Ir. J. Boel
Section Free-flying Models (O):	Ir. A. J. Marx Ir. G. Y. Fokkinga
Section Flight Mechanics and Flight Testing (V):	Ir. A. J. Marx Ir. T. van Oosterom
Documentation and Library:	Dra. G. Scherpenhuijsen Rom
Administration:	G. J. Hendriks.

The staff of the laboratory consisted of 59 scientists, 34 graduates of Technical Colleges, 105 technicians, 36 clerical staff and 18 others, in total 253. 13 members of the staff, among whom 6 scientists, were in military service.

1.2 *Windtunnels and equipment.*

The Pilottunnel ($1.4 \times 1.83\ \mathrm{ft}^2$) has been tested; the Schlieren system and strain gauge balances functioned satisfactorily. A transonic test section is being developed.

In the construction of the High Speed Tunnel ($5.3 \times 6.7\ \mathrm{ft}^2$) together with the new building annexes good progress was made.

The design studies for the Supersonic Tunnel resulted in a project for a blow-down tunnel, test section $4 \times 5\ \mathrm{ft}^2$, with a flexible nozzle for Ma-numbers from 1.3 to 4 approximately, measuring time of about 20 sec, energy supply by compressed air of 40 atm.

In the worpshops a new automatic planing and duplicating machine with additional facilities for heavy milling work will assist in the model construction for the high-speed windtunnels.

The linear analog-computor was delivered and has been successfully applied to computations in the field of stability, flutter, gust loads etc. Additional non-linear elements appeared to be useful for future work. An electronic digital computor developed by the Netherlands P.T.T. has been ordered.

Complete equipment for telemetering has been supplied to the Free-flying Models Section at the end of the year.

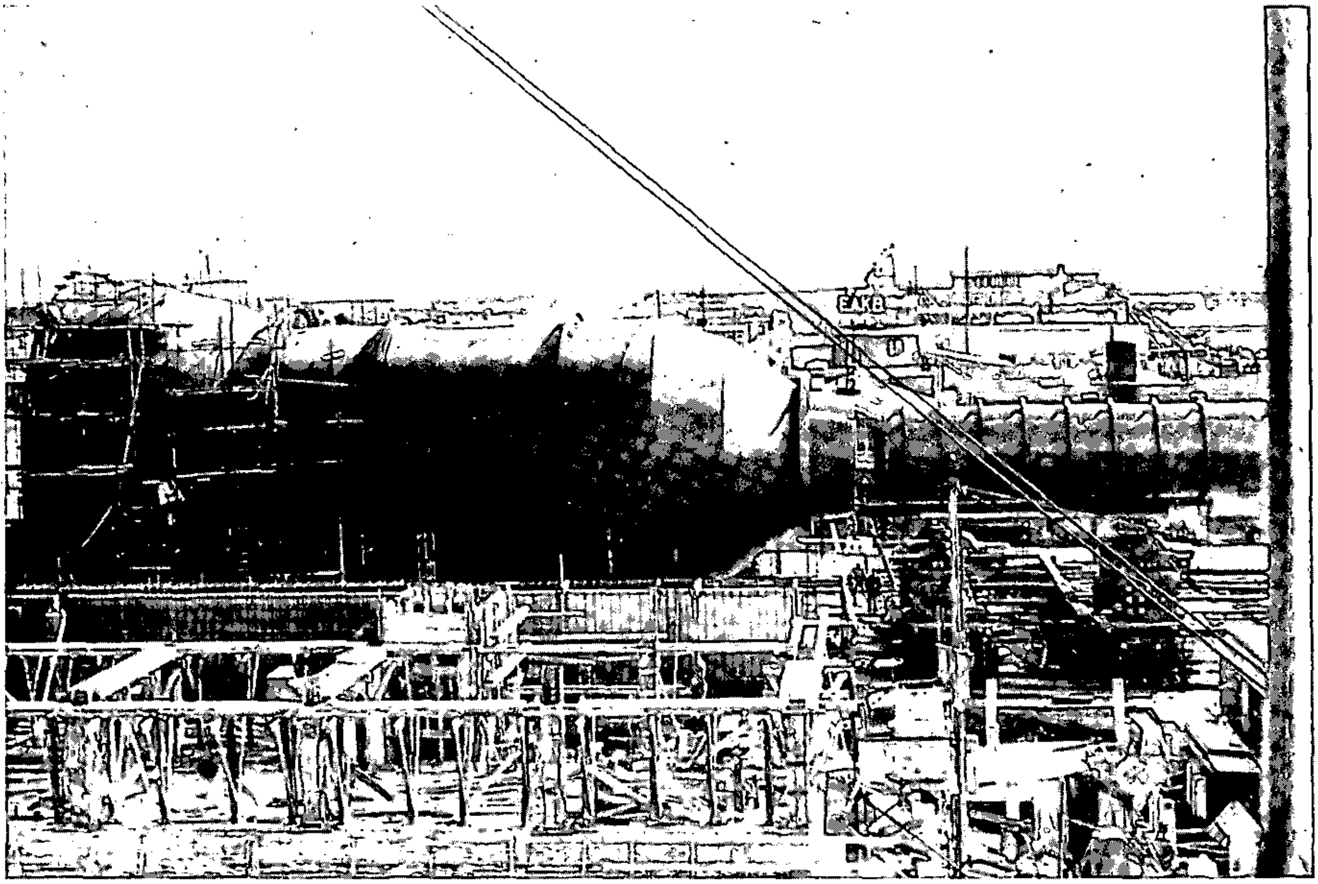

The high-speed tunnel under construction, the test section is being placed.

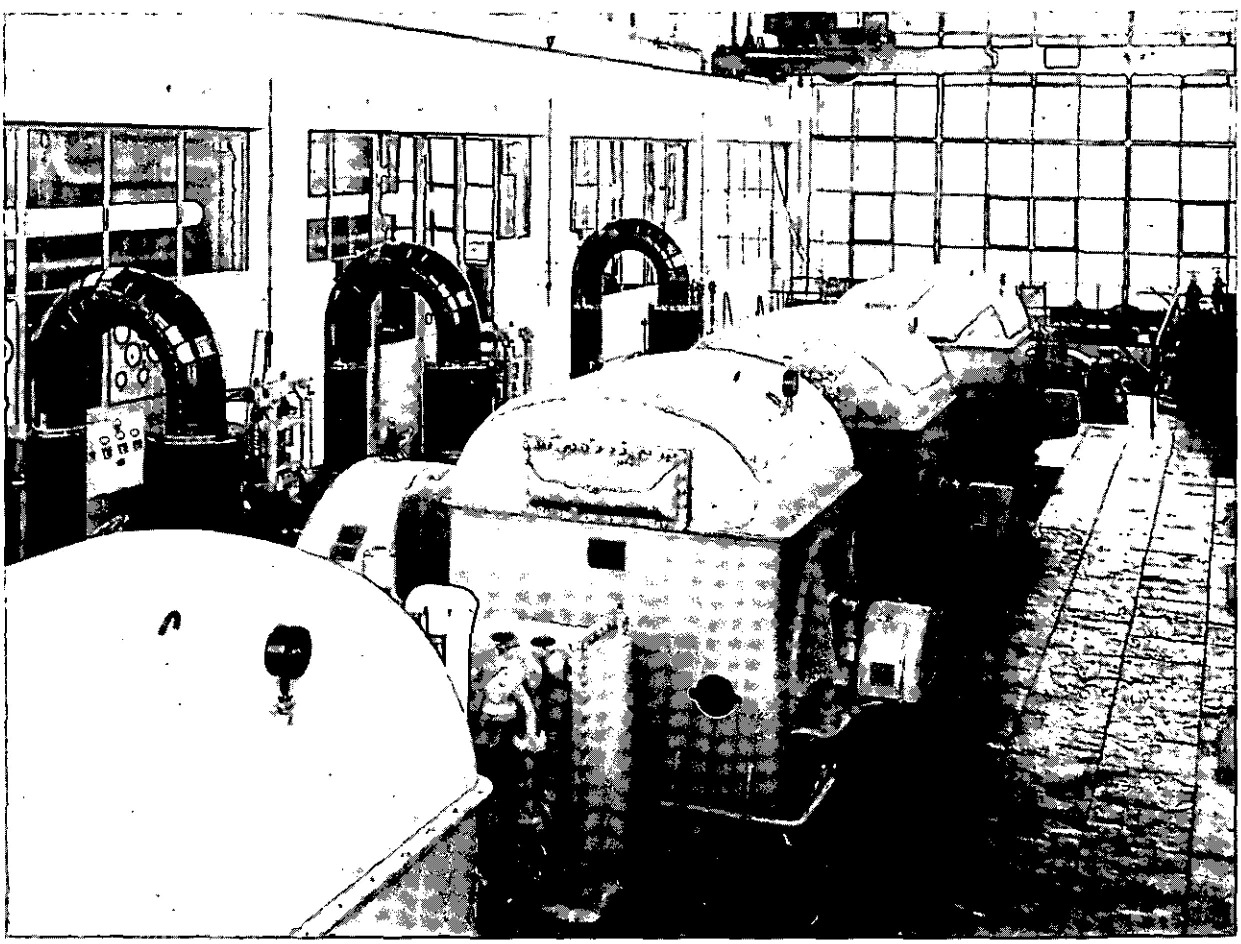

Power station for the new tunnels.
Four turbo-electric aggregates of 6000 hp each are installed.

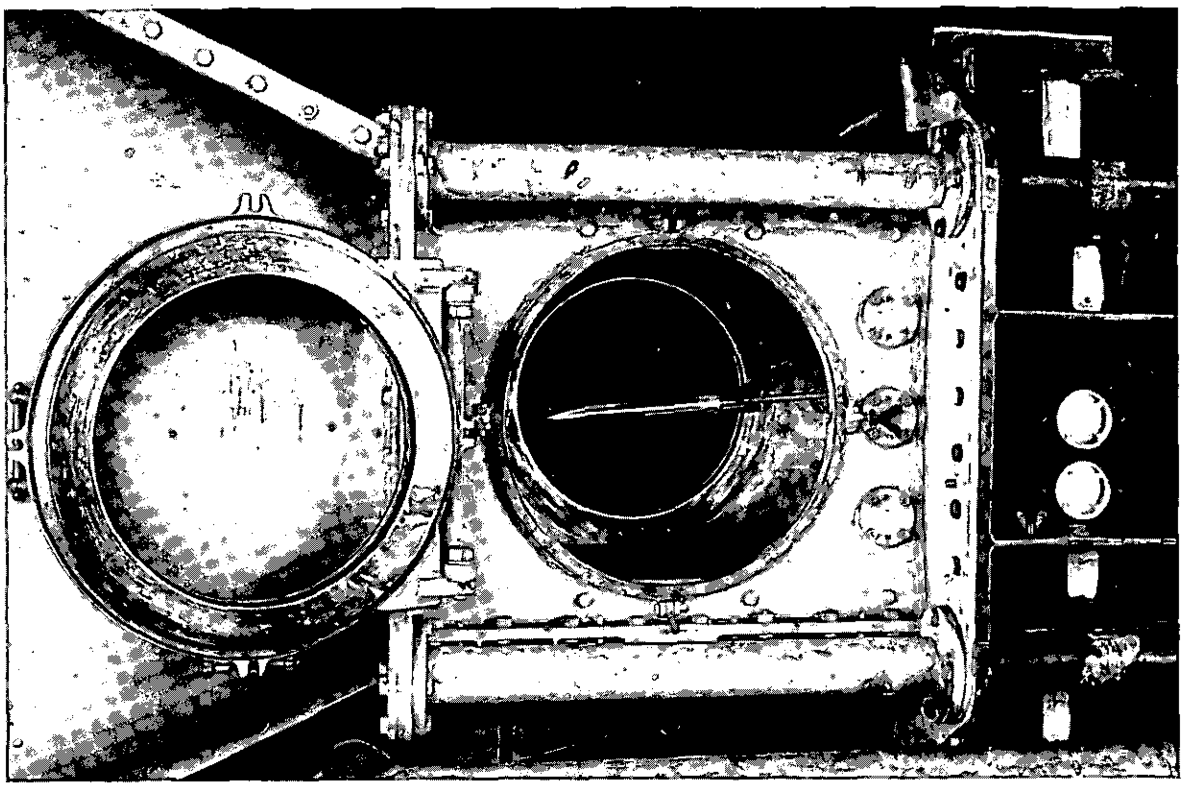

AGARD standard model in the test section of the Pilot tunnel.

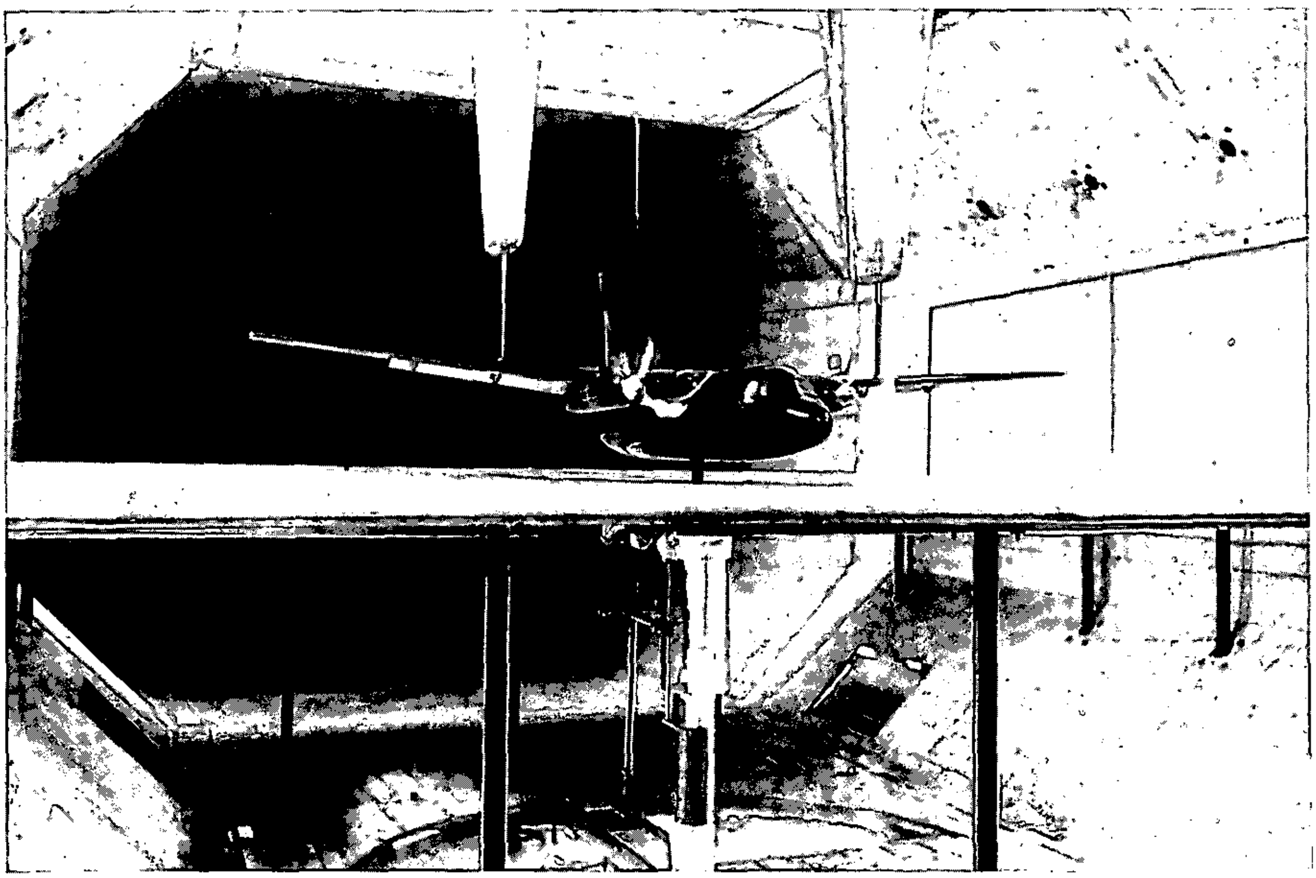

The model of the Fokker F-27 with turning propellers, tested under take-off and landing conditions.

1.3 *Research Contracts.*

Contract work for the Netherlands Aircraft Development Board (N.I.V.) comprised extensive investigations in connection with the F-27 project, and a helicopter project. Also contracts covering theoretical and experimental research in view of future development have been awarded.

Contracts by the Royal Netherlands Air Force and the Royal Netherlands Navy included mainly ad-hoc research. For the Royal Dutch Airlines, K.L.M., work has been done in the field of take-off and landing calculations, noise measurements and instrument development.

The N.L.L. cooperated with the Department of Civil Aviation in the Committee for Strength Specifications for Civil Aircraft and gave advices on Air Regulations and flight testing.

A number of orders from industry, including testing and calibration of apparatus and wind-tunnel measurements on ship models, buildings etc. have been carried out.

1.4 *International Cooperation.*

International cooperation in the Advisory Group for Aeronautical Research and Development (AGARD) of the NATO in various fields, to which Structures and Materials have now been added, continued to be of great benefit. The General Assembly of AGARD in Ottawa and a journey of Dr. van de Vooren as AGARD-consultant through the United States brought close contact with American and Canadian scientists and institutes.

In the International Committee on Aeronautical Fatigue in which Belgium, England, the Netherlands, Sweden and Switzerland are represented, the N.L.L. having the secretariat, a fruitful exchange of ideas could take place.

2 *Aerodynamics Section.*

Fokker F-27 (Friendship).

The static stability and control characteristics of a complete model (1:15) have been measured both for normal flight, and for take-off and landing conditions with ground influence, also in the case of one-engine failure.

Detailed measurements with a large tailplane model and a wing-tip model with various types of ailerons have been concluded.

A free-flying model has been launched above a water surface in order to investigate the ditching characteristics.

The Fokker S-14 (Machtrainer).

Pressure-distribution and three-component measurements at low speeds have been made with various shapes of cockpit hood in order to investigate where the first development of shock waves could be expected when entering the transonic regime.

With a model of this aeroplane also ditching characteristics have been investigated.

The Aviolanda AT-21 (pilotless target plane).

Performance measurements have been made on the complete model, and on tail-plane and wing-tip models.

Swept wings.

The contribution of the horizontal tail-plane to the stability of a swept-wing model at low speeds has been determined as a function of its position behind the wing. In order to know the influence of the downwash on the tailplane the wake has been examined.

A comparison has been made on the aerodynamic characteristics of a complete and a half-model (with plate in the plane of symmetry) of a swept-wing with fuselage.

Various subjects.

Tests have been carried out for various industries concerning e.g. wind and smoke nuisance on ships, ventilation for buildings, streamlining of trains, etc.

3 *Flutter and Theoretical Aerodynamics Section.*

Boundary layer theory.

The method for calculating the three-dimensional boundary layer about a wing has been considerably simplified (report F. 184). The simplification is based upon the assumption that the displacement and momentum thicknesses of the boundary layer cross flow are small compared with the same quantities taken in the direction of the main flow. The results for the flat yawed ellipsoid under zero angle of incidence have been compared with the results formerly obtained by aid of the original method (F. 165). The agreement is very satisfactory.

Load distributions of wings in steady flow.

The load distribution of circular wings for arbitrary camber distribution in incompressible flow has been calculated according to a new method which allows the Kutta condition to be satisfied in all points of the trailing edge (report F. 189).

Transonic flow.

A method for calculating the two-dimensional flow about arbitrary profiles in the transonic region has been presented (report F. 185). The flow about a wedge was the subject of an introductory study.

The phenomenon of shock reflection at the walls of a transonic test section has been considered and certain conclusions could be drawn for the cases of transversal and longitudinal slots (report F. 167).

Aerodynamic forces on oscillating aerofoils.

The general method, described in report F. 157, for the asymptotic solution of the wave equation, has now been applied to the two-dimensional aerofoil oscillating either at high frequencies or in a subsonic flow with Mach number near to 1. Numerical results are being evaluated.

The damping in pitch of a rectangular wing oscillating slowly about an arbitrary spanwise axis in a subsonic flow of high Mach number has been calculated. There exists an important difference between the results obtained by quasi-steady or by unsteady theory.

Measurements of aerodynamic forces on oscillating wing-aileron combinations at low speed have been continued. A report (F. 175) was completed dealing with the measurements performed with an aileron without aerodynamic balance. The boundary layer of an oscillating wing was made visible by a smoke method and photographs were taken by aid of stroboscopic illumination.

Aeroelasticity and flutter.

Flutter calculations have been made (report F. 168) for swept wings using the strip theory which has formerly been developed at the NLL (report F. 146). In many cases the deviations from the results obtained, by taking into account only the velocity component perpendiculum to the wing are small.

A criterion for the prevention of flutter for binary aileron-spring tab systems has been presented (F. 182).

An investigation has been performed concerning the influence of the finite torsional stiffness of a flexible wing on gust loads (report F. 191). This may lead to considerably higher bending moments than for a wing of infinite torsional stiffness.

4 *Gasdynamic Section.*

Transonic test-section.

The reflection of shock waves by slotted walls has been investigated in the 3×3 cm² supersonic tunnel.

Supersonic tunnel components.

Three possible methods of nozzle construction have been compared, one with exchangeable fixed sections and two flexible constructions. It appeared to be possible to realize an adjustable nozzle for Mach numbers varying from 1.2 through 4.

A heat exchanger has been designed for compensating the temperature drop caused by expansion of the pressurized air used for driving the proposed blowdown-type tunnel.

The study and design of Schlieren systems has been continued.

5 *Structures and Materials Section.*

Theoretical structures research.

During the whole of the year the capacity for carrying out structural research was severely restricted by urgent duties in connection with the airworthiness certification and the preparations for full-scale strength tests of the Fokker F-27 transport aeroplane, as well as the structural design of the transonic windtunnel of the N.L.L.

The stress and deflection analysis of semi-infinite swept boxes clamped at the root was continued.

A report was prepared on methods suitable for determining the compressive strength of bonded stiffened panels (Report S. 463).

A search was made of the literature concerning impact loading of non-linear components such as beams bent in the plastic range and buckling columns (Report S. 455).

Investigations were started on the effect of airplane flexibility on the ground loads during landing manoeuvres. Several other investigations relating to airworthiness requirements (gust loads (Report S 457), checked manoeuvre loads, design for fatigue) are being carried out.

Static testing of structural components.

A swept box was designed and manufactured, on which tests to verify the results of theoretical analyses will be carried out.

Tests to determine the effective width in the plastic range of clad 75 S-T and half-hard aluminium flat plates were carried out. A diagram for determining the ultimate strength of plates buckled in compression was derived (Report S. 465).

A report on the plastic buckling tests carried out in 1954 was completed also containing an empirical design formula (Report S. 444).

Fatigue.

Various investigations running from 1954 could be completed or were continued, viz.:

Cumulative damage tests on 24 S-T alclad strips and on riveted joints at two stress levels. A critical review of the literature on cumulative damage in light alloys was also included (Reports M. 1982 and M. 1999):

Endurance tests of flexible steel cables used in aircraft (Report M. 1978).

Tests to determine the most important parts of the fatigue diagrams (Goodman diagrams) of riveted joints (Report M. 1980) and simple lugs.

Investigations were started concerning the fatigue strength of Redux-bonded single lap joints at low and elevated temperatures, and on the propagation of fatigue cracks.

Adhesives and plastics.

The investigations concerning the strength of Redux-bonded lap joints at low temperatures was completed (Report M. 1973). A new investigation was started on the short-term and long-term strengths of Redux-bonded clad 75 S-T lap joints at elevated temperatures.

The tests to determine the mechanical properties of glassfiber-polyester laminates were completed (Report M. 1991).

Miscellaneous work.

Research was carried out concerning ultrasonic inspection of adhesive-bonded joints (Report M. 1995) and of jet engine compressor and turbine blades.

A study was made of the effect of elevated temperatures up to 350°C on the mechanical properties of various aircraft materials (Report M. 1987).

Rapid-loading tests with single welded frames, glued metal joints and lugs showed no significant deviations from the ultimate static strengths (Report S. 466).

6 *Flight Testing and Instrumentation Section.*

Response measurements.

The study of measuring techniques for the determination of dynamic aircraft characteristics has been continued.

A second series response measurements with the Siebel laboratory aeroplane has been carried out and better insight has been gained in various data reduction methods (V. 1745).

Stability and Control.

The influence of elastic deformation, at high subsonic air speeds, of high aspect-ratio swept wings on static longitudinal stability has been investigated. A simplified method for the calculation of the lift distribution and resulting accompanying deformation gave satisfactory results in comparison with the exact theory (V. 1754).

The static longitudinal stability and control at transonic and supersonic speeds for swept and delta wings has been studied from literature (V. 1780).

Flight testing.

The flight-testing of the prototype F-27 started at the end of the year after extensive preparations. Some performance testing of the prototype S-14 Nene and of the S-14 Derwent production version has been carried out.

The trajectory of the jettisoned cockpit hood of the S-14 has been measured in flight from two accompanying Meteors. The results have been compared with windtunnel measurements (Film).

Some ad-hoc measurements on cabin noise, position error of pitot systems and control characteristics of various types of aircraft have been carried out.

With the Siebel Laboratory aeroplane flight tests have been carried out on the effect of slotted wing-roots on the flying characteristics at large angles of attack. Comparison with windtunnel measurements was satisfactory (V. 1763).

Landing-gear accelerations have been measured during simulated deck-landings.

Instrumentation.

The planning and development of the flight-test instrumentation for the prototype F 27 took much time. Two large automatic observers have been built together with many devices built in in the aeroplane.

A new calibrating apparatus for accelerometers has been put in operation.

7 *Helicopter Section.*

The performance of ramjets as influenced by the dimensions of various components and by various atmospheric circumstances has been studied, in order to be able to reduce performance measurements to other circumstances.

Methods for the calculation of take-off and landing characteristics of helicopters have been studied, in particular one-engine take-off of a twin-engined helicopter and autorotation landings.

The influence of the position of the tip-ramjets on the rise of temperature and contamination of the intake air by the preceding ramjet has been studied in still air and in the wind tunnel.

The influence of the centrifugal accelerations on the fuel transport to the bladetips is being investigated.

8 *Free-flying models section.*

The test results of the launching of some NACA RM-10 models gave satisfactory agreement with existing data. A new model with built-in programming mechanism has been designed for the investigation of stability and control, and flight loads.

A study has been made of a Doppler-radar installation and its construction from surplus stock is in good progres. A readily available telemetering system has been ordered and received.

Both installations are mounted on trailers in order to have a mobile system.

9 *Combustion Section.*

The experimental investigation of the performance and fuel consumption of the NHI-ramjet has been continued. The measuring methods for the investigation of the combustion processes in a ramjet have been improved, and the influence of various modifications on the output have been investigated.

10 *Documentation and Publications.*

Catalogue of Aerodynamic Measurements (CAM).

The number of subscribers and the number of cards issued increased. A complete report covering systematical and alphabetical indexes, description and procedures has been issued. A report has been delivered to the Congrès Internationale des Bibliothèques in Brussels.

Central Aeronautical Abstracting Service (CLD).

Also here the number of cards issued and the number of subscribers increased. It has been decided to change over gradually to the Universal Decimal Classification, as far as the existing U.D.C. chapters are satisfactory or can be improved. An intensive international contact through the AGARD Documentation committee has been maintained.

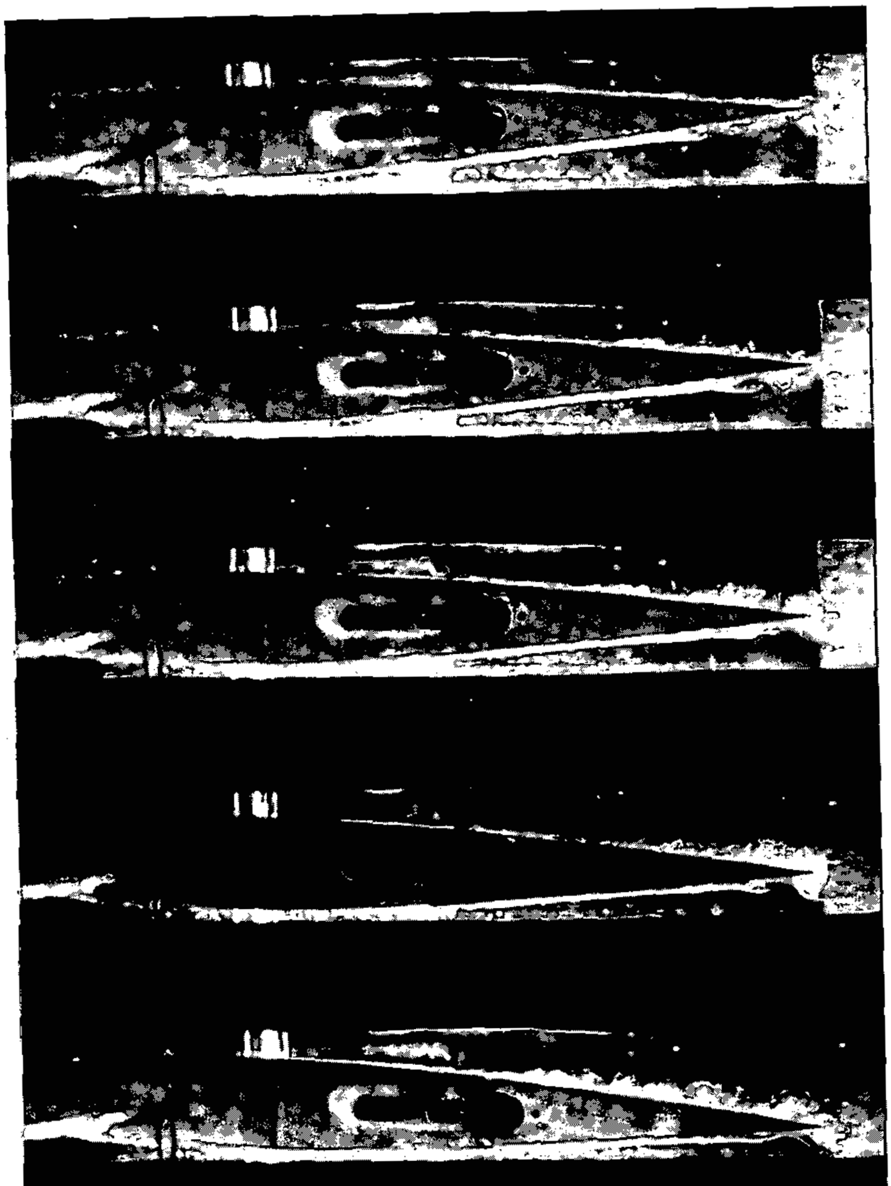

The boundary layer on an oscillating wing in various positions, visualized by smoke. N.B. the formation of a turbulent boundary layer at the trailing edge.

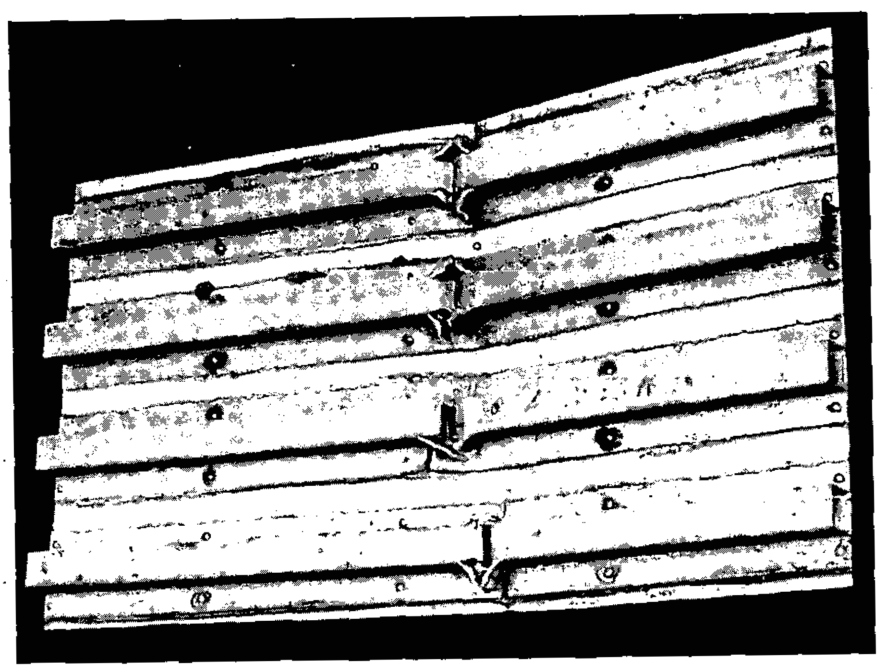

A skin panel of the Fokker F-27 with bonded stiffeners after failure at the 150-tons compression machine. This panel could absorb a load of 118 tons.

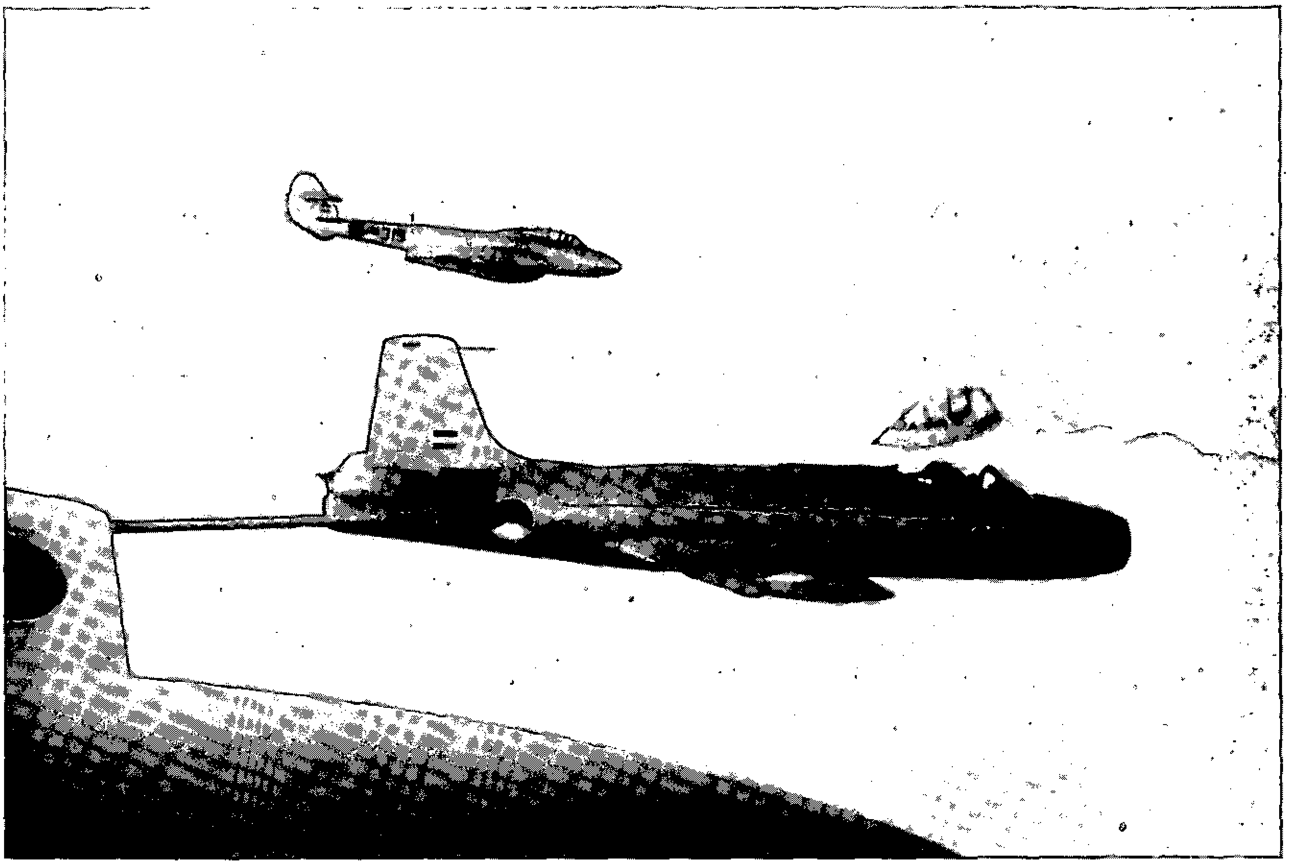

The cockpit hood of the Fokker S 14 Mach trainer immediately after jettisoning in flight, filmed from two accompanying Meteors.

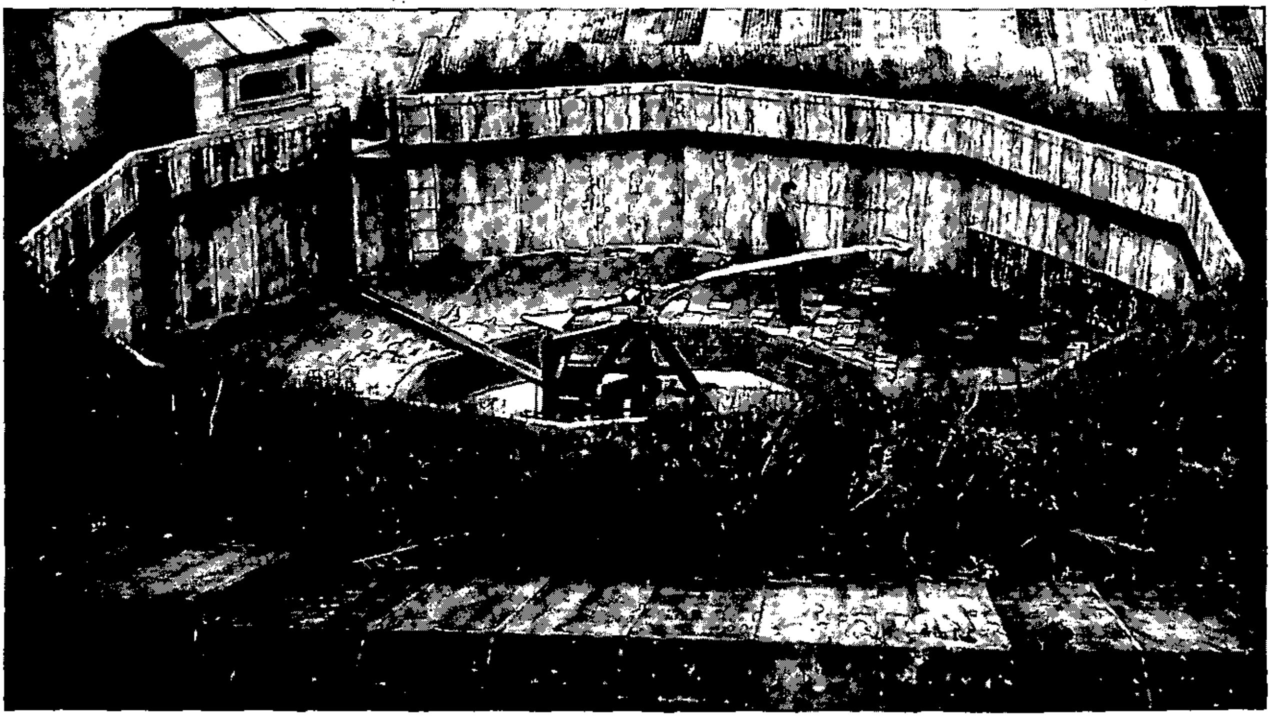

The test stand for the investigation of rotors and ram jets for helicopters.

Publications.

In 1955 146 reports were completed, of which the following were published, in addition to those published in this volume:

a) *Multigraphed and ozalided reports:*

A. 1370	Buntsma, W.	Investigation of the Wall Influence on a Half Model of a Swept Wing with Fuselage. (In Dutch.)
A. 1373	Boersma, G. and Landstra, J. A.	Properties of Internally Balanced and Non-Balanced Ailerons with Trim Tabs. (In Dutch.)
F. 152	De Jager, E. M.	The Theory of Conical Flows. 1955. (In Dutch.)
F. 156	De Leeuw, J. H., Eckhaus, W. and Van de Vooren, A. I.	The Solution of the Generalized Prandtl Equation for Swept Wings.
F. 157	Burger, A. P.	On the Asymptotic Solution of Wave Propagation and Oscillation Problems.
F. 161	Burgerhout, Th. J.	The Electric Digital Computer "Zebra". Part. I. General Survey for Programmers. (In Dutch.)
F. 163	Zaat, J. A.	Literature Survey of Two-Dimensional Transonic Flows. (In Dutch.)
F. 164	De Jager, E. M.	Lateral Stability Derivatives for a Swept Wing in Supersonic Flow. (In Dutch.)
F. 166	Bosschaert, A. C. A.	The Influence of the Chord-, Span-, and Gear Ratios on Binary Aileron-Springtab Flutter.
F. 167	Eckhaus, W.	On the Theory of Shock Reflection on Walls with Slots.
F. 170	De Jager, E. M. and Van de Vooren, A. I.	Slender Body Theory. (In Dutch.)
M. 1969	Jacobs, F. A. and Hartman, A.	The Effect of Sheet Thickness and Overlap on the Fatigue Strength at Repeated Tension of Redux Bonded 75 S-T Clad Single Lap Joints.
M. 1973	Hartman, A.	The Low-Temperature Strength of Redux-Bonded Single Lap Joints in 24 S-T Alclad and Clad 75 S-T. (In Dutch.)
M. 1978	Hartman, A.	Comparative Investigation on the Fatigue Strength of Flexible Preformed Steel Cable. (In Dutch.)
M. 1980	Klaassen, W. and Hartman, A.	The Fatigue Diagram for Fluctuating Tension of Single Lap Joints of Clad 24 S-T and 75 S-T Aluminum Alloy with 2 Rows of 17 S Rivets.
M. 1982	Schijve, J. and Jacobs, F. A.	Fatigue Tests on Notched and Unnotched Clad 24 S-T Sheet Specimens to Verify the Cumulative Damage Hypothesis.
M. 1987	Hartman, A.	Mechanical Properties of Aluminium Alloys, Stainless Steel, Titanium and Titanium Alloys at Elevated Temperatures up to 450°C. (In Dutch.)
M. 1995	Schijve, J.	Investigation on the Ultrasonic Testing of Glued Metal Joints.
S. 444	Besseling, J. F.	On the Buckling Problem in the Plastic Range for Struts and Plates. Part III. Experiments and Non-Dimensional Buckling Curves.
S. 446	Botman, M.	Shear Tests on 24 S-T Unstiffened and Stiffened Webs with Flanged Holes. Part 2.
S. 455	Benthem, J. P.	Step and Impact Loads on Some Non-Linear Structural Elements.
S. 457	Plantema, F. J.	Some Observations on Gust Load Requirements.
S. 460	Hakkeling, B.	Comparison of the British, U. S. and ICAO Strength Requirements for Flight Loads. (In Dutch.)
S. 465	Botman, M.	The Effective Width in the Plastic Range of Flat Plates under Compression. Part III.
S. 466	Benthem, J. P. and de Vries, G.	Investigation on the Strength of Redux-Bonded 75 S-T Clad Simple Lap Joints and of 24 S-T Lugs at Rapidly Applied Loads.

V. 1650	Burgerhout, Th. and Pool, A.	NACA Standard Atmosphere with Intervals of 10 m (33 ft). (In Dutch.)
V. 1671	Molier, W. J.	Manual for the Measurement of Lag in Aircraft Pitot Systems. (In Dutch.)
V. 1722	Willekens, A. J. L.	An Investigation of the Dynamic Characteristics of the N.L.L. Pressure-Sensing Elements. (In Dutch.)
V. 1725	Buhrman, J.	The "Tightening" Phenomenon of Aircraft and a Few Related Problems. (In Dutch.)
V. 1727	Lucassen, L. R.	Study of Literature on Combustion in Ramjet Engines. (In Dutch.)
V. 1734	Molier, W. J.	Comparison of the Calculated and Measured Lag in a Few Models of Aircraft Pitot Systems. (In Dutch.)
V. 1737	Greebe, F. W.	Siebel PH-NLL, type Si 204 D-1. Measurements of the Deformation of Fuselage and Stabilo during Flight. (In Dutch.)
V. 1745	Buhrman, J. and Marx, A. J.	An Investigation of the Longitudinal Stability and Control Characteristics of Aircraft by Means of Response Measurements. (In Dutch.)
V. 1748	Lucassen, L. R.	Helicopter Ground Resonance.
V. 1754	Kalkman, C. M.	A Numerical Investigation of the Effect of Aero-Elastic Deformations on the Longitudinal Static Stability of an Aircraft with a Swept Back Wing with Large Aspect Ratio. (In Dutch.)
V. 1761	Van Oosterom, T.	Balloon Race at 's Hertogenbosch (Coupe Andries Blitz 1955). Calculations of and Check on Gas Content and Handicap Ballast of the Balloons. (In Dutch.)
V. 1763	De Boer, I. and Greebe, F. W.	Siebel PH-NLL, type Si 204 D-1. A Flight Investigation of the Effects of Slots in the Wing Root on the Flying Characteristics at Large Angles of Attack. (In Dutch.)
V. 1769	Buhrman, J.	The Shorts Analogue Computor. (In Dutch.)

b) *Miscellaneous publications:*

MP. 109	Besseling, J. F.	Analysis of the Plastic Collaps of a Cruciform Column with Initial Twist Loaded in Compression. Journ. of Aero. Sci. Jan. 1956, Vol. 23, no. 1, p. 49.
MP. 110	Timman, R. und Zaat, J. A.	Eine Rechenmethode für dreidimensionale laminare Grenzschichten. (Prandtl-Gedenkboek) 50 Jahre Grenzschichtforschung, Vieweg und Sohn, 1955, p. 432.
MP. 115	Scherpenhuijsen Rom, G.	General Decimal Classification Systems for Aeronautical Use. AGARD March 1955.
MP. 116	Burgerhout, Th. J.	On Certain Linear Invariant Relations between the Elements of a Square Matrix. Proc. Kon. Ned. Ak. Wet. Ser. A, Vol. 58, nr. 3 (1955), p. 315. Indag. Math. Vol. 17, nr. 3 (1955), p. 315.
MP. 118	Besseling, J. F.	The Effective Width in the Plastic Range of Flat Plates under Compression. Lecture before AFITA, Paris, Dec. 1954.
MP. 119	Van de Vooren, A. I.	Two Lectures on Unsteady Aerodynamics. June '55.
MP. 120	Plantema, F. J.	Some Investigations on Cumulative Damage. Colloquium on Fatigue. Stockholm May 25—27, 1955. Proceedings, p. 218.
MP. 121	Schijve, J.	The Possibilities of Ultrasonic Materials Testing. Ingenieur Vol. 67, nr. 41 (14 Oct. 1955), p. L 49. (In Dutch.)
MP. 122	De Kock, A. C. and Van de Vooren, A. I.	Some Remarks on the Classificative Part of the N.L.L. Card Catalogue of Aerodynamic Measurements. FID Conference, Brussels, Sept. 1955.
MP. 123	Wijker, H.	Charts for the Estimation of the Permissible Humidity in Supersonic Windtunnels. Publ. Sci. Tech. Min. de l'Air "Hors Série" 1954.
MP. 124	Hartman, A.	Some Fatigue Problems in Aeronautics. Ingenieur, Vol. 67, nr. 20 (1955), p. L. 25 (1955). (In Dutch.)

MP. 125	Douwes Dekker, F. E.	Flight Tests. Performance Measurements on Jet Aircraft in Symmetrical Flight. Blue papers of Students Soc., "Leonardi da Vinci", 1955. (In Dutch.)
MP. 126	Eckhaus, W.	Theoretical Background of the Design of Transonic Test Sections in Wind Tunnels. Ingenieur, Vol. 68, nr. 3 (20 jan. 1956), p. L. 1. (In Dutch.)
MP. 127	Van Asselt, B. J.	The High-Speed Tunnel of the N.L.L. Ingenieur, Vol. 68, nr. 3 (20 jan. 1956), p. L. 6. (In Dutch.)
MP. 128	Schijve, J.	General Survey of Fatigue. Lecture before Kon. Inst. v. Ing. 25 nov. 1955. (In Dutch.)
MP. 129	Schijve, J.	Fatigue and Aircraft Engineering. Lecture before Kon. Inst. v. Ing. 25 nov. 1955. (In Dutch.)

C.C.L. Class. D 050 : D 011 : D 031

REPORT F. 165.

The Threedimensional Laminar Boundary Layer Flow about a Yawed Ellipsoid at Zero Incidence

by

J. A. ZAAT, E. VAN SPIEGEL *and* R. TIMMAN.

Summary.

Using TIMMAN's two parameter method for three dimensional laminar boundary layers the velocity distribution in the laminar boundary layer of a yawed ellipsoid at zero incidence will be calculated. The momentum equations in streamline direction and perpendicular to this direction can be reduced to a set of quasi-linear first order partial differential equations.

The initial conditions necessary for solving the system of differential equations are determined from the behaviour of the differential equations in the stagnation point.

Contents.

This investigation has been sponsored by the Netherlands Aircraft Development Board (N.I.V.).

1 Introduction.

In this paper a calculation of the laminar boundary layer about a three dimensional body will be made. In ref. 1 TIMMAN has developed a general theory for the calculation of three dimensional laminar boundary layers. This general theory will be applied to the laminar boundary layer of a yawed ellipsoid at zero incidence. The axes of the ellipsoid are chosen as $a = 3$, $b = 1$, $c = 0{,}15$ and the direction of the undisturbed flow as $(-1, -1, 0)$. For the calculation of the laminar boundary layer the potential flow about the body is necessary to be known. In the general case of a body of arbitrary shape this potential flow is not known. A case which is of considerable interest is that of the boundary layer of a swept back wing. To simulate conditions on a swept back wing a yawed ellipsoid at zero incidence is examined. The formulae for the potential flow about an ellipsoid are well known and can be found in the references 2, 3 and 4.

In TIMMAN's theory for three dimensional boundary layers a similar procedure as in the two-dimensional case is followed. The boundary layer equations can be replaced by a set of two first order partial differential equations in two unknown functions. These functions are two parameters, characterizing the velocity profiles in the direction of the streamline at the outer edge of the boundary layer and in a direction parallel to the surface and normal to the streamline direction.

A short survey of TIMMAN's theory for three dimensional incompressible laminar boundary layers is given. After the introduction of suitable velocity profiles and after a short treatment of the potential flow about the ellipsoid the boundary layer calculations are performed.

2 List of symbols.

y^i	Cartesian coordinates $(i = 1, 2, 3)$
x^α	Gaussian coordinates $(\alpha = 1, 2)$
x^0	coordinate measured along the normal to the surface
φ, ψ	streamline coordinates
U^i	contravariant components of the velocity vector in the free stream at the outer edge of the boundary layer
U_i	covariant components of the velocity vector in the free stream at the outer edge of the boundary layer
u	velocity components in the boundary layer
$g_{\alpha\beta}$, $\gamma_{\lambda\mu}$	covariant components of the metric tensor
$g^{\alpha\beta}$, $\gamma^{\lambda\mu}$	contravariant components of the metric tensor
ds	line-element
$\sqrt{T}$	absolute value of the velocity vector
$\sqrt{\rho}$	integration factor
ν_1	kinematic viscosity

$\Gamma^{\alpha}_{\beta\lambda}$: Riemann-Christoffel symbol
ζ, ζ_a, η coordinates
σ, Ω profile parameters
δ_a displacement thickness vector
$\delta_{a\beta}$ momentum thickness tensor
Δ_a dimensionless displacement thickness vector
$\theta_{a\beta}$ dimensionless momentum thickness vector
f, g, h functions of η
$\left.\begin{array}{l} a_a, b_a, c_a, \ldots f_a \\ p_0, q_0, r_0, s_0, t_0 \\ M, N, \Lambda \end{array}\right\}$ coefficients (functions of φ and ψ)
$p_1, p_2, \ldots\ldots, p_{15}$ constants
$\left.\begin{array}{l} f^1, f^2, g^1, g^2 \\ F^1, F^2, G^1, G^2 \\ \gamma^1, \gamma^2, \gamma^{11}, \gamma^{12}, \gamma^{22} \\ \Gamma^1, \Gamma^2, \Gamma^{11}, \Gamma^{12}, \Gamma^{22} \end{array}\right\}$ functions of the parameters σ and Ω and of the coordinates φ and ψ
x, y, z Cartesian coordinates
a, b, c axes of the ellipsoid
U, V velocity components of the undisturbed flow
p, q covariant velocity components on the surface of the ellipsoid
α_0, β_0 constants
η_1, η_2, η_3 coordinates introduced in section 5
$l, \lambda, \mu, \nu, \kappa$ constants
$A_{ij}, B_{ij}, P, Q, R, S, T, V, W, Z$ functions of the surface coordinates introduced in section 6.

3 The momentum equations in streamline coordinates.

The potential flow about a body in three-dimensional space with Cartesian coordinates y^i $(i=1,2,3)$ is completely determined by its velocity potential $\varphi(y^i)$. This velocity potential $\varphi(y^i)$ must satisfy the condition that the gradient $\dfrac{\partial\varphi}{\partial y^i}$ is tangential to the surface F of the body.

Introduce the curvilinear coordinates x^α $(\alpha=0,1,2)$, x^0 being the Euclidean distance from a point in space to the surface measured along the normal to the surface through this point and x^1 and x^2 the coordinates on the surface F. The line element for these coordinates is then

$$ds^2=(dy^i)^2=g_{a\beta}\,dx^\alpha dx^\beta + (dx^0)^2 \;(\alpha,\beta=1,2) \qquad (3.1)$$

where

$$g_{a\beta}=\frac{\partial y^i}{\partial x^\alpha}\cdot\frac{\partial y^i}{\partial x^\beta}. \qquad (3.2)$$

In the Cartesian coordinates y^i there is no difference between co- and contravariant components of the velocity vector

$$U_i=U^i=\frac{\partial\varphi}{\partial y_i}=\frac{\partial\varphi}{\partial y^i}. \qquad (3.3)$$

In the curvilinear coordinates the covariant components of the velocity vector are

$$U_a=U_i\frac{\partial y^i}{\partial x^\alpha}=\frac{\partial\varphi}{\partial y^i}\;\frac{\partial y^i}{\partial x^\alpha}=\frac{\partial\varphi}{\partial x^\alpha}\,(\alpha=1,2)$$
$$U_0=U_i\frac{\partial y^i}{\partial x^0}=\frac{\partial\varphi}{\partial y^i}\;\frac{\partial y^i}{\partial x^0}=\frac{\partial\varphi}{\partial x^0}. \qquad (3.4)$$

The fact that the velocity vector is tangential to the surface F requires $U_0=0$ for $x^0=0$. Hence, on the surface the velocity vector is fully determined by its two components in the Gaussian system. Introduce now again a curvilinear orthogonal coordinate system $\xi^\lambda\,(\lambda=1,2)$ on the surface defined by requiring the covariant components of the velocity vector to assume the form

$$\overline{U}_1=1,\;\;\overline{U}_2=0. \qquad (3.5)$$

From the transformation formulae

$$U_a=\frac{\partial\xi^\lambda}{\partial x^\alpha}\overline{U}_\lambda \qquad (3.6)$$

it follows

$$U_1=\frac{\partial\xi^1}{\partial x^1},\;\;U_2=\frac{\partial\xi^1}{\partial x^2}. \qquad (3.7)$$

The formulae (3.4) and (3.7) show that

$$\xi^1=\varphi(x^\alpha), \qquad (3.8)$$

taking the value of the constant of integration to be zero.

The second coordinate ξ^2 can be determined from the orthogonality conditions.

Denoting the new metric tensor by $\gamma_{\lambda\mu}$ the line element is

$$ds^2=g_{a\beta}\,dx^\alpha\,dx^\beta=\gamma_{\lambda\mu}\,d\xi^\lambda\,d\xi^\mu. \qquad (3.9)$$

Owing to the orthogonality holds

$$\gamma_{12}=\gamma_{21}=0 \qquad (3.10)$$

and thus

$$\gamma=|\det\gamma_{\lambda\mu}|=\gamma_{11}\gamma_{22}. \qquad (3.11)$$

The contravariant components $\gamma^{\lambda\mu}$ are

$$\gamma^{11}=\frac{\gamma_{22}}{\gamma}=\frac{1}{\gamma_{11}}\;;\;\gamma^{22}=\frac{1}{\gamma_{22}}\;;$$
$$\gamma^{12}=\gamma^{21}=0. \qquad (3.12)$$

From the last relation $\gamma^{12}=\gamma^{21}=0$ the equation for ξ^2 can be derived

$$\gamma^{12}=\gamma^{21}=g^{\alpha\beta}\frac{\partial\xi^1}{\partial x^\alpha}\;\frac{\partial\xi^2}{\partial x^\beta}=$$
$$=g^{\alpha\beta}\,U_\alpha\frac{\partial\xi^2}{\partial x^\beta}=U^\beta\,\frac{\partial\xi^2}{\partial x^\beta}=0$$

or explicitly

$$U^1\frac{\partial\xi^2}{\partial x^1}+U^2\frac{\partial\xi^2}{\partial x^2}=0. \qquad (3.13)$$

Denoting ξ^2 by ψ this differential equation can be solved by putting

$$\frac{\partial\psi}{\partial x^2}=\sqrt{\rho g}\,U^1,\;\;\frac{\partial\psi}{\partial x^1}=-\sqrt{\rho g}\,U^2 \quad (3.14)$$

where

$$g=|\det g_{a\beta}|$$

and ρ is a function which must satisfy the equation

$$\frac{\partial \sqrt{\rho g}\, U^1}{\partial x^1} + \frac{\partial \sqrt{\rho g}\, U^2}{\partial x^2} = 0. \qquad (3.15)$$

Let the square of the velocity vector be denoted by T, then

$$\gamma^{11} = g^{\alpha\beta} \frac{\partial \xi^1}{\partial x^\alpha} \cdot \frac{\partial \xi^1}{\partial x^\beta} = g^{\alpha\beta} U_\alpha U_\beta = T$$

and

$$\gamma^{22} = g^{\alpha\beta} \frac{\partial \xi^2}{\partial x^\alpha} \frac{\partial \xi^2}{\partial x^\beta} = \rho g \,\{\, g^{11}(U^2)^2 -$$
$$- 2\, g^{12} U^1 U^2 + g^{22} (U^1)^2 \,\} = \rho g_{\alpha\beta} U^\alpha U^\beta = \rho T. \quad (3.16)$$

The line-element in the new streamline coordinates φ and ψ is now

$$ds^2 = \frac{1}{T}\left(d\varphi^2 + \frac{1}{\rho}\, d\psi^2\right). \qquad (3.17)$$

Introducing for the coordinate normal to the surface a new variable by putting

$$\zeta = \frac{x^0}{\sqrt{\nu_1}}, \qquad (3.18)$$

where ν_1 is the kinematic viscosity
and replacing the velocity component U_0 in this direction by

$$w = \frac{U_0}{\sqrt{\nu_1}}, \qquad (3.19)$$

then according to LIN (ref. 5) the boundary layer equations assume the form

$$\left\{\begin{aligned} & u^\beta u_{\alpha,\beta} + w \frac{\partial u_\alpha}{\partial \zeta} = U^\beta U_{\alpha,\beta} + \frac{\partial^2 u_\alpha}{\partial \zeta^2} \; (\alpha, \beta = 1, 2) \\ & u^\beta{}_{,\beta} + \frac{\partial w}{\partial \zeta} = 0 \end{aligned}\right. \qquad (3.20)$$

The comma's denote covariant differentiation in the coordinates $x^\alpha\,(\alpha = 1, 2)$, so that

$$\begin{aligned} u_{\alpha,\beta} &= \frac{\partial u_\alpha}{\partial x^\beta} - \Gamma^\lambda_{\alpha\beta}\, u_\lambda \\ u^\beta{}_{,\alpha} &= \frac{\partial u^\beta}{\partial x^\alpha} + \Gamma^\beta_{\alpha\lambda}\, u^\lambda \end{aligned} \qquad (3.21)$$

where

$$\Gamma^\lambda_{\alpha\beta} = \tfrac{1}{2}\, \gamma^{\lambda\lambda} \left\{ \frac{\partial \gamma_{\alpha\lambda}}{\partial \xi^\beta} + \frac{\partial \gamma_{\beta\lambda}}{\partial \xi^\alpha} - \frac{\partial \gamma_{\alpha\beta}}{\partial \xi^\lambda} \right\}. \qquad (3.22)$$

U^α denote the contravariant components of the velocity vector in the free stream at the outer edge of the boundary layer; u^α the components in the boundary layer.

From the equations (3.20) the momentum equation is found by integration with respect to ζ from 0 to ∞

$$U_{\alpha,\beta} \int_0^\infty (U^\beta - u^\beta)\, d\zeta +$$
$$+ \int_0^\infty \{(U_\alpha - u_\alpha) u^\beta\}_{,\beta}\, d\zeta = \left[\frac{\partial u_\alpha}{\partial \zeta}\right]_0. \quad (3.23)$$

Introduction of the displacement thickness vector

$$\delta_\alpha = \int_0^\infty (U_\alpha - u_\alpha)\, d\zeta$$

and the momentum thickness tensor (3.24)

$$\vartheta_{\alpha\beta} = \int_0^\infty (U_\alpha - u_\alpha)\, u_\beta\, d\zeta$$

gives to the equations (3.23) the form

$$U_{\alpha,\beta}\, \delta^\beta + \vartheta_\alpha{}^\beta{}_{,\beta} = \left[\frac{\partial u_\alpha}{\partial \zeta}\right]_0. \qquad (3.25)$$

In streamline coordinates φ and ψ the covariant components of the free stream velocity vector are

$$U_1 = 1, \; U_2 = 0$$

and the covariant derivatives $U_{\alpha,\beta}$ become

$$U_{\alpha,\beta} = -\Gamma^1_{\alpha,\beta}. \qquad (3.26)$$

Using the relations $\gamma^{11} = T$, $\gamma^{22} = \rho T$ and $\gamma^{12} = \gamma^{21} = 0$ one can write for the Riemann-Christoffel symbols

$$\Gamma^1_{11} = -\frac{T_\varphi}{2\,T}, \; \Gamma^1_{12} = \Gamma^1_{21} = -\frac{1}{\rho}\, \Gamma^2_{11} = -\frac{T_\psi}{2\,T}$$
$$\Gamma^1_{22} = -\frac{1}{\rho} \Gamma^2_{12} = \frac{1}{2\,\rho}\left(\frac{T_\varphi}{T} + \frac{\rho_\varphi}{\rho}\right); \qquad (3.27)$$
$$\Gamma^2_{22} = -\frac{1}{2}\left(\frac{T_\psi}{T} + \frac{\rho_\psi}{\rho}\right).$$

Taking account of the identities

$$\delta^\beta = \gamma^{\beta\varepsilon} \delta_\varepsilon, \; \vartheta_\alpha{}^\beta = \gamma^{\beta\varepsilon} \vartheta_{\alpha\varepsilon}$$
$$\vartheta_{\alpha\varepsilon,\beta} = \frac{\partial \vartheta_{\alpha\varepsilon}}{\partial \xi^\beta} - \Gamma^\lambda_{\alpha\beta}\, \vartheta_{\lambda\varepsilon} - \Gamma^\lambda_{\varepsilon\beta}\, \vartheta_{\alpha\lambda} \qquad (3.28)$$

the momentum equations become

$$\frac{\partial \vartheta_{11}}{\partial \varphi} + \rho \frac{\partial \vartheta_{12}}{\partial \psi} + \frac{T_\varphi}{2\,T} (\delta_1 + \vartheta_{11} + \rho \vartheta_{22}) +$$
$$+ \frac{\rho_\varphi}{2\,\rho} (\rho \vartheta_{22} - \vartheta_{11}) + \frac{\rho_\psi}{2}\, \vartheta_{12} = \frac{1}{T} \left[\frac{\partial u_1}{\partial \zeta}\right]_0$$
$$(3.29)$$
$$\frac{\partial \vartheta_{21}}{\partial \varphi} + \rho \frac{\partial \vartheta_{22}}{\partial \psi} + \frac{T_\psi}{2\,T} (\delta_1 + \vartheta_{11} + \rho \vartheta_{22}) -$$
$$- \frac{\rho_\varphi}{2\,\rho}\, \vartheta_{21} + \rho_\psi \vartheta_{22} = \frac{1}{T} \left[\frac{\partial u_2}{\partial \zeta}\right]_0.$$

4 The solution of the momentum equations.

The momentum equations, derived in the preceding section, are not sufficient to determine completely the boundary layer flow. In fact, the boundary value problem formed by the boundary layer equations together with the boundary conditions at the wall and in infinity is equivalent to the momentum equation and a set of infinitely many boundary conditions for $\zeta = 0$ and $\zeta = \infty$, obtained from (3.20) by differentiation with respect to ζ and putting $\zeta = 0$ and $\zeta = \infty$. The first of these boundary conditions at the wall reads

$$- U^\beta U_{\alpha,\beta} = \left[\frac{\partial^2 u_\alpha}{\partial \zeta^2}\right]_{\zeta=0}. \tag{4.1}$$

Using the equation of continuity the second boundary conditions at the wall can be written as

$$\left[u_{\alpha,\beta}\frac{\partial u^\beta}{\partial \zeta} + \frac{\partial u_\alpha}{\partial \zeta}\,\frac{\partial w}{\partial \zeta}\right]_{\zeta=0} =$$

$$= \left[u_{\alpha,\beta}\frac{\partial u^\beta}{\partial \zeta} - u^\beta{}_{,\beta}\frac{\partial u_\alpha}{\partial \zeta}\right]_{\zeta=0} = \left[\frac{\partial^3 u_\alpha}{\partial \zeta^3}\right]_{\zeta=0}. \tag{4.2}$$

From the relations $[u_{\alpha,\beta}]_{\zeta=0} = 0$ and $[u^\beta{}_{,\beta}]_{\zeta=0} = 0$ this boundary condition can be reduced to

$$\left[\frac{\partial^3 u_\alpha}{\partial \zeta^3}\right]_{\zeta=0} = 0. \tag{4.3}$$

The following boundary conditions contain derivatives of unknown functions as is seen by differentiating (3.20) once more with respect to ζ and putting $\zeta = 0$ and hence cannot be taken into account without greatly complicating the calculations. In the streamline coordinates (4.1) becomes

$$- \tfrac{1}{2} T_\varphi = \left[\frac{\partial^2 u_1}{\partial \zeta^2}\right]_{\zeta=0}$$

$$- \tfrac{1}{2} T_\psi = \left[\frac{\partial^2 u_2}{\partial \zeta^2}\right]_{\zeta=0}. \tag{4.4}$$

The set of partial differential equations (3.29) will be replaced by a set of two quasi-linear first order partial differential equations in two unknown functions. These functions are two parameters, characterizing the velocity profiles in the direction of the streamline at the outer edge of the boundary layer and in the direction parallel to the surface and normal to this streamline direction.

In order to specify the velocity profiles in the boundary layer the covariant components of the velocity profiles which are dimensionless quantities, are considered. For $\zeta \to \infty$ these covariant components tend to the components of the free stream velocity $U_1 = 1$, $U_2 = 0$.

The profiles are introduced as functions of a dimensionless variable

$$\zeta_\alpha = \zeta \sigma_\alpha^{-\frac{1}{2}} \quad (\alpha = 1, 2) \tag{4.5}$$

where σ_α is a measure for the boundary layer thickness. σ_α is taken different in the two directions. In the streamline coordinates one can write for the velocity profiles

$$u_\alpha = U_\alpha - (a_\alpha + b_\alpha\zeta_\alpha + c_\alpha\zeta_\alpha^2 + \ldots)e^{-\zeta_\alpha^2} - f_\alpha \int_{\zeta_\alpha}^{\infty} e^{-\eta^2} d\eta \quad (\alpha = 1, 2). \tag{4.6}$$

The boundary conditions that must be taken into account are

$$\begin{aligned} &\text{for} \quad \zeta_\alpha \to \infty \quad u_\alpha \to U_\alpha; \\ &\qquad u_\alpha' = u_\alpha'' = \ldots\ldots = 0 \\ &\text{for} \quad \zeta_\alpha = 0 \quad u_\alpha = u_\alpha''' = 0; \\ &\qquad u_1'' = -\tfrac{1}{2} T_\varphi \sigma_1;\ u_2'' = -\tfrac{1}{2} T_\psi \sigma_2 \end{aligned} \tag{4.7}$$

where the accent denotes differentiation with respect to ζ_α.

From (4.6) can now be derived for $\zeta_\alpha = 0$

$$\begin{aligned} u_\alpha &= U_\alpha - a_\alpha - \frac{\sqrt{\pi}}{2} f_\alpha & u_\alpha'' &= 2(a_\alpha - c_\alpha) \\ & & u_\alpha''' &= 2(3b_\alpha - f_\alpha) \\ u_\alpha' &= f_\alpha - b_\alpha & u_\alpha'''' &= 6(4c_\alpha - 2a_\alpha) \end{aligned} \tag{4.8}$$

Writing

$$\begin{aligned} &\sigma = \sigma_1 \quad \eta = \zeta_1 = \Omega\zeta_2; \quad \tfrac{1}{2} T_\varphi \sigma = \Lambda \\ &2\,c_1 = -N \quad c_2 = 0 \quad \tfrac{1}{2}\sqrt{\rho}\, T_\psi \sigma = M \end{aligned} \tag{4.9}$$

the velocity profiles can be expressed in the form

$$\begin{aligned} u_1 &= f(\eta) - \Lambda g(\eta) - N h(\eta) \\ \sqrt{\rho}\, u_2 &= -\Omega^2 M g\left(\frac{\eta}{\Omega}\right) \end{aligned} \tag{4.10}$$

with

$$\begin{aligned} 1 - f(\eta) &= 2g(\eta) + e^{-\eta^2} = \\ &= 2h(\eta) + (1 + \eta^2)e^{-\eta^2} = \\ &= \frac{2}{3\sqrt{\pi}}\eta e^{-\eta^2} + \frac{2}{\sqrt{\pi}}\int_\eta^\infty e^{-\eta^2} d\eta \end{aligned} \tag{4.11}$$

and the boundary conditions for $\eta = 0$

$$\begin{aligned} &f = g = h = f'' = h'' = f''' = g''' = h''' = f'''' = 0 \\ &f' = -2g' = -2h' = \frac{4}{3\sqrt{\pi}} \\ &g'' = 1 \\ &g'''' = -h'''' = -6. \end{aligned} \tag{4.12}$$

As the covariant components of the displacement thickness vector and the momentum thickness tensor have the dimension of the coordinate ζ, it is convenient to introduce new quantities by putting

$$\Delta_1 = \sigma^{-\frac{1}{2}}\,\delta_1 = \int_0^\infty (1-u_1)\,d\eta = p_1 + p_2\,\Lambda + p_3\,N$$

$$\Delta_2 = \rho^{\frac{1}{2}}\,\sigma^{-\frac{1}{2}}\,\delta_2 = -\int_0^\infty \sqrt{\rho}\,u_2\,d\eta = p_2\,M\Omega^3$$

$$\theta_{11} = \sigma^{-\frac{1}{2}}\,\vartheta_{11} = \int_0^\infty (1-u_1)u_1\,d\eta = p_4 - p_5\Lambda -$$
$$- p_6 N - p_7\,\Lambda^2 - p_8 N^2 - 2\,p_9\,N\Lambda \qquad (4.13)$$

$$\theta_{21} = \rho^{1/2}\sigma^{-1/2}\vartheta_{21} = -\int_0^\infty \sqrt{\rho}\,u_2\,u_1\,d\eta = \Delta_2 + \theta_{12}$$

$$\theta_{22} = \rho\sigma^{-\frac{1}{2}}\vartheta_{22} = -\int_0^\infty \rho\,u_2^2\,.\,d\eta = -p_7\,M^2\Omega^5.$$

As the component $\theta_{12} = \rho^{1/2}\sigma^{-1/2}\,\vartheta_{12}$ for $\Omega \neq 1$ turns out to be a complicated expression, the function $u_1 = u_1(\zeta_1)$ will be approximated by

$$u_1 = 1 - (p_0 + q_0\zeta_2 + r_0\zeta_2^2 + s_0\zeta_2^3)\,e^{-\zeta_2^2} -$$
$$- t_0 \int_{\zeta_2}^\infty e^{-\eta^2}\,d\eta \qquad (4.14)$$

where p_0, q_0, r_0, s_0 and t_0 must be calculated from the first four boundary conditions at the wall and from the unchanged value of Δ_1.

These conditions give the expressions

$$u_1 = 1 - p_0 - \frac{\sqrt{\pi}}{2}\,t_0 = 0$$

$$\frac{\partial u_1}{\partial \eta} = \frac{\partial u_1}{\partial \zeta_2}\,\frac{1}{\Omega} = \frac{1}{\Omega}\,(t_0 - q_0) = \frac{2}{3\sqrt{\pi}}(2 + \Lambda + N)$$

$$\frac{\partial^2 u_1}{\partial \eta^2} = \frac{\partial^2 u_1}{\partial \zeta_2^2}\,\frac{1}{\Omega^2} = \frac{2}{\Omega^2}\,(p_0 - r_0) = -\Lambda \qquad (4.15)$$

$$\frac{\partial^3 u_1}{\partial \eta^3} = \frac{\partial^3 u_1}{\partial \zeta_2^3}\,\frac{1}{\Omega^3} = \frac{2}{\Omega^3}\,(3\,q_0 - 3\,s_0 - t_0) = 0$$

$$\frac{1}{\Omega}\,(p_1 + p_2\,\Lambda + p_3\,N) =$$
$$= \frac{\sqrt{\pi}}{2}\,(p_0 + \tfrac{1}{2}\,r_0) + \tfrac{1}{2}\,(q_0 + s_0 + t_0).$$

The approximate formula for θ_{12} takes now the form

$$\theta_{12} = \rho^{1/2}\sigma^{-1/2}\,\vartheta_{12} = \sqrt{\rho}\int_0^\infty (1-u_1)u_2\,d\eta = -\Delta_2 -$$
$$- \Omega\sqrt{\rho}\int_0^\infty u_2(\zeta_2)u_1(\zeta_2)\,d\zeta_2 =$$
$$= M\Omega^2\,[p_{10} + p_{11}\,\Lambda + p_{12}\,N + p_{13}\,\Omega + p_{14}\,(2 +$$
$$+ \Lambda + N)\,\Omega^2 + p_{15}\,\Lambda\,\Omega^3]\ ^{*}). \qquad (4.16)$$

Using the relations (4.13) and (4.16) the momentum equations (3.29) become

$$f^1\sigma_\varphi + f^2\sigma_\psi + g^1\Omega_\varphi + g^2\Omega_\psi = d = \frac{\gamma}{T} + \gamma^1\,\frac{\rho_\varphi}{\rho} - \gamma^{11}T_{\varphi\varphi} - \gamma^{12}\sqrt{\rho}T_{\varphi\psi} - \gamma^{22}\sqrt{\rho}\,(\sqrt{\rho}T_\psi)_\psi$$
$$(4.17)$$
$$F^1\sigma_\varphi + F^2\sigma_\psi + G^1\Omega_\varphi + G^2\Omega_\psi = D = \frac{\Gamma}{T} + \Gamma^1\,\frac{\rho_\varphi}{\rho} - \Gamma^{11}T_{\varphi\varphi} - \Gamma^{21}\,\frac{(\sqrt{\rho}T_\psi)_\varphi}{\sqrt{\rho}T_\psi} - \Gamma^{22}\sqrt{\rho}\,(\sqrt{\rho}T_\psi)_\psi$$

where

$$f^1 = 2\,\Lambda\,\theta_{11\Lambda} + \theta_{11} \qquad MF^1 = 2\,\Lambda\theta_{21\Lambda} + 2\,M\,\theta_{21M} + \theta_{21}$$

$$f^2 = \sqrt{\rho}(2\,M\,\theta_{12M} + 2\,\Lambda\,\theta_{12\Lambda} + \theta_{12}) \qquad MF^2 = (2\,M\,\theta_{22M} + \theta_{22})\sqrt{\rho}$$

$$g^1 = 0 \qquad MG^1 = 2\,\sigma\,\theta_{21\Omega}$$

$$g^2 = 2\,\sigma\sqrt{\rho}\,\theta_{12\Omega} \qquad MG^2 = 2\,\sigma\,\theta_{22\Omega}\sqrt{\rho}$$

and

$$\gamma = 2\left[\left(\frac{\partial u_1}{\partial \eta}\right)_0 - \Lambda\,(\Delta_1 + \theta_{11} + \theta_{22})\right] \qquad M\Gamma = 2\left[\left(\frac{\partial u_2}{\partial \eta}\right)_0\sqrt{\rho} - M\,(\Delta_1 + \theta_{11} + \theta_{22})\right]$$

$$\gamma^1 = \sigma(\theta_{11} - \theta_{22}) \qquad M\Gamma^1 = 2\,\sigma\,\theta_{21}$$

$$\gamma^{11} = \sigma^2\,\theta_{11\Lambda} \qquad M\Gamma^{11} = \sigma^2\,\theta_{21\Lambda}$$

$$\gamma^{12} = \sigma^2\,\theta_{12\Lambda} \qquad \Gamma^{21} = 2\,\sigma\,\theta_{21M}$$

$$\gamma^{22} = \sigma^2\,\theta_{12M} \qquad M\Gamma^{22} = \sigma^2\,\theta_{22M}.$$

---

*) The constants used in the formulae (4.13) and (4.16) are

$p_1 = 0.75225$	$p_6 = 0.08670$	$p_{11} = -0.00121$
$p_2 = -0.06699$	$p_7 = 0.00380$	$p_{12} = -0.00523$
$p_3 = -0.28854$	$p_8 = 0.04774$	$p_{13} = 0.03522$
$p_4 = 0.28943$	$p_9 = 0.01108$	$p_{14} = -0.00585$
$p_5 = -0.00734$	$p_{10} = 0.01364$	$p_{15} = 0.00327$

Just as in TIMMAN's method for two-dimensional boundary layers (ref. 6) only the first four boundary conditions are taken into account for the region of accelerated flow. Therefore N will be taken zero there. In the case of retarded flow this approximation fails. Because of the fact that in the separation point the fifth boundary condition becomes zero (vanishing of the skin friction in the streamline direction) it will be supposed that in this region N is equal to Λ. The solutions for accelerated and retarded flow agree very well in the transition region, where holds $T_\varphi = 0$.

5 The potential flow about a three-axial ellipsoid.

From a practical point of view the calculation of the boundary layer of a swept back wing is of great importance. In order to simulate conditions on a swept back wing a yawed ellipsoid at zero incidence is considered. The formulae for the potential flow about an ellipsoid are well known and can be applied directly.

If the ellipsoid is given by the equation

$$\frac{x^2}{a^2} + \frac{y^2}{b^2} + \frac{z^2}{c^2} = 1 \quad a > b > c \tag{5.1}$$

then the expression for the velocity potential $\varphi(x, y, z)$ on the surface of the ellipsoid for a flow, with velocity components $-U$, $-V$, 0 in infinity, is given by (ref. 2 and 3)

$$\varphi = -p\,x - q\,y \tag{5.2}$$

where

$$-p = \frac{2\,U}{2 - \alpha_0}, \quad -q = -\frac{2\,V}{2 - \beta_0}.$$

are the covariant components of the velocity vector and

$$\alpha_0 = abc \int_0^\infty \frac{d\xi}{(a^2 + \xi)L}, \quad \beta_0 = abc \int_0^\infty \frac{d\xi}{(b^2 + \xi)L},$$

$$L = \sqrt{(a^2 + \xi)(b^2 + \xi)(c^2 + \xi)}.$$

In order to give a better description of the streamlines new variables are introduced defined by a system of oblique coordinates, with origin in the stagnation point and axis in the x-y plane formed by the tangent to the ellips in the stagnation point and its conjugate median; the third axis being parallel to the z-axis (ref. 4)

$$\begin{aligned} 1 - \eta_1 &= \frac{px + qy}{l} = \cos\vartheta\cos\theta \\ \eta_2 &= \frac{bqx}{al} - \frac{apy}{bl} = \sin\vartheta \\ \eta_3 &= \frac{z}{c} = \cos\vartheta\sin\theta \end{aligned} \tag{5.3}$$

if l is defined by $l = \sqrt{a^2p^2 + b^2q^2}$.

The velocity potential φ is then

$$\varphi = -l(1 - \eta_1) \tag{5.4}$$

and the equation for the ellipsoid in the new coordinatss becomes

$$(1 - \eta_1)^2 + \eta_2^2 + \eta_3^2 = 1. \tag{5.5}$$

Two of these η-coordinates can be taken as coordinates on the surface of the ellipsoid.

The covariant components of the velocity vector in these coordinates η_1 and η_2 are then

$$U_1 = \frac{\partial\varphi}{\partial\eta_1} = l, \quad U_2 = \frac{\partial\varphi}{\partial\eta_2} = 0. \tag{5.6}$$

Putting $G = \frac{\eta_2}{1 - \eta_1}$ and $F = \frac{\eta_3}{1 - \eta_1}$, the line element takes the form

$$\begin{aligned} ds^2 &= c^2\left(\mu + \frac{1}{F^2}\right)d\eta_1^2 - 2\,c^2\left(\nu + \frac{G}{F^2}\right)d\eta_1\,d\eta_2 + \\ &\quad + c^2\left(\lambda + \frac{G^2}{F^2}\right)d\eta_2^2 = \\ &= g_{11}\,d\eta_1^2 + 2\,g_{12}\,d\eta_1\,d\eta_2 + g_{22}\,d\eta_2^2. \end{aligned} \tag{5.7}$$

The contravariant components of the metric tensor are

$$g^{11} = \frac{g_{22}}{g}; \quad g^{12} = -\frac{g_{12}}{g}; \quad g^{22} = \frac{g_{11}}{g},$$

where $g = g_{11}g_{22} - g_{12}^2$.

The contravariant components of the velocity vector become thus

$$\begin{aligned} U^1 &= g^{11}U_1 + g^{12}U_2 = \frac{c^2 l}{g}\left(\lambda + \frac{G^2}{F^2}\right) \\ U^2 &= g^{21}U_1 + g^{22}U_2 = \frac{c^2 l}{g}\left(\nu + \frac{G}{F^2}\right). \end{aligned} \tag{5.8}$$

The square of the velocity vector can be written as

$$T = U_1U^1 + U_2U^2 = \frac{l^2}{c^2}\;\frac{G^2 + \lambda F^2}{\lambda - 2\,\nu G + \mu G^2 + \kappa F^2} \tag{5.9}$$

with

$$\lambda = \frac{a^2b^2(p^2 + q^2)}{l^2c^2}; \quad \nu = \frac{(a^2 - b^2)abpq}{l^2c^2};$$

$$\mu = \frac{a^4p^2 + b^4q^2}{l^2c^2}; \quad \lambda\mu - \nu^2 = \frac{a^2b^2}{c^4} = \kappa.$$

For a thin ellipsoid the values of λ, ν, μ and κ are very large.

The equation of the streamlines expresses that everywhere on the surface they are tangent to the velocity vector. Hence this equation is (ref. 4)

$$\frac{d\eta_2}{d\eta_3} = \frac{\eta_2(1 - \eta_1) + \nu\eta_3^2}{\eta_3\{\lambda(1 - \eta_1) - \nu\eta_2\}}. \tag{5.10}$$

In the neighbourhood of the stagnation point $(\eta_1 = \eta_2 = \eta_3 = 0)$ the equation can be approximated by

$$\frac{d\eta_2}{d\eta_3} \approx \frac{\eta_2}{\lambda\eta_3} \tag{5.11}$$

with the solution

$$\eta_3 = e^{-\psi}\,\eta_2^{\lambda}. \tag{5.12}$$

From this formula one sees that the streamlines have a point of contact of very high order in common with the equator of the ellipsoid. In the central part of the surface ($\eta_1 \to 1$, $\eta_3 \to 1$) the approximation formula

$$\frac{d\eta_2}{d\eta_1} = \frac{U^2}{U^1} = \frac{(1-\eta_1)\eta_2 + \nu\eta_3^2}{\eta_2^2 + \lambda\eta_3^2} \sim \frac{\nu}{\lambda} \tag{5.13}$$

can be used.

In this region the equation of the streamlines takes the form

$$\eta_2 + \frac{\nu}{\lambda}(1-\eta_1) = \psi = \cos\alpha. \tag{5.14}$$

This means that the streamlines can be approximated by straight lines in the considered region.

As numerical example an ellipsoid with axes $a = 3$, $b = 1$, and $c = 0{,}15$ will be chosen. The direction of the uncoming flow will be $(-1, -1, 0)$.

The values of the different parameters are then

$\lambda = 87.2666$	$l = 3.27829$
$\mu = 357.179$	$p = 1.02485$
$\nu = 115.723$	$q = 1.13770$
$\kappa = 17777.8$	

In the figures 1, 2 and 3, taken from ref. 4, the streamlines about the considered ellipsoid are given.

In relation with (5.14) the initial conditions are chosen as

$$\eta_1 = 1,\quad \eta_2 = \cos\alpha,\quad \eta_3 = \sin\alpha;$$
$$\alpha = 30^\circ,\ 60^\circ,\ 90^\circ,\ 120^\circ,\ 150^\circ.$$

From the relations

$$G(1-\eta_1) = \eta_2,\quad 1 + G^2 + F^2 = \frac{1}{(1-\eta_1)^2} = \frac{l^2}{\varphi^2}$$

and the orthogonality of the curvilinear coordinates

$$\frac{\partial\psi}{\partial\eta_2} = \sqrt{\rho g}\,U^1 \qquad \frac{\partial\psi}{\partial\eta_1} = -\sqrt{\rho g}\,U^2 \tag{5.15}$$

it can be easily derived

$$GG_\varphi = -\frac{G}{\varphi}\left(G + \frac{G + \nu F^2}{G^2 + \lambda F^2)}\right)$$

$$FF_\varphi = -\frac{F}{\varphi}\left(F + \frac{\lambda F - \nu G F}{G^2 + \lambda F^2}\right) = -$$

$$-\left(\frac{l^2}{\varphi^3} + GG_\varphi\right) \tag{5.16}$$

$$\sqrt{\rho}\,FF_\psi = -\sqrt{\rho}\,GG_\psi = \frac{GF^2\sqrt{g}}{c^2(G^2+\lambda F^2)\varphi}.$$

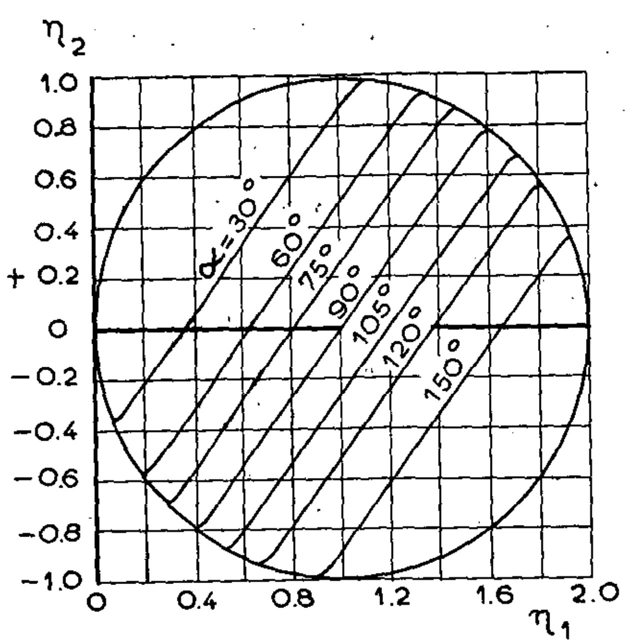

Fig. 1. The streamlines in the coordinates η_1 and η_2.

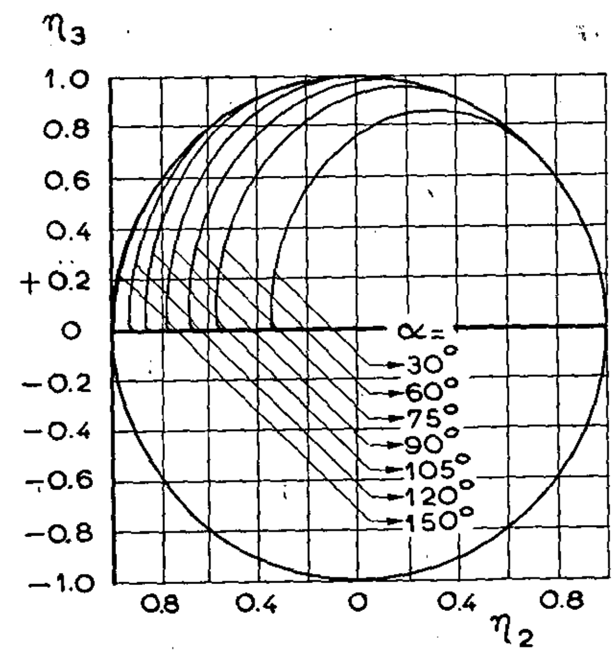

Fig. 2. The streamlines on the upper surface in the coordinates η_2 and η_3.

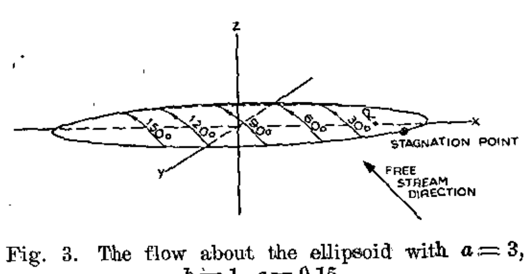

Fig. 3. The flow about the ellipsoid with $a = 3$, $b = 1$, $c = 0{,}15$.
The direction of the free flow bisects the angle between X and Y axes.

The derivatives T_φ, $\sqrt{\rho}\,T_\psi$, $T_{\varphi\varphi}$, $(\sqrt{\rho}\,T_\psi)_\varphi$ and $\sqrt{\varphi}\,(\sqrt{\rho}\,T_\psi)_\psi$, necessary for the boundary layer calculations, can be calculated by differentiating formula (5.9). Using the relations (5.16) one finds

$$T_\varphi = -\frac{2c^2}{l^2}\,\frac{T^2}{\varphi}\,\frac{(\lambda-\nu G)}{(G^2+\lambda F^2)^3}\left[(G^2+\nu F^2)^2+(G+\nu F^2)^2+(\lambda-\nu G)^2F^2\right]$$

$$\sqrt{\varphi}\,T_\psi = -\frac{2c\nu}{l}\,\frac{T^{3/2}}{\varphi}\,\frac{F(\lambda-\nu G)}{(G^2+\lambda F^2)^{3/2}}\left(G^2+F^2+\frac{1-\lambda}{\nu}\,G\right) \tag{5.17}$$

$$\frac{T_{\varphi\varphi}}{T_\varphi} = \frac{2T_\varphi}{T}-\frac{1}{\varphi}-\frac{\nu G_\varphi}{\lambda-\nu G}-\frac{6GG_\varphi+6\lambda FF_\varphi}{G^2+\lambda F^2}+\frac{\left[(G^2+\nu F^2)^2+(G+\nu F^2)^2+(\lambda-\nu G)^2F^2\right]_\varphi}{(G^2+\nu F^2)^2+(G+\nu F^2)^2+(\lambda-\nu G)^2F^2}$$

$$\frac{(\sqrt{\rho}T_\psi)_\varphi}{\sqrt{\rho}T_\psi} = \frac{3T_\varphi}{2T}-\frac{1}{\varphi}+\frac{F_\varphi}{F}-\frac{\nu G_\varphi}{\lambda-\nu G}-\frac{5GG_\varphi+5\lambda FF_\varphi}{G^2+\lambda F^2}+\frac{2GG_\varphi+2FF_\varphi+\frac{1-\lambda}{\nu}G_\varphi}{G^2+F^2+\frac{1-\lambda}{\nu}G}$$

$$\frac{\sqrt{\rho}\,(\sqrt{\rho}T_\psi)_\psi}{\sqrt{\rho}T_\psi} = \frac{3\sqrt{\rho}T_\psi}{2T}-\frac{\sqrt{\rho}GG_\psi}{F^2}-\frac{\nu\sqrt{\rho}G_\psi}{\lambda-\nu G}+\frac{5(\lambda-1)GG_\psi}{G^2+\lambda F^2}+\frac{\frac{1-\lambda}{\nu}\sqrt{\rho}\,G_\psi}{G^2+F^2+\frac{1-\lambda}{\nu}G}.$$

From the relation

$$\frac{\partial(\sqrt{\rho g}U^1)}{\partial\eta_1}+\frac{\partial(\sqrt{\rho g}U^2)}{\partial\eta_2}=0$$

it can be derived

$$\frac{\rho_\varphi}{2\rho} = \frac{\lambda(1+\lambda)-\nu(1+3\lambda)G+(\lambda+\lambda\mu+2\nu^2)G^2-\nu(1+\mu)G^3+(\lambda^2+\nu^2+\kappa)F^2-\nu(\lambda+\mu)GF^2}{\varphi(G^2+\lambda F^2)(\lambda-2\nu G+\mu G^2+\kappa F^2)} \tag{5.18}$$

At the equator holds $F=\tan\theta=0$ and $G=\tan\vartheta$. Therefore the basic functions at the equator read

$$T=\frac{l^2}{c^2}\,\frac{G^2}{\lambda-2\nu G+\mu G^2};\quad \frac{T_\varphi}{T}=-\frac{2(G^2+1)(\lambda-\nu G)}{\varphi G^2(\lambda-2\nu G+\mu G^2)}$$

$$\sqrt{\rho}T_\psi=0;\quad \frac{T_{\varphi\varphi}}{T_\varphi}=\frac{2T_\varphi}{T}+\frac{\lambda G^2-3\nu G+4\lambda}{\varphi G^2(\lambda-\nu G)}$$

$$\frac{(\sqrt{\rho}T_\psi)_\varphi}{\sqrt{\rho}T_\psi}=\frac{T_{\varphi\varphi}}{T_\varphi}-\frac{T_\varphi}{2T}+\frac{\left(\nu-\frac{\lambda-1}{\nu}\right)G^2-2\lambda G+\frac{\lambda-1}{\nu}\left(\frac{\lambda-1}{\nu}+1\right)}{\varphi G^2\left(G-\frac{\lambda-1}{\nu}\right)} \tag{5.19}$$

$$\sqrt{\varphi}(\sqrt{\rho}T_\psi)_\psi=-\frac{\sqrt{\rho}GG_\psi}{F^2}\sqrt{\rho}T_\psi=-\frac{2}{c^2}\,\frac{G^2+1}{G^2}\,\frac{(\lambda-\nu G)(1-\lambda+\nu G)}{\lambda-2\nu G+\mu G^2}$$

$$\frac{\rho_\varphi}{2\rho}=\frac{(1+G^2)(\lambda-\nu G)}{G^2\varphi}\left[\frac{1}{1+G^2}+\frac{1}{\lambda-2\nu G+\mu G^2}\right]=\frac{\lambda-\nu G}{G^2\varphi}-\frac{T_\varphi}{2T}.$$

From the differential equation (5.10) follows that the equation of the streamlines near the equator can be written as

$$\eta_3{}^2=e^{-2\psi}f(\eta_2)=1-\eta_2{}^2-(1-\eta_1)^2. \tag{5.20}$$

Differentiation of this expression gives the relation

$$-\eta_2\,d\eta_2+(1-\eta_1)d\eta_1=-\eta_3{}^2\,d\psi+\eta_3\left(\frac{d\eta_3}{d\eta_2}\right)_{\text{streamline}}d\eta_2. \tag{5.21}$$

From the formulae (5.15) and (5.8) one finds

$$\frac{\partial\psi}{\partial\eta_1}=-\frac{1-\eta_1}{\eta_3{}^2}=-\sqrt{\rho g}\,U^2=-\sqrt{\rho g}\,c^2l\,\frac{G+\nu F^2}{gF^2}. \tag{5.22}$$

Near the equator the function $\sqrt{\rho}$ can be written apart from a constant factor as

$$\sqrt{\rho}\approx\frac{\sqrt{gF}}{c^2l\eta_3}\,\frac{1}{G+\nu F^2}=-\frac{\sqrt{g}}{c^2\varphi(G+\nu F^2)}\approx O\left(\frac{1}{F}\right). \tag{5.23}$$

At the equator the function ρT_ψ remains finite.

Furthermore hold in connection with (5.16) in the neighbourhood of the equator the relations

$$\vartheta_\varphi \approx \frac{1}{l \sin \vartheta} + 0\,(F^2) \qquad \vartheta_\psi \approx 0\,(F^2)$$

$$\theta_\varphi \approx 0(F). \qquad \theta_\psi \approx 0\,(F) \tag{5.24}$$

6 The boundary layer flow about the ellipsoid.

A consideration of the momentum equations

$$\begin{aligned} f^1\sigma_\varphi + f^2\sigma_\psi + \qquad\qquad + g^2\Omega_\psi &= d \\ F^1\sigma_\varphi + F^2\sigma_\psi + G^1\Omega_\varphi + G^2\Omega_\psi &= D \end{aligned} \tag{6.1}$$

shows that the righthand sides of these equations can be written as

$$d = \sum_{i=0}^{3} \sum_j A_{ij}\,\Omega^j\sigma^i, \quad D = \sum_{i=0}^{2} \sum_j B_{ij}\,\Omega^j\sigma^i, \tag{6.2}$$

with the coefficients A_{ij} and B_{ij} as functions of the coordinates φ and ψ only.

Putting

$$P = T_\varphi,\ Q = \sqrt{\rho}\,T_\psi,\ R = \frac{\rho_\varphi}{2\,\rho},\ S = T_{\varphi\varphi},\ T = T,\ V = \sqrt{\rho}\,(\sqrt{\rho}\,T_\psi)_\psi$$

and

$$W = \frac{(\sqrt{\rho}\,T_\psi)_\varphi}{\sqrt{\rho}\,T_\psi} \tag{6.3}$$

the following relations can be given

$$\begin{aligned}
\Sigma A_{0j}\,\Omega^j &= \frac{2\,p_1}{T} \\
\Sigma A_{1j}\,\Omega^j &= (-\tfrac{1}{2}\,p_1 + \tfrac{1}{2}\,p_1\,i - p_4)\,\frac{P}{T} + 2\,p_4\,R \\
\Sigma A_{2j}\,\Omega^j &= -\left(\frac{p_2 - p_5}{2} + \frac{p_3 - p_6}{2}\,i\right)\frac{P^2}{T} - (p_5 + p_6\,i)\,(PR - S) - (p_{10}\Omega^2 + p_{13}\Omega^3 + 2\,p_{14}\Omega^4)\,V \\
\Sigma A_{3j}\,\Omega^j &= \left(\frac{p_7}{2} + \frac{p_8 + 2\,p_9}{2}\,i\right)\left(2\,PS - P^2R + \frac{P^3}{2\,T}\right) + \frac{p_7}{4}\,Q^2\left(\frac{P}{T} + 2\,R\right)\Omega^5 - \\
&\quad - \left(\frac{p_{11} + p_{12}i}{2}\,\Omega^2 + \frac{p_{14} + p_{14}i}{2}\,\Omega^4 + \frac{p_{15}}{2}\,\Omega^5\right)(Q^2W - Q^2R + VP) \\
\Sigma B_{0j}\,\Omega^j &= -(p_1 + p_4)\,\frac{2}{T} + p_1\frac{\Omega}{T} \\
\Sigma B_{1j}\,\Omega^j &= [p_5 - p_2 + (p_6 - p_3)i]\,\frac{P}{T} + 2\,[p_{10}\Omega^2 + (p_2 + p_{13})\Omega^3 + 2\,p_{14}\Omega^4]\,(2\,R - W) \\
\Sigma B_{2j}\,\Omega^j &= \left(\frac{p_7}{2} + \frac{p_8 + p_9}{2}\,i\right)\frac{P^2}{T} + 2\,p_7\left(\frac{Q^2}{4\,T} + V\right) + \\
&\quad + [(p_{11} + p_{12}\,i)\Omega^2 + p_{14}(1+i)\Omega^4 + p_{15}\Omega^5]\,(2\,RP - S - WP).
\end{aligned} \tag{6.4}$$

The coefficients in the left hand sides of the equations (6.1) read now

$$\begin{aligned}
f^1 &= p_4 - \frac{3}{2}\,(p_5 + p_6\,i)P\sigma - \frac{5}{4}\,[p_7 + (p_8 + 2\,p_9)i]P^2\sigma^2 \\
F^1 &= 3\,p_{10}\Omega^2 + 3(p_{13} + p_2)\Omega^3 + 6\,p_{14}\Omega^4 + \frac{5}{2}[p_{11} + p_{12}i + (1+i)p_{14}\Omega^2 + p_{15}\Omega^3]\,P\Omega^2\sigma \\
G^1 &= [4\,p_{10} + 6\,(p_{13} + p_2)\Omega + 16\,p_{14}\Omega^2]\,\Omega\sigma + [2\,(p_{11} + p_{12}i) + 4\,(1+i)p_{14}\Omega^2 + 5\,p_{15}\Omega^3]\,P\Omega \\
f^2 &= \frac{1}{2}\,Q\sigma\,[F^1 - 3\,p_2\Omega^3]\,\sqrt{\rho} \\
F^2 &= -\frac{5}{2}\,p_7Q\sigma\Omega^5\sqrt{\rho} \\
g^2 &= \frac{1}{2}\,Q\sigma\,[G^1 - 6\,p_2\Omega^2\sigma]\,\sqrt{\rho} \\
G^2 &= -5\,p_7Q\sigma^2\Omega^4\sqrt{\rho}\,.
\end{aligned} \tag{6.5}$$

In the expressions (6.4) and (6.5) $i=0$ must be substituted for accelerated flow and $i=1$ for retarded flow.

Supposing the functions σ and Ω are regular in the variables ϑ and θ, it can be derived from the relations (5.24) that the derivatives σ_ψ and Ω_ψ vanish at the equator.

Writing the momentum equations in the coordinates ϑ and θ, these equations read at the equator

$$\begin{aligned} f^1\sigma_\vartheta \frac{l}{c^2}\sin\vartheta &= d\frac{l^2}{c^2}\sin^2\vartheta = d_1 = \sum_{i=0}^{3}\sum_{j} \overline{A}_{ij}\Omega^j\sigma^i \\ (F^1\sigma_\vartheta + G^1\Omega_\vartheta)\frac{l}{c^2}\sin\vartheta &= D\frac{l^2}{c^2}\sin^2\vartheta = D_1 = \sum_{i=0}^{2}\sum_{j} \overline{B}_{ij}\Omega^j\sigma^i . \end{aligned} \tag{6.6}$$

From the requirement that σ_ϑ and Ω_ϑ must be finite in the stagnation point follows

$$d_1 = D_1 = 0. \tag{6.7}$$

Similar as in POHLHAUSEN's method for two-dimensional boundary layers this condition of boundedness gives the initial values for the parameters σ and Ω. In this manner one gets two algebraic equations which can be solved numerically. As starting value σ_0 will be chosen the positive root of the equation $d_1 = D_1 = 0$ that increases along the equator.

The magnitude of σ_0 is in good agreement with the value found for the boundary layer about an elliptic cylinder with the same pressure distribution (Appendix 1).

Numerical calculations at the equator show that the terms on the left hand side of the equations (6.6) are very small. Thus an approximation can be made by neglecting these terms and then solving the algebraic equations in every point. Substituting the derivatives σ_ϑ and Ω_ϑ found by numerical differentiation of the first approximate values in the left side of (6.6) and then solving the new algebraic equations gives a new set of values σ and Ω. These new values of σ and Ω can be considered as a second approximation. This process can now be repeated thus performing an iteration procedure. After two or three steps the values of σ and Ω are accurate enough. For the calculations the reader is referred to table I.

For the boundary layer calculations on the upper part of the ellipsoid the equations (4.17) will be used. At first an estimation will be made of the magnitude of the terms on the left of these equations. These terms can be expressed in powers of the quantity c. For a thin ellipsoid with a small value of c these considerations lead to a less complicated calculation method. On the upper part of the ellipsoid the following approximate formulae hold

$$T \sim 0(1)\,; \quad T_\varphi \sim \sqrt{\rho}\,T_\psi \sim c^2.$$

Writing under each term of the equations the order of magnitude one finds

$$\begin{array}{cccccc} f^1\sigma_\varphi & + \; f^2\rho_\psi & + & & + \; g^2\Omega_\psi & = d \\ \sigma & \sigma^2c^2\sqrt{\rho} & & & \sigma^2c^2\sqrt{\rho} & \\ F^1\sigma_\varphi & + \; F^2\sigma_\psi & + \; G^1\Omega_\varphi & & + \; G^2\Omega_\psi & = D \\ \sigma & \sigma^2c^2\sqrt{\rho} & \sigma & & \sigma^2c^2\sqrt{\rho}. & \end{array} \tag{6.8}$$

As on the top of the ellipsoid the function $\sqrt{\rho}$ is of order 1 (Appendix 2), for a first approximation the terms with σ_ψ and Ω_ψ can be neglected.

Near the equator $\sqrt{\rho}$ can reach large values and consequently the terms with σ_ψ and Ω_ψ cannot be neglected in this region.

Using the relations

$$\varphi = -l(1-\eta_1)\,; \quad \left(\frac{\partial\psi}{\partial\eta_2}\right)_{\eta_1=\text{constant}} = \sqrt{\rho g}\,U^1$$

and

$$\left(\frac{\partial\sigma}{\partial\eta_2}\right)_{\eta_1=\text{constant}} = \left(\frac{\partial\sigma}{\partial\varphi}\right)_\psi \left(\frac{\partial\varphi}{\partial\eta_2}\right)_{\eta_1} + \left(\frac{\partial\sigma}{\partial\psi}\right)_\varphi \left(\frac{\partial\psi}{\partial\eta_2}\right)_{\eta_1} = \sqrt{\rho g}\,U^1 \left(\frac{\partial\sigma}{\partial\psi}\right)_{\varphi=\text{constant}}$$

the following expressions can be derived

$$\left(\frac{\partial\sigma}{\partial\varphi}\right)_{\psi=\text{constant}} = \frac{1}{l}\left(\frac{\partial\sigma}{\partial\eta_1}\right)_{\text{streamline}} \tag{6.9}$$

$$\sqrt{\rho}\left(\frac{\partial\sigma}{\partial\psi}\right)_{\varphi=\text{constant}} = \frac{1}{\sqrt{gU^1}}\left(\frac{\partial\sigma}{\partial\eta_2}\right)_{\eta_1=\text{constant}} = \frac{F\sqrt{\lambda - 2\nu G + \mu G^2 + \kappa F^2}}{l(G^2+\lambda F^2)}\left(\frac{\partial\sigma}{\partial\eta_2}\right)_{\eta_1=\text{constant}} \tag{6.10}$$

Now the behaviour of the unknown functions σ and Ω near the equator will be examined. In the neighbourhood of a streamline the values of σ and Ω can be considered approximately as constants at the circles $(1-\eta_1)^2 + \eta_2^2 = \text{constant}$.

From the relation

$$(1-\eta_1)^2 + \eta_2^2 = \text{constant}$$

follows

$$(1-\eta_1)\Delta\eta_1 = \eta_2\,\overline{\Delta\eta_2}\,.$$

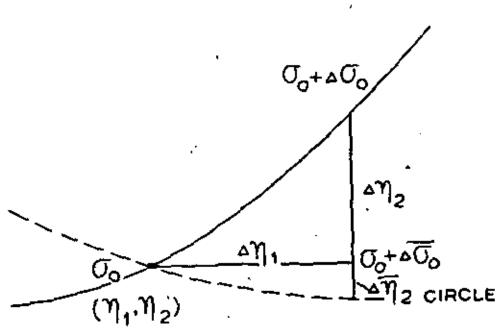

Fig. 4.

Further figure 4 shows

$$\left(\frac{\partial\sigma}{\partial\eta_2}\right)_{\eta_1=\text{constant}} = \lim_{\Delta\to 0}\frac{\Delta\sigma_0-\overline{\Delta\sigma_0}}{\Delta\eta_2} =$$

$$= \lim_{\Delta\to 0}\frac{\Delta\sigma_0}{\Delta\eta_2-\overline{\Delta\eta_2}} = \left(\frac{\partial\sigma}{\partial\eta_1}\right)_\psi \frac{1}{\left(\frac{d\eta_2}{d\eta_1}\right)_\psi - \left(\frac{d\eta_2}{d\eta_1}\right)_{\text{circle}}}$$

$$\left(\frac{d\eta_2}{d\eta_1}\right)_{\text{streamline}} - \left(\frac{d\eta_2}{d\eta_1}\right)_{\text{circle}} = \frac{G+\nu F}{G^2+\lambda F^2} - \frac{1}{G} = -\frac{F^2(\lambda-\nu G)}{G(G^2+\lambda F^2)}.$$

With these formulae the relation (6.10) can be transformed into

$$\sqrt{\rho}\left(\frac{\partial\sigma}{\partial\psi}\right)_{\varphi=\text{constant}} = -\frac{G\sqrt{\lambda-2\nu G+\mu G^2+\kappa F^2}}{lF(\lambda-\nu G)}\left(\frac{\partial\sigma}{\partial\eta_1}\right)_\psi = \left(\frac{Z}{l}\right)\left(\frac{\partial\sigma}{\partial\eta_1}\right)_{\text{streamline}}.$$

In the neighbourhood of the equator the differential equations (6.8) can be approximated by

$$\begin{aligned}&\left(f^1+Z\frac{f^2}{\sqrt{\rho}}\right)(\sigma_{\eta_1})_{\text{streamline}} + Z\frac{g^2}{\sqrt{\rho}}(\Omega_{\eta_1})_{\text{streamline}} = ld\\ &\left(F^1+Z\frac{F^2}{\sqrt{\rho}}\right)(\sigma_{\eta_1})_{\text{streamline}} + \left(G^1+Z\frac{G^2}{\sqrt{\rho}}\right)(\Omega_{\eta_1})_{\text{streamline}} = lD.\end{aligned} \tag{6.11}$$

The numerical calculations show that the estimates used in the equations (6.8) are relevant.

The integration of the equations (6.11) along the streamlines will now be performed in the following way.

Near the equator the same method as for the equator itself be used.

Neglecting the terms on the left of the equations (6.11) and solving the resulting algebraic equations a first approximation for σ and Ω can be found. Then the derivatives σ_{η_1} and Ω_{η_1} are determined by differentiation with respect to η_1 of the values of σ and Ω. Substituting the values of these derivatives in the left hand sides of (6.11) one finds a new system of algebraic equations for the unknown functions σ and Ω. The solution of these algebraic equations gives now a second approximation for σ and Ω. Repeating this process two or three times one finds the values of σ and Ω with sufficient accuracy.

Now it seems that the values of σ and Ω along a great part of the streamlines are equal to the values of σ and Ω in corresponding points at the equator, within the required accuracy.

Therefore the calculation of σ and Ω at the streamline does not need to be started in the stagnation point.

With the prescribed method it is possible to find the initial values necessary to start the numerical integration.

It appears that near the equator the inequality $\sigma \ll \Omega$ holds. This implies that convergence of the iteration process may be slow. To guard against such difficulties a special procedure will be applied. Consider the values of the functions σ and Ω and their derivatives with respect to η in three successive points η_{-2}, η_{-1} and η_0. The values σ_0, Ω_0, σ_{η_0} and Ω_{η_0} must then satisfy LAGRANGE's integration formula

$$\begin{aligned}\sigma_0 &= \sigma_{-1} + q_1\sigma_{\eta-2} + r_1\sigma_{\eta-1} + s_1\sigma_{\eta_0}\\ \Omega_0 &= \Omega_{-1} + q_1\Omega_{\eta-2} + r_1\Omega_{\eta-1} + s_1\Omega_{\eta_0}\end{aligned} \tag{6.12}$$

where q_1, r_1 and s_1 are coefficients which can be determined by integrating LAGRANGE's interpolation formula with respect to η from η_{-1} to η_0

$$\sigma_\eta = \sigma_{\eta-2}\frac{(\eta-\eta_{-1})(\eta-\eta_0)}{(\eta_{-2}-\eta_{-1})(\eta_{-2}-\eta_0)} + \sigma_{\eta_{-1}}\frac{(\eta-\eta_{-2})(\eta-\eta_0)}{(\eta_{-1}-\eta_{-2})(\eta_{-1}-\eta_0)} + \sigma_{\eta_0}\frac{(\eta-\eta_{-2})(\eta-\eta_{-1})}{(\eta_0-\eta_{-2})(\eta_0-\eta_{-1})}$$

$$\begin{aligned}q_1 &= \frac{(\eta_{-1}-\eta_0)^3}{6(\eta_{-2}-\eta_{-1})(\eta_{-2}-\eta_0)};\\ r_1 &= -\frac{(\eta_{-1}-\eta_0)(3\eta_{-2}-2\eta_{-1}-\eta_0)}{6(\eta_{-2}-\eta_{-1})};\\ s_1 &= -\frac{(\eta_{-1}-\eta_0)(3\eta_{-2}-\eta_{-1}-2\eta_0)}{6(\eta_{-2}-\eta_0)}.\end{aligned} \tag{6.13}$$

With the aid of the values of σ, Ω and their derivatives in the points η_{-2} and η_{-1} an estimate of σ and Ω in the point η_0 can be made. From the approximate differential equations (6.11) σ_η and Ω_η can then be calculated. The values obtained for σ, Ω, σ_η and Ω_η will, in general, not satisfy the integration formula of LAGRANGE. To satisfy LAGRANGE's formula it will be necessary to change σ and Ω by small amounts $\Delta\sigma$ and $\Delta\Omega$. Consequently σ_η and Ω_η will change too. Denoting these alterations by $\Delta\sigma_\eta$ and $\Delta\Omega_\eta$ the approximate relations can be given

$$\begin{aligned}\sigma_{\eta_0}-\sigma_\eta &= \Delta\sigma_\eta = a\Delta\sigma + b\Delta\Omega\\ \Omega_{\eta_0}-\Omega_\eta &= \Delta\Omega_\eta = c\Delta\sigma + d\Delta\Omega.\end{aligned} \tag{6.14}$$

Putting $\Delta\Omega = 0$ the values of $\bar{\sigma}_\eta = \sigma_\eta + \overline{\Delta\sigma}_\eta$ and $\bar{\Omega}_\eta = \Omega_\eta + \overline{\Delta\Omega}_\eta$ can be determined from the differential equations (6.11); the constants a and b follow immediately from (6.14)

$$a = \frac{\overline{\Delta\sigma}_\eta}{\Delta\sigma}, \quad c = \frac{\overline{\Delta\Omega}_\eta}{\Delta\sigma}.$$

Now putting $\Delta\sigma = 0$ one finds in the same manner $\tilde{\sigma}_{\eta} = \sigma_{\eta} + \Delta\tilde{\sigma}_{\eta}$, $\tilde{\Omega}_{\eta} = \Omega_{\eta} + \Delta\tilde{\Omega}_{\eta}$ and from (6.14)

$$b = \frac{\Delta\tilde{\sigma}_{\eta}}{\Delta\sigma}, \quad d = \frac{\Delta\tilde{\Omega}_{\eta}}{\Delta\Omega}.$$

Substituting the calculated values of a, b, c and d in (6.14), these relations read then

$$\sigma_{\eta_0} = \sigma_{\eta} + \Delta\sigma_{\eta} = \sigma_{\eta} + a\Delta\sigma + b\Delta\Omega$$
$$\Omega_{\eta_0} = \Omega_{\eta} + \Delta\Omega_{\eta} = \Omega_{\eta} + c\Delta\sigma + d\Delta\Omega$$

belonging to

$$\sigma_0 = \sigma + \Delta\sigma,$$
$$\Omega_0 = \Omega + \Delta\Omega.$$

The quantities $\Delta\sigma$ and $\Delta\Omega$ are calculated from the relations (6.12). This integration process was developed by Mr. T. BURGERHOUT of the computational department of the National Aeronautical Research Institute.

For the streamline $\alpha = 90°$ the basic functions P, Q, R, S, T, V, W, Z and the solutions $\sqrt{\sigma}$ and Ω as functions of the coordinate η are given in table 2.

Table 3 contains $\sqrt{\sigma}$ and Ω for the streamlines $\alpha = 30°$, $60°$, $120°$ and $150°$.

Near the point where the accelerated flow passes into the retarded flow the numerical integration gives some difficulties. This point is characterized by the formula

$$T_{\varphi} = 0 \quad \text{or} \quad G = \frac{\eta_2}{1-\eta_1} = \frac{\lambda}{\nu}.$$

In this region the value of

$$M = \tfrac{1}{2}\sqrt{\rho}\, T_{\psi}\, \sigma = \tfrac{1}{2} Q\sigma$$

approaches also zero and thus the component of the velocity vector perpendicular to the streamline vanishes there. The second momentum equation loses there its importance with regard to the first momentum equation. As a consequence of this it appears that the function Ω varies very strongly, whereas the function σ varies nearly linearly in the considered region. From physical considerations too one can expect that the function σ will vary slowly there. Beyond the point

$$G = \frac{\eta_2}{1-\eta_1} = \frac{\lambda}{\nu}$$

the values of σ and σ_{η} can be determined by extrapolation; Ω and Ω_{η} can then be calculated in the ordinary manner.

The integration can be continued till the transition line has been reached. This transition line can be considered as the envelope of the directions, determined by the velocity vectors approaching the wall.

This direction can be written in the form

$$\lim_{\zeta \to 0} \frac{u_2}{u_1}.$$

The considered envelope can be approximated by the curve passing through the points where the component of the shear stress in the streamline direction vanishes. Thus the curve can be characterized by the formula

$$\Lambda = \tfrac{1}{2}\sigma T_{\varphi} = \tfrac{1}{2}\sigma P = -1.$$

In the figures 5 and 6 the functions $\sqrt{\sigma}$ and Ω are drawn for the equator and some streamlines.

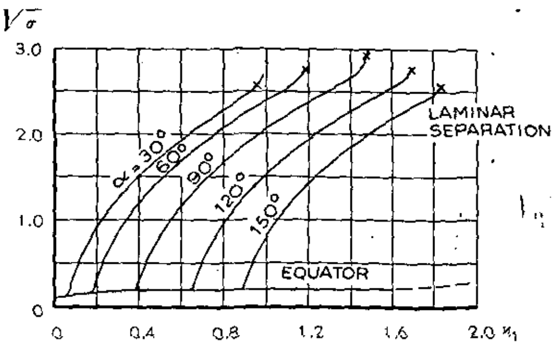

Fig. 5. Variation of $\sqrt{\sigma}$ with η_1, for the equator and the streamlines.

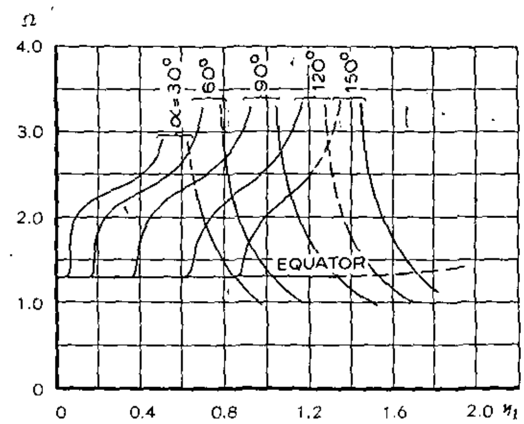

Fig. 6. Ω against η_1, for the equator and the streamlines on the surface.

7 The velocity profiles in the boundary layer.

For a good description of the velocity profiles it is necessary to consider the contravariant components of the velocity vector. These contravariant components can be written as

$$u^1 = \gamma^{11} u_1 = T u_1$$
$$u^2 = \gamma^{22} u_2 = \rho T u_2 .$$

Normalizing these components with the component U^1 of the free stream they read

$$\bar{u}^1 = \frac{u^1}{U^1} = \frac{T u_1}{T} = u_1$$

$$\bar{u}^2 = \frac{u^2}{U^1} = \frac{\rho T u_2}{T} = \rho u_2 .$$

From the line element

$$ds^2 = \frac{1}{T}\left(d\varphi^2 + \frac{1}{\rho}\, d\psi^2\right)$$

one sees immediately that for a good comparison the components $\overline{u}^1$ and $\dfrac{\overline{u}^2}{\sqrt{\rho}}$ must be considered.

$$\overline{u}^1 = u_1 = f(\eta) - \Lambda\, g(\eta) - N\, h\,(\eta)$$

$$\frac{\overline{u}^2}{\sqrt{\rho}} = u_2 \sqrt{\rho} = -\,\Omega^2 M\, g\left(\frac{\eta}{\Omega}\right).$$

In the figures 7 and 8 the velocity profiles in the two directions are drawn for several points of the streamline $\alpha = 90°$.

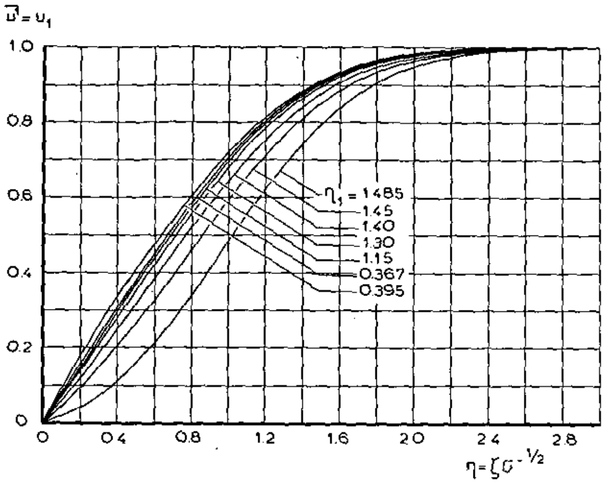

Fig. 7. The velocity profiles in the boundary layer in streamline direction for different points of the streamline $\alpha = 90°$.

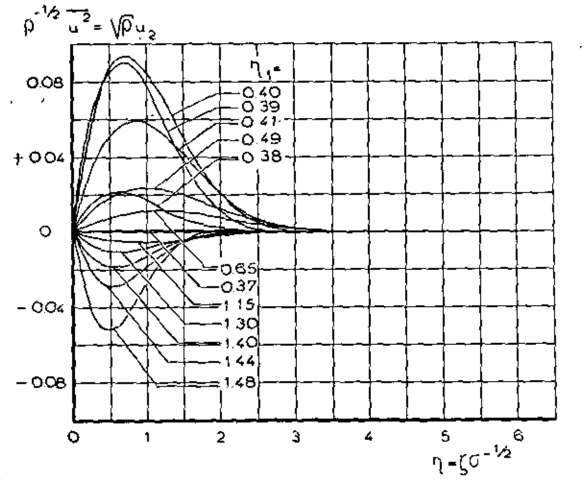

Fig. 8. The velocity profiles in the boundary layer perpendicular to the streamline direction for different points of the streamline $\alpha = 90°$.

The direction of the velocity vector at the wall can be expressed by the formula

$$\lim_{\eta \to 0} \frac{\overline{u}^2/\sqrt{\rho}}{\overline{u}^1} =$$

$$= \frac{-\,\Omega M g'(0)}{f'(0) - \Lambda g'(0) - N h'(0)} = \frac{\Omega M}{2 + \Lambda + N}.$$

Figure 9 shows this direction as a function of η_1 for the streamlines $\alpha = 30°$, $60°$, $90°$, $120°$ and $150°$.

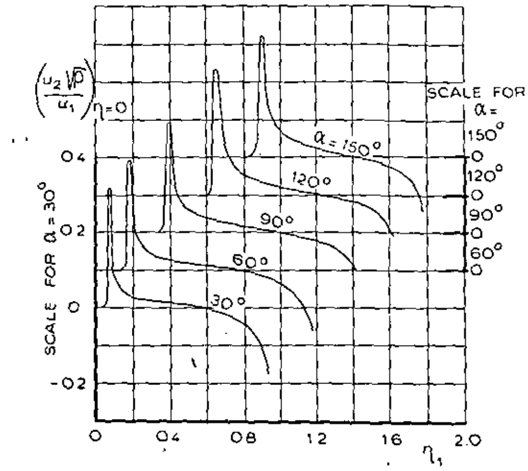

Fig. 9. The proportion $\dfrac{u_2\sqrt{\rho}}{u_1}$ on the wall for the streamlines on the surface.

The calculations have been performed in the computational department of the National Aeronautical Research Institute under the direction of Mssr. Burgerhout and Wouters. A part of the numerical integrations has been performed on the electronic machine ARRA of the Mathematical Centre.

8 References.

1 Timman, R. A. Calculation Method for Three-Dimensional Laminar Boundary-Layers. Report F. 66 of the National Aeronautical Research Institute. 1951.

2 Lamb, H. Hydrodynamics 5th Ed. 1935 Cambridge University Press.

3 Munk, M. Durand: Aerodynamic Theory I. 1934, Springer, Berlin.

4 Timman, R. The Potential Flow about a Yawed Ellipsoid at Zero Incidence. Report F. 74 of the National Aeronautical Research Institute. 1950.

5 Michal, A. D. Matrix and Tensor Calculus. Galcit Aeron. Series 1947. John Wiley and Sons, New York.

6 Timman, R. A One-Parameter Method for the Calculation of Laminar Boundary Layers. Report F. 35 of the National Aeronautical Research Institute. 1949.

APPENDIX 1.

The value of the parameter σ in the stagnation-point for an infinite elliptic cylinder.

A comparison will be made of the value of the parameter σ in the stagnation point for an ellipsoid with axes $a = 3$, $b = 1$, $c = 0{,}15$ and uncoming flow direction $(-1, -1, 0)$ and for an infinite elliptic cylinder with axes $a_1 = \infty$, $b_1 = \sqrt{2}$, $c_1 = 0{,}15$ and uncoming flow direction$(0, -1, 0)$.

The calculation of the boundary layer about the infinite cylinder is a two-dimensional problem.

At first the transformation formulae for the coordinate directed along the normal on the surface must be considered.

For the two-dimensional problem this formula reads

$$\frac{\eta}{y} = \alpha = \sqrt{\frac{1}{\nu_1 \lambda} \frac{dU}{ds}}$$

and for the three-dimensional case

$$\frac{\eta}{y} = \sigma^{-1/2} \nu_1^{-1/2}.$$

The two-dimensional flow satisfies thus the relation

$$\sigma^{-1} = \nu_2 \alpha^2 = \frac{1}{\lambda} \frac{dU}{ds}. \qquad \text{(A.1)}$$

The quantity λ is a dimensionless parameter, characterizing the family of velocity profiles for the two-dimensional laminar boundary layer.

In the stagnation point λ takes the value $\lambda = 0{,}830$ (ref. 6). To calculate the potential flow about the infinite elliptic cylinder it is usual to map the cross section of the cylinder on a circle with radius r.

Writing the equation of the circle as

$$\zeta = r\, e^{i\varphi} \qquad \text{(A.2)}$$

the conformal transformation can be expressed by the formula

$$z = \zeta + \frac{\lambda_1 r^2}{\zeta} \qquad \text{(A.3)}$$

or

$$x = r(1 + \lambda_1) \cos\varphi = b_1 \cos\varphi;$$
$$y = r(1 - \lambda_1) \sin\varphi = c_1 \sin\varphi. \qquad \text{(A.4)}$$

As the complex potential is invariant for conformal mapping the following relations between the velocities in corresponding points can be given.

$$\left| v_c \right| = \left| \frac{dF}{d\zeta} \right| = \left| \frac{d\Phi}{dz} \right| \left| \frac{dz}{d\zeta} \right| = \left| v_e \right| \left| \frac{dz}{d\zeta} \right| \qquad \text{(A.5)}$$

where

$$\left| \frac{dz}{d\zeta} \right| = \left| 1 - \frac{\lambda_1 r^2}{\zeta^2} \right| = \sqrt{(1 + \lambda_1)^2 - 4\lambda_1 \cos^2\varphi.} \qquad \text{(A.6)}$$

In this formula $\Phi(z)$ denotes the complex potential of the flow about the ellips and $F(\zeta)$ the complex potential of the flow about the circle. Supposing the velocity V_0 of the oncoming flow is directed along the x-axis the velocity distribution about the circle is given by

$$\left| \frac{v_c}{v_0} \right| = 2 \left| \sin\varphi \right|. \qquad \text{(A.7)}$$

From the relation (A.5) the velocity distribution about the ellips follows as

$$U = \left| \frac{v_e}{v_0} \right| = \frac{|2 \sin\varphi|}{\sqrt{(1 + \lambda_1) - 4\lambda_1 \cos^2\varphi}}. \qquad \text{(A.8)}$$

The relations (A.8) and (A.4) give for the stagnation point $\varphi = 0$ the expression

$$\frac{dU}{ds} = \frac{dU}{d\varphi} \frac{r d\varphi}{ds} \frac{1}{r} = \frac{1}{r} \left| \frac{d\zeta}{dz} \right| \frac{dU}{d\varphi} =$$
$$= \frac{1}{r} \frac{2}{(1 - \lambda_1)^2} = \frac{b_1 + c_1}{c_1^2}. \qquad \text{(A.9)}$$

In the considered two-dimensional case one finds easily from (A.1) and (A.9) for the value of σ in the stagnation point $\sigma = 0{,}012$.

In the three-dimensional case the value $\sigma = 0{,}0122$ has been found. It appears that the two values of σ agree very well.

APPENDIX 2.

The calculation of the function $\sqrt{\rho}$.

In section 5 it has been shown that on the upper part of the ellipsoid the streamlines can be approximated by the straight lines

$$\psi = \eta_2 + \frac{\nu}{\lambda}(1 - \eta_1) = \frac{l}{ab(p^2 + q^2)}(qx - py). \qquad \text{(A.1)}$$

The velocity potential has been written as

$$\varphi = -l(1 - \eta_1) = -px - qy. \qquad \text{(A.2)}$$

Replacing the stream function ψ by $\Psi = \frac{ab(p^2 + q^2)}{l}\psi$ the formula (A.1) is transformed into

$$\Psi = \frac{ab(p^2 + q^2)}{l}\,\psi = qx - py. \qquad \text{(A.3)}$$

In this approximation the covariant components of the metric tensor (see formula (5.7)) can be written as

$$g_{11} = c^2\mu,\ g_{12} = g_{21} = -c^2\nu,\ g_{22} = c^2\lambda$$
$$g = g_{11}g_{22} - g_{12}{}^2 = c^4(\lambda\mu - \nu) = c^4\kappa = a^2b^2. \qquad \text{(A.4)}$$

The contravariant components of the velocity vector are then

$$U^1 = g^{11} U_1 + g^{12} U_2 = \frac{g_{22}}{g} U_1 = \frac{c^2 l\lambda}{a^2b^2}$$
$$\qquad \text{(A.5)}$$
$$U^2 = g^{21} U_1 + g^{22} U_2 = -\frac{g_{12}}{g} U_1 = \frac{c^2 l\nu}{a^2b^2}$$

where use has been made of the formulae

$$U_1 = \frac{\partial \varphi}{\partial \eta_1} = l, \quad U_2 = \frac{\partial \varphi}{\partial \eta_2} = 0.$$

Using the orthogonality of the curvilinear coordinates one can write

$$\frac{\partial \Psi}{\partial \eta_2} = \frac{ab(p^2 + q^2)}{l} = \sqrt{\rho g}\, U^1 = \sqrt{\rho}\, \frac{c^2 l \lambda}{ab}. \quad \text{(A.6)}$$

From this relation (A.6) follows

$$\sqrt{\rho} = \frac{a^2 b^2 (p^2 + q^2)}{c^2 l^2 \lambda} = 1. \quad \text{(A.7)}$$

It appears that on the upper part of the ellipsoid, where the streamlines can be approximated by straight lines, the function $\sqrt{\rho}$ has the value 1. Starting from this value the function $\sqrt{\rho}$ can be calculated by numerical integration of the differential equation (5.18) along the streamlines.

TABLE 1.

The basicfunctions P, R, S, T, V, W and the solutions $\sqrt{\sigma}$ *and* Ω
as functions of the coordinate ϑ for the equator.

ϑ	P	R	S	T	V	W	$\sqrt{\sigma}$	Λ
0	3.3392	$-26.9246\,\vartheta^{-2}$	$4.05221\,\vartheta^{-1}$	$5.47349\,\vartheta^{-2}$	$7668.14\,\vartheta^{-2}$	$0.227392\,\vartheta^{-2}$	0.110	1.3158
− 6	2.2064	− 2784.5	− 24.930	0.045672	689060	2728.0	0.119	1.3151
− 12	1.4958	− 777.41	− 7.7511	0.14142	167130	762.97	0.128	1.3146
− 18	1.0556	− 381.44	− 3.2522	0.25192	71925	374.86	0.137	1.3141
− 24	0.77802	− 234.84	− 1.5801	0.36263	39352	231.09	0.146	1.3137
− 30	0.59818	− 163.45	− 0.84570	0.46837	24670	161.02	0.154	1.3133
− 36	0.47840	− 122.80	− 0.48501	0.56794	16914	121.11	0.161	1.3130
− 48	0.34072	− 79.977	− 0.18221	0.75067	9504.4	79.026	0.174	1.3126
− 60	0.27572	− 58.654	− 0.070744	0.91878	6268.0	58.058	0.183	1.3124
− 72	0.25028	− 46.323	− 0.016170	1.0817	4609.0	45.917	0.190	1.3124
− 84	0.25294	− 38.406	+ 0.023198	1.2489	3662.4	38.112	0.194	1.3124
− 96	0.28326	− 32.779	+ 0.067604	1.4309	3059.6	32.537	0.197	1.3125
− 102	0.31098	− 30.405	+ 0.097116	1.5313	2818.6	30.157	0.197	1.3128
− 108	0.34902	− 28.125	+ 0.13404	1.6404	2585.3	27.844	0.198	1.3130
− 114	0.39878	− 25.778	+ 0.17744	1.7598	2331.9	25.400	0.199	1.3141
− 120	0.45924	− 23.133	+ 0.21517	1.8906	2020.8	22.542	0.203	1.3165
− 126	0.52096	− 19.854	+ 0.19461	2.0318	1603.3	18.761	0.211	1.3204
− 132	0.54726	− 15.372	− 0.073592	2.1758	1036.3	12.931	0.231	1.3278
− 134	0.53238	− 13.455	− 0.30145	2.2211	813.95	10.055	0.244	1.3367

TABLE 2.

The basicfunctions P, Q, R, S, T, V, W, Z and the solutions $\sqrt{\sigma}$ and Ω as functions of the coordinate η_1 for the streamline $\alpha = 90°$.

η_1	P	Q	R	S	T	V	W	Z	$\sqrt{\sigma}$	Ω
0.3668	+ 0.32531	+ 0.67595	− 73.956	+ 0.41194	0.78956	+ 8550.9	+ 73.069	+ 115.95	0.17618	1.31275
0.3689	+ 0.33014	+ 1.0660	− 73.619	+ 1.2805	0.79190	+ 8494.7	+ 72.749	+ 115.75	0.17631	1.31276
0.3711	+ 0.34367	+ 1.6808	− 73.268	+ 3.3971	0.79430	+ 8434.1	+ 72.375	+ 115.53	0.17645	1.31280
0.3731	+ 0.37918	+ 2.6522	− 72.920	+ 8.6271	0.79662	+ 8367.2	+ 71.928	+ 115.30	0.17659	1.31291
0.3751	+ 0.46889	+ 4.1789	− 72.512	+ 21.544	0.79934	+ 8269.1	+ 71.297	+ 114.95	0.17674	1.31322
0.3772	+ 0.69212	+ 6.5633	− 71.917	+ 53.026	0.80312	+ 8090.8	+ 70.169	+ 114.33	0.17692	1.31395
0.3793	+ 1.2407	+ 10.242	− 70.915	+ 127.59	0.80923	+ 7729.5	+ 67.761	+ 113.03	0.17715	1.31580
0.3815	+ 2.5509	+ 15.718	− 68.902	+ 292.26	0.82124	+ 6946.7	+ 62.461	+ 110.13	0.17756	1.32048
0.3838	+ 5.4866	+ 23.182	− 64.600	+ 594.25	0.84755	+ 5329.0	+ 50.891	+ 103.55	0.17842	1.33185
0.3861	+ 11.085	+ 31.150	− 55.867	+ 902.27	0.90665	+ 2601.9	+ 28.472	+ 89.756	0.18033	1.35707
0.3888	+ 18.328	+ 34.499	− 40.835	+ 646.36	1.0346	− 260.35	− 4.3704	+ 65.754	0.18560	1.41371
0.3905	+ 20.636	+ 32.259	− 31.581	+ 221.14	1.1386	− 1006.3	− 20.102	+ 50.901	0.19146	1.46037
0.3926	+ 20.587	+ 27.174	− 22.400	− 194.05	1.2737	− 1124.6	− 31.352	+ 36.135	0.20153	1.51745
0.3953	+ 17.882	+ 20.346	− 14.435	− 397.50	1.4362	− 843.27	− 36.361	+ 23.294	0.21796	1.58591
0.3990	+ 13.384	+ 13.464	− 8.4365	− 362.49	1.6138	− 479.90	− 35.326	+ 13.614	0.24433	1.66004
0.4012	+ 10.954	+ 10.458	− 6.2214	− 296.45	1.7032	− 332.09	− 33.132	+ 10.034	0.26099	1.69585
0.4042	+ 8.6452	+ 7.8840	− 4.4811	− 223.69	1.7903	− 218.40	− 30.235	+ 7.2240	0.28410	1.73693
0.4074	+ 6.6144	+ 5.7991	− 3.1718	− 158.11	1.8716	− 137.92	− 26.978	+ 5.1071	0.30853	1.77464
0.4114	+ 4.9011	+ 4.1548	− 2.1999	− 105.11	1.9469	− 83.544	− 23.570	+ 3.5365	0.33861	1.81214
0.4165	+ 3.5325	+ 2.9103	− 1.5005	− 66.393	2.0149	− 48.892	− 20.234	+ 2.4074	0.37551	1.85193
0.4227	+ 2.4822	+ 1.9968	− 1.0080	− 40.088	2.0749	− 27.739	− 17.109	+ 1.6125	0.41809	1.89247
0.4304	+ 1.7067	+ 1.3465	− 0.66879	− 23.303	2.1269	− 15.342	− 14.284	+ 1.0661	0.46775	1.93400
0.4403	+ 1.1468	+ 0.89025	− 0.43708	− 13.040	2.1717	− 8.2479	− 11.777	+ 0.6935	0.52698	1.97703
0.4453	+ 0.93340	+ 0.71916	− 0.35172	− 9.6383	2.1914	− 5.9896	− 10.651	+ 0.5559	0.55522	1.99474
0.4595	+ 0.60956	+ 0.46416	− 0.22586	− 5.1499	2.2258	− 3.1142	− 8.6527	+ 0.3546	0.63035	2.03873
0.4684	+ 0.48865	+ 0.37044	− 0.18007	− 3.7177	2.2409	− 2.2255	− 7.7694	+ 0.2817	0.67391	2.06612
0.4723	+ 0.40845	+ 0.30757	− 0.14965	− 2.8542	2.2519	− 1.6844	− 7.1187	+ 0.2321	0.69235	2.07644
0.4886	+ 0.30992	+ 0.23294	− 0.11338	− 1.9000	2.2668	− 1.1172	− 6.2295	+ 0.1756	0.76595	2.10737
0.5013	+ 0.24470	+ 0.18328	− 0.089409	− 1.3420	2.2782	− 0.78387	− 5.5612	+ 0.1377	0.81891	2.13821
0.5320	+ 0.14956	+ 0.11137	− 0.054753	− 0.65223	2.2974	− 0.37705	− 4.4061	+ 0.0832	0.93630	2.20436
0.5739	+ 0.088170	+ 0.065345	− 0.032535	− 0.30375	2.3132	− 0.17433	− 3.4703	+ 0.0486	1.07840	2.27954
0.65	+ 0.041943	+ 0.030942	− 0.015766	− 0.10831	2.3285	− 0.061641	− 2.5936	+ 0.0229	1.30093	2.40035
0.75	+ 0.019423	+ 0.014292	− 0.007464	− 0.042806	2.3380	− 0.024030	− 2.2087	+ 0.0105	1.54958	2.57172
0.85	+ 0.009125	− 0.006706	− 0.003561	− 0.023284	2.3426	− 0.012809	− 2.5538	+ 0.0049	1.76624	2.84810
0.90	+ 0.005667	+ 0.004163	− 0.002222	− 0.019138	2.3438	− 0.010426	− 3.3789	+ 0.0031	1.86548	3.09870
0.95	+ 0.002718	+ 0.001997	− 0.001069	− 0.016976	2.3445	− 0.009180	− 6.2459	+ 0.0015	1.96010	
1.05	− 0.002718	− 0.001997	+ 0.001069	− 0.016976	2.3445	− 0.009180	+ 6.2459	0	2.13752	2.95
1.10	− 0.005667	− 0.004163	+ 0.002222	− 0.019138	2.3438	− 0.010426	+ 3.3789	0	2.22126	2.30
1.15	− 0.009125	− 0.006706	+ 0.003561	− 0.023284	2.3426	− 0.012809	+ 2.5538	0	2.30304	2.00
1.20	− 0.013491	− 0.009919	+ 0.005229	− 0.030446	2.3408	− 0.016929	+ 2.2602	0	2.38160	1.750
1.25	− 0.019423	− 0.014292	+ 0.007464	− 0.042806	2.3380	− 0.024030	+ 2.2087	0	2.45683	1.568
1.30	− 0.028108	− 0.020705	+ 0.010690	− 0.065070	2.3342	− 0.036797	+ 2.3224	0	2.52864	1.409
1.35	− 0.041943	− 0.030942	+ 0.015766	− 0.10831	2.3285	− 0.061641	+ 2.5936	0	2.59634	1.275
1.3997	− 0.066400	− 0.049113	+ 0.024656	− 0.20321	2.3198	− 0.11625	+ 3.0790	0	2.66289	1.165
1.4261	− 0.088170	− 0.065345	+ 0.032535	− 0.30375	2.3132	− 0.17433	+ 3.4703	0	2.70370	1.113
1.4489	− 0.11551	− 0.085788	+ 0.042416	− 0.44803	2.3057	− 0.25793	+ 3.9128	0	2.75354	1.072
1.4680	− 0.14956	− 0.11137	+ 0.054753	− 0.65223	2.2974	− 0.37705	+ 4.4061	0	2.81471	1.0483
1.4845	− 0.19196	− 0.14333	+ 0.070149	− 0.93968	2.2882	− 0.54566	+ 4.9540	0	3.00982	1.029
1.4987	− 0.24470	− 0.18328	+ 0.089409	− 1.3420	2.2782	− 0.78387	+ 5.5612	0	3.83406	1.011

TABLE 3.

The solutions $\sqrt{\sigma}$ and Ω as functions of the coordinate η_1, for the streamlines $\alpha = 30°$, $60°$, $120°$ and $150°$ (for $\alpha = 90°$ see table 2).

$\alpha = 30°$

η_1	σ	$\sqrt{\sigma}$	Ω
0.0622	0.01976	0.14057	1.3139
0.0632	0.01983	0.14081	1.3139
0.0642	0.01988	0.14099	1.3149
0.0653	0.01986	0.14092	1.3213
0.0665	0.01944	0.13942	1.3591
0.0675	0.01880	0.13713	1.4449
0.0685	0.01894	0.13764	1.5641
0.0693	0.02018	0.14204	1.6417
0.0704	0.02292	0.15139	1.7092
0.0720	0.02822	0.16800	1.7725
0.0743	0.03738	0.19333	1.8263
0.0759	0.04399	0.20975	1.8631
0.0779	0.05254	0.22922	1.9086
0.0803	0.06514	0.25522	1.9222
0.0834	0.08147	0.28543	1.9448
0.0873	0.10288	0.32074	1.9701
0.0921	0.13031	0.36098	1.9969
0.0980	0.16522	0.40648	2.0236
0.1061	0.21469	0.46335	2.0548
0.1108	0.24393	0.49389	2.0718
0.1222	0.31603	0.56217	2.1055
0.1368	0.41102	0.64111	2.1416
0.1677	0.61695	0.78546	2.1988
0.1890	0.76141	0.87259	2.2301
0.2155	0.94310	0.97113	2.2631
0.2499	1.18148	1.0870	2.3001
0.30	1.53271	1.2380	2.3514
0.35	1.88752	1.3739	2.4108
0.40	2.24606	1.4987	2.4942
0.45	2.60672	1.6145	2.624
0.50	2.969	1.7231	
0.55	3.332	1.8254	
0.60	3.695	1.9222	
0.65	4.058	2.0144	2.519
0.70	4.433	2.1055	2.000
0.75	4.815	2.1943	1.689
0.80	5.203	2.2810	1.467
0.85	5.596	2.3656	1.289
0.90	5.990	2.4474	1.150
0.95	6.553	2.5599	1.041

$\alpha = 60°$

η_1	σ	$\sqrt{\sigma}$	Ω
0.1684	0.025107	0.15845	1.31315
0.1695	0.025153	0.15860	1.31315
0.1707	0.025200	0.15875	1.31320
0.1718	0.025242	0.15888	1.31328
0.1728	0.025283	0.15901	1.31340
0.1740	0.025327	0.15914	1.31389
0.1751	0.025370	0.15928	1.31506
0.1763	0.025409	0.15940	1.31805
0.1776	0.025451	0.15953	1.32532
0.1789	0.025513	0.15973	1.34037
0.1803	0.025728	0.16040	1.37590
0.1813	0.026142	0.16168	1.41350
0.1821	0.026777	0.16364	1.44659
0.1832	0.028224	0.16800	1.49909
0.1846	0.031024	0.17614	1.56062
0.1866	0.036505	0.19106	1.63106
0.1893	0.045823	0.21406	1.69971
0.1909	0.052219	0.22851	1.72981
0.1934	0.063066	0.25113	1.76823
0.1956	0.072513	0.26928	1.80023
0.2028	0.111877	0.33448	1.83922
0.2077	0.127507	0.35708	1.96160
0.2221	0.214328	0.46296	1.96612
0.2268	0.243167	0.49312	1.98294
0.2322	0.276585	0.52591	2.00078
0.2382	0.314258	0.56059	2.01936
0.2451	0.358215	0.59851	2.03971
0.2617	0.470970	0.68627	2.06117
0.2717	0.536730	0.73262	2.08540
0.2833	0.613717	0.78340	2.11069
0.3034	0.748481	0.86515	2.15486
0.3116	0.803842	0.89657	2.17223
0.3293	0.924728	0.96163	2.19798
0.35	1.06695	1.03293	2.22870
0.40	1.41423	1.18921	2.29570
0.45	1.76553	1.32873	2.36030
0.50	2.12029	1.45612	2.43060
0.55	2.47847	1.57432	2.51705
0.60	2.84040	1.68535	2.64706
0.65	3.20561	1.79042	2.85860
0.70	3.55982	1.88675	3.27702
0.80	4.286	2.07027	2.824
0.85	4.654	2.15731	2.100
0.90	5.025	2.24165	1.794
0.95	5.594	2.36516	1.572
1.00	5.760	2.40000	1.403
1.05	6.104	2.47063	1.244
1.10	6.432	2.53614	1.109
1.1497	6.819	2.61132	1.025
1.1929	10.358	3.21838	0.852
1.2267	25.772	5.07661	0.110

$\alpha = 120°$

η_1	σ	$\sqrt{\sigma}$	Ω
0.6172	0.035356	0.18803	1.31251
0.6204	0.035392	0.18813	1.31252
0.6234	0.035426	0.18822	1.31255
0.6266	0.035471	0.18834	1.31261
0.6299	0.035522	0.18847	1.31282
0.6331	0.035587	0.18865	1.31343
0.6365	0.035700	0.18894	1.31491
0.6394	0.035891	0.18945	1.31824
0.6428	0.036394	0.19077	1.32716
0.6469	0.037668	0.19408	1.34908
0.6509	0.040274	0.20068	1.39128
0.6536	0.044064	0.20991	1.43233
0.6565	0.049652	0.22283	1.47839
0.6601	0.058981	0.24286	1.53794
0.6646	0.073940	0.27192	1.60415
0.6708	0.099293	0.31511	1.67775
0.6749	0.118206	0.34381	1.71744
0.6795	0.140956	0.37544	1.75557
0.6860	0.175176	0.41854	1.80167
0.6929	0.213392	0.46194	1.84683
0.7025	0.269336	0.51898	1.89203
0.7142	0.340078	0.58316	1.94052
0.7293	0.434494	0.65916	1.99502
0.7482	0.556106	0.74573	2.05253
0.8071	0.949619	0.97448	2.19138
0.8503	1.24554	1.11604	2.27777
0.9	1.59088	1.26130	2.36882
0.95	1.94196	1.39354	2.46248
1.0	2.29695	1.51557	2.56754
1.05	2.65618	1.62978	2.68295
1.10	3.02173	1.73831	2.83780
1.15	3.40545	1.84539	3.20876
1.20	3.90364	1.97576	3.90364
1.40	5.182	2.276	1.742
1.45	5.534	2.352	1.550
1.50	5.875	2.424	1.396
1.55	6.199	2.490	1.268
1.60	6.500	2.550	1.159
1.65	6.819	2.611	1.071
1.6707	7.014	2.648	1.042
1.6884	7.341	2.709	1.022
1.6966	7.680	2.771	1.017

$\alpha = 150°$

η_1	σ	$\sqrt{\sigma}$	Ω
0.8477	0.037503	0.19366	1.31247
0.8507	0.037526	0.19372	1.31247
0.8537	0.037547	0.19377	1.31251
0.8568	0.037569	0.19383	1.31250
0.8600	0.037603	0.19391	1.31240
0.8633	0.037645	0.19402	1.31306
0.8667	0.037711	0.19419	1.31359
0.8702	0.037782	0.19438	1.31295
0.8741	0.037934	0.19477	1.31521
0.8788	0.038366	0.19587	1.32133
0.8822	0.038983	0.19744	1.32729
0.8859	0.0402717	0.20068	1.34224
0.8878	0.0414942	0.20370	1.35791
0.8904	0.0440677	0.20992	1.38576
0.8932	0.0480123	0.21912	1.41976
0.8963	0.0541265	0.23265	1.46423
0.8979	0.0581175	0.24108	1.48780
0.8998	0.0636221	0.25223	1.51562
0.9039	0.0779099	0.27912	1.56943
0.9066	0.0890268	0.29837	1.59822
0.9101	0.104709	0.32359	1.63048
0.92	0.15402	0.39245	1.70511
0.93	0.20431	0.45201	1.76788
0.94	0.26211	0.51197	1.81501
0.95	0.32201	0.56746	1.85779
0.96	0.38357	0.61933	1.89357
0.97	0.44641	0.66814	1.92812
0.98	0.51022	0.71430	1.96090
0.99	0.57488	0.75821	1.99114
1.00	0.64025	0.80016	2.01888
1.05	0.97414	0.98699	2.14142
1.10	1.31546	1.14694	2.25037
1.20	2.01191	1.41842	2.48330
1.45	3.807	1.95115	3.194
1.50	4.176	2.04353	2.300
1.55	4.533	2.12908	1.983
1.60	4.880	2.20907	1.739
1.65	5.212	2.28298	1.543
1.70	5.517	2.34883	1.387
1.7501	5.790	2.40624	1.261
1.7626	5.854	2.41950	1.229
1.7740	5.911	2.43125	1.199
1.7845	5.963	2.44193	1.175
1.7941	6.024	2.45438	1.154
1.8030	6.101	2.47002	1.133
1.8110	6.196	2.48918	1.116
1.8188	6.339	2.51774	1.101
1.8257	6.545	2.55832	1.088
1.8323	6.819	2.61132	1.077

REPORT M. 1999.

Research on Cumulative Damage in Fatigue of Riveted Aluminum Alloy Joints

by

J. SCHIJVE and F. A. JACOBS.

Summary.

Two-step tests and interval tests were performed on 24 S-T Alclad riveted lap joints to study the cumulation of fatigue damage in this type of joint and to verify the linear cumulative damage rule.
Available data on light alloy specimens are reviewed and compared with the results of the present investigation. It is tried to establish some general trends of the cumulative damage phenomenon. Some proposed cumulative damage rules are discussed with respect to the experimental results and general accepted features of the fatigue phenomenon. Some remarks are made on the life estimation of structures under service loading. Proposals for further investigation are made.

Contents.

The research reported in this document has been sponsored by the AIR RESEARCH AND DEVELOPMENT COMMAND, UNITED STATES AIR FORCE, under contract no. AF 61(514—812, through the European Office, ARDC.

1 Introduction.

This investigation is an extension of a previous research (ref. 33) on the cumulation of fatigue damage in tests with varying load ranges. In ref. 33 unnotched and simply notched specimens of 24 S-T Alclad were tested. It was thought advisable, subsequently to test a typical aircraft joint in a similar way and for this purpose a 24 S-T Alclad riveted lap joint was chosen. However, now the mean stress was kept constant, whereas in ref. 33 all tests were performed at $R = 0$ (minimum stress zero). A constant mean stress is more realistic with respect to actual service loading.

The cumulative-damage tests were of a very simple nature. Only two different stress amplitudes were used in one test. Simple load sequences were thought necessary to obtain a clear picture of the cumulation of fatigue damage. Furthermore, with the results the well-known linear cumulative-damage rule was checked although in ref. 33 it was already stated that this rule has no general validity.

The results of the present investigation are compared with the results of other investigations. This necessitates a literature review and it turned out that a fair comparison is quite difficult owing to the great variety of test programs. Nevertheless it has been tried to establish some general trends of cumulative damage in precipitation-hardening light alloys. Taking account of these trends and of our knowledge of the fatigue phenomenon the cumulative-damage concepts, published by different authors are discussed. Since it turns out that insufficient rational back-ground for any cumulative-damage rule is available some proposals are made to clarify the gaps of our knowledge.

The significance of the reviewed test data for the practical fatigue testing and life estimation of complete aircraft structures is considered and some suggestions for ad-hoc research on this subject are given.

For the literature review valuable references were received from Dr. Gassner, Dr. Heywood and Prof. Shanley, which is gratefully acknowledged here.

This research was conducted under the auspices

of the Air Research and Development Command, United States Air Force under contract no. AF 61(514)—812, through its European Office at Brussels.

2 Nomenclature and notations.

Fatigue curve = S-N curve = Wöhlercurve.
Fatigue diagram = Smith diagram = modified Goodman diagram.
Fatigue limit = Endurance limit = S_l.
Load range $\triangleq$ Stress range = $S_m \pm S_a$.
Cumulative damage test = Fatigue test with varying load range.

Two-step test = Fatigue test in which the load range is varied once. First the pre-stress and then the test stress is applied.
H-L test = Two step test in which a high pre-stress is followed by a low test stress.
L-H test = Two step test in which a low pre-stress is followed by a high test stress.
Spectrum test = Fatigue test in which the load range varies periodically, stepwise or continuously, each period being small with respect to the endurance.
Interval test = Spectrum test in which only two different load ranges are employed.

Pre-loading: One high pre-load is applied before the fatigue test (test loading).

Cyclic pre-loading = H-L test.

Cycle ratio = $\frac{n}{N}$

n = Number of load cycles.
n_1 = ,, ,, ,, ,, at pre-stress (two step test).
n_2 = ,, ,, ,, ,, at test stress (two step test).
n_H = ,, ,, ,, ,, at high stress range.
n_L = ,, ,, ,, ,, at low stress range.
N = Endurance (suffixes 1, 2, H and L are used in the same way as for n)
N' = Endurance in a spectrum test.
S = Stress (all stresses, if not specified otherwise, are nominal stresses in the net section).
S_{min} = Minimum stress in a load cycle.
S_{max} = Maximum stress in a load cycle or in a spectrum test.
S_m = Mean stress in a load cycle.
S_a = Stress amplitude.
S_{a_H} = High stress amplitude in a two-step or interval test.
S_{a_L} = Low stress amplitude in a two-step or interval test.
S_l = Fatigue limit = endurance limit.
$S_{0.2}$ = Yield stress.
S_u = Ultimate stress.
R = Stress ratio= $\frac{S_{min}}{S_{max}}$
r = radius.
k_t = theoretical stress concentration factor.
σ = Standard deviation.

In general the dimensions are given in metric units (mm; kg/mm²). In the text the English equivalents are given in inches and kips (1000 p.s.i.) between brackets. At the bottom of the tables and figures conversion factors are given, if necessary.

1 mm = 0.04 inch.
1 inch = 25.4 mm.
1 kg/mm² = 1.422 kips = 0.635 t.s.i.
1 kips = 0.703 kg/mm².
1 t.s.i. = 2.240 kips = 1.574 kg/mm².

3 Test procedure.

3.1 *Material, specimens and static tests.*

The material used for the specimens was 24 S-T alclad sheet with a nominal thickness of 0.8 mm (0.032″). The sheet thickness of each specimen was measured accurately within 1/100 mm. The sheet material was obtained from two manufacturers: the Vereinigte Leichtmetall Werke (VLW) and the Nederlandse Aluminium Maatschappij (NAM). From both sheet materials normal tensile test specimens were tested by the Royal Netherlands Aircraft Factories Fokker, the manufacturer of the specimens, to determine the mechanical properties. These properties were found to be:

24 S-T alclad from NAM:
$S_{0.2}$ = 34.9 kg/mm² (49.6 kips)
S_u = 44.5 ,, (63.2 ,,)
Elong. = 13.4 %.

24 S-T alclad from VLW:
$S_{0.2}$ = 34.4 kg/mm² (48.8 kips)
S_u = 46.9 ,, (66.6 ,,)
Elong. = 16.6 %.

One type of riveted joint was used, a simple lapjoint with two rows of eight rivets each, see fig. 3.1. The rivets were of the brazier type of 17 S material. The specimens were manufactured by Fokker according to common workshop practice. This includes the following features: The diameters of the holes and the rivets were 3.1 and 3.0 mm respectively (about ⅛ inch). After drilling the holes the burrs were removed. The snapheads were made by pneumatic rivet hammers with a flat head at 3600 blows per minute.

The material of the rivets was 17 S, according to Fokker specification 5.312. This includes a chemical composition of: Cu 3.5—4 %; Mg 0.4—0.9 %; Mn 0.4—0.7 %; Si < 0.7 %; Fe < 0.7 %; Ti < 0.3 % and the remainder Al. The minimum ultimate shear stress was 25.2 kg/mm² (35.8 kips). The rivets were solution heat treated at 495° C ± 5° C during 20 minutes and quenched in cold water. The riveting occurred within two hours after quenching.

In the ends of the specimens holes were drilled for clamping purposes (see fig. 3.1). The specially designed grips were also used in previous investigations as given by ref. 17.

Tension tests were executed on two specimens in an Amsler hydraulic tensile testing machine. The ultimate loads (shearing of the rivets) were 3630 kg (8004 lbs) and 3640 kg (8026 lbs). The mean corresponds to a stress of 33.7 kg/mm² (47.9 kips), based on the critical net section of the sheet.

3.2 *Fatigue machines and fatigue tests.*

The fatigue tests were run on a 10 tons Amsler high-frequency pulsator which is an electromagnetic type of resonance machine (see fig. 3.2). The frequency used was 6000 c/min.

When a fatigue crack has propagated sufficiently in a specimen, the resonance frequency of the loading system decreases. The machine is no longer adapted then to the frequency and switches off automatically. That moment was considered as the end of a test. The specimens were not completely fractured but a well defined crack was visible. As the maximum load in the fatigue test did not exceed 2000 kg (4409 lbs) a 2 tons dynamometer was used in the machine.

Two test programs which were quite similar were performed; one at a mean stress of 9.0 kg/mm² (12.8 kips) and the other at a mean stress of 7.2 kg/mm² (10.1 kips). $S_m = 9.0$ kg/mm² corresponds to an ultimate load factor of 3.75 with respect to the static strength. $S_m = 7.2$ kg/mm² corresponds to an ultimate load factor of ca. 4.7. A lower value of S_m was avoided as then compressive forces in the fatigue tests had to be used, which would have necessitated a special arrangement for preventing buckling.

At each mean stress only two different stress amplitudes were used. Each test program consisted of H-L tests, L-H tests and interval tests (see chapter 2 for nomenclature). A number of different cycle ratios were employed in all types of tests.

To a certain extent the test program was similar to the program of ref. 33, in which unnotched and notched specimens were used. However, in ref. 33 all tests were performed at $R = 0$ whereas now all tests were performed at a constant mean stress. This was thought more realistic with respect to aircraft loading.

The main purpose of the test program was to verify the linear cumulative damage rule:

$$\Sigma \frac{n_i}{N_i} = 1.$$

Further the interaction of two different stress amplitudes applied in one test could be studied. In this way it was hoped to gain some understanding of the cumulation of damage in a common aircraft joint, because in ref. 33 it turned out that the linear cumulative damage rule did not possess general validity.

Four spare specimens were given a high preload of 22.4 kg/mm² (31.9 kips) and then fatigue-tested at 7.2 ± 3.2 kg/mm² (10.1 ± 4.6 kips).

4 Results and discussion of the normal fatigue tests.

Table 4.1 and fig. 4.1 give the results of the normal fatigue tests. The mean of the endurances as well as the standard deviations have been determined logarithmically. This is more adequate as several investigators have pointed out; see for instance refs. 8 and 38. For the tests at a mean stress of 9.0 kg/mm² (12.8 kips) 20 specimens were used for each stress amplitude. This number was thought necessary in view of the scatter which is inherent to the fatigue phenomenon. In fig. 4.1 a comparison with the results of ref. 24 for the same type of specimen has been made. The results of ref. 24 were obtained with a different type of fatigue machine and a lower test frequency; for details see fig. 4.1. The present results are slightly better but still the agreement is good. Moreover it turned out that the scatter in the fatigue tests, was quite low. For these reasons a number of 10 specimens for each stress amplitude at the mean stress of 7.2 kg/mm² (10.1 kips) was considered sufficiently high.

To check whether a normal logarithmic distribution curve is valid here, the results for the tests at a mean stress of 9.0 kg/mm² (12.8 kips) were normalized

$$y_i = \frac{\log N_i - \overline{\log N}}{\sigma} \; (i = 1, 2, 3 \ldots 20). \quad (4.1)$$

The average probability of failure at the endurance N_i may be denoted by

$$P_i = \frac{i}{m+1} \quad (4.2)$$

m = number of similarly tested specimens.

In fig. 4.2 P_i is plotted against y_i. A normal distribution should give the straight line given in the figures. It may be concluded that indeed a normal logarithmic distribution may be a good approximation in the range of probabilities of failures considered here but it can not be said whether this approximation is reliable for very low values of the probability of failure which is a rather important range with respect to providing some margin of safety.

The "extreme value distribution function" as proposed by Freudenthal and Gumbel (ref. 10) is certainly more realistic as it assumes a minimum life for which a probability of failure is zero. This distribution has not been considered here as the sample size is too small to discriminate between this distribution function and the "log-normal distribution function".

The scatter in the results is extremely low for fatigue tests. To illustrate this point $\sigma/\overline{\log N}$ has also been given in table 4.1. In ref. 47 Weibull, testing 1088 flat 24 S-T Alclad specimens with two drilled holes, concludes that the shortest life, even in a not very large sample, may be expected to be about $^1/_3$ of the average life. For the results in table 4.1 this value is about $^2/_3$ or higher. Probably the small scatter has mainly to be attributed to the type of specimen. The riveted lapjoint has eight rivets in each line. So the specimens may be considered as consisting of eight specimens. The weakest one will determine the endurance and so the chance of obtaining high endurances will be reduced. This reasoning has also been advanced to explain a small scatter in the fatigue life of complete structures.

From table 4.1 it may be seen that there is more scatter at the lower stress amplitude than at the higher stress amplitude. This generally recognized feature is more evident at $S_m = 9.0$ kg/mm² (12.8 kips) than at $S_m = 7.2$ kg/mm² (10.1 kips).

5 Results of the cumulative damage tests.

In the tables 5.1, 5.2, 5.3 and figs. 5.1 and 5.2 the results of the two-step tests and the interval tests are given. The type of test is denoted schematically. In the figures $\Sigma \frac{n}{N}$ is plotted as a horizontal line, each line representing one test. For the two-step tests the beginning of the line corresponds to the end of the prestress and the end of the line corresponds to the end of the test. (Only the latter applies to the plotting of the results of the interval tests).

As mentioned in chapter 3.1 for the tests with a mean stress of 9.0 kg/mm² (12.8 kips), specimens of VLW sheet material and NAM sheet material were used. Only a small number of these tests were performed with specimens of NAM sheet material. The results of these tests are indicated by dotted lines in fig. 5.1. For those tests which allow a comparison it would seem that the VLW material is slightly better. If the results obtained with the NAM material are omitted, the mean results are hardly affected, however. For the tests at $S_m = 7.2$ kg/mm² (10.2 kips) only NAM material was used.

One of the most remarkable features about the results of the two-step tests is that the mean values of $\Sigma \frac{n}{N}$ deviate so little from unity for both mean stresses used. As these two mean stresses (9.0 and 7.2 kg/mm² $\triangleq$ 12.8 and 10.2 kips) do not differ very much it is not unexpected that the results of both test programs show a similar character.

Since the deviations of the $\Sigma \frac{n}{N}$ values from unity are small, they do not reveal any systematical relation and for the two-step tests the linear cumulative damage rule seems to be a good approximation. It is more or less surprising to notice that $\Sigma \frac{n_i}{N_i}$ in the interval tests is not much, but still noticeably beyond unity. The lowest value was obtained for $S_m = 9.0$ kg/m² (12.8 kips), $\frac{n_L}{N_L} = 0.10$ and $\frac{n_H}{N_H} = 0.03$. However, 5 of the 10 specimens tested were of NAM material, which is believed to give somewhat lower fatigue results. If these specimens are omitted the mean value of $\Sigma \frac{n}{N}$ for the remaining 5 specimens becomes 1.32. The mean results are once more summarized below:

		$S_m = 7.2$ kg/mm²		
$\frac{n_L}{N_L}$	$\frac{n_H}{N_H}$	$\Sigma \frac{n_L}{N_L}$	$\Sigma \frac{n_H}{N_H}$	$\Sigma \frac{n}{N}$
0.05	0.05	0.61	0.61	1.22
0.10	0.03	1.25	0.38	1.63
0.10	0.01	1.45	0.15	1.60
0.20	0.01	1.87	0.09	1.96
0.05	0.01	1.53	0.30	1.83
		$S_m = 9.0$ kg/mm²		
$\frac{n_L}{N_L}$	$\frac{n_H}{N_H}$	$\Sigma \frac{n_L}{N_L}$	$\Sigma \frac{n_H}{N_H}$	$\Sigma \frac{n}{N}$
0.05	0.05	0.66	0.65	1.31
0.10	0.03	1.02	0.30	1.32*
		*NAM specimens omitted		

These results hardly reveal any trend with respect to the effect of the cycle ratios at the high and the low stress amplitudes. If the tests are considered as fatigue tests at the low stress amplitude which are periodically interrupted for applying a batch of higher load-cycles, the effect of the latter is a slowing down of the fatigue rate at the low stress amplitude. $\Sigma \frac{n_L}{N_L} > 1$ except for $\frac{n_H}{N_H} = 0.05$. This value was sufficiently high to add a substantial damage increment. The smallest value of $\frac{n_H}{N_H}$ is 0.01 and gives the highest values of $\Sigma \frac{n_L}{N_L}$. The effect of the frequency of the batch of high loads does not turn out in some clearly defined way. It is remarkable that for $\frac{n_L}{N_L} = 0.20$ and $\frac{n_H}{N_H} = 0.01$ the highest endurances are obtained.

In table 5.1 the results for four pre-loaded specimens tested at 7.2 ± 3.2 kg/mm² (10.2 ± 4.6 kips) are given. The pre-loading consisted of applying a load of $^2/_3 \cdot S_u$ (22.2 kg/mm² $\triangleq$ 31.6 kips) to which an endurance of ca. 20000 load cycles (at minimum load zero) corresponds (see ref. 24). After this pre-loading the stress returned to zero and then the fatigue test started, giving the results at the bottom of table 5.1. The mean endurance obtained then was about one and a half times the original value given in table 4.1. Although the pre-load was fairly high, the gain of endurance is still moderate.

Some more comments on the cumulative damage tests are given in chapters 6 and 7.

Also in the cumulative damage tests the scatter is not large. No systematical variation as a function of the pre-stress cycle ratio could be observed.

The distribution of $\Sigma \frac{n}{N}$ has not been considered. Also for cumulative damage tests the probability of failure may be approximated by relation

(4.2). In ref. 33 it was remarked that for the calculation of $\Sigma \frac{n}{N}$ the values of N_1 and N_2 with the same probability of failure as that of the test result itself could be used. This has been proposed by LEVY (ref. 26) as a method to obtain more information from apparently similar tests. LEVY postulates that a specimen with a certain probability of failure, determined by performing many identical tests of a certain type would have obtained the same probability of failure in other fatigue tests of the same type but different loading program. He reasons that fatigue is a rather localized phenomenon and local weak spots which initiate the fatigue crack remain weak under all circumstances. LEVY applies this to two-step tests for deriving the relation between the pre-stress cycle ratio and $\Sigma \frac{n}{N}$. He performs 20 tests at the low stress amplitude (Sa_L), 20 tests at the high stress amplitude (Sa_H) and 20 L-H tests with 400.000 pre-stress load cycles (n_L) at Sa_L and n_H load cycles at the test stress Sa_H. So the L-H tests were meant to be identical (all have the same number of pre-stress load cycles). Owing to scatter different values for n_H are obtained. The results are then arranged in increasing order.

$$\text{Endurance at } Sa_L = N_{L_1},\ N_{L_2},\ \dots,\ N_{L_j},\ \dots,\ N_{L_{20}} \qquad \text{(a)}$$

$$\text{,, } \quad \text{,, } \quad Sa_H = N_{H_1},\ N_{H_2},\ \dots,\ N_{H_j},\ \dots,\ N_{H_{20}} \qquad \text{(b)}$$

$$n_H = n_{H_1},\ n_{H_2},\ \dots,\ n_{H_j},\ \dots,\ n_{H_{20}} \qquad \text{(c)}$$

$$\text{Prestress cycle ratio} = \dots,\ \dots,\ \dots,\ \frac{400{,}000}{N_{L_j}},\ \dots,\ \dots \qquad \text{(d)}$$

$$\text{Teststress cycle ratio} = \dots,\ \dots,\ \dots,\ \frac{n_{H_j}}{N_{H_j}},\ \dots,\ \dots \qquad \text{(e)}$$

$$\Sigma \frac{n}{N} = \dots,\ \dots,\ \dots,\ \frac{400{,}000}{N_{L_j}} + \frac{n_{H_j}}{N_{H_j}},\ \dots \qquad \text{(f)}$$

The pre-stress cycle ratio (line d) thus obtained is different for all tests and since the scatter in N_L was quite large the pre-stress cycle ratio ranged from 0.10 to 0.91 and covers almost the entire range (0 to 1). Combining line d and line f gives $\Sigma \frac{n}{N}$ as a function of $\frac{n_L}{N_L}$.

If this method of treating the test results were correct the results of $\Sigma \frac{n}{N}$ would be hardly affected by scatter. Scatter would only originate from slight deviations from relation (4.2), which are possible if a limited number of specimens is used. However, WEIBULL (ref. 46) has shown that this type of scatter will be rather small for 20 identical tests. So indeed more information from 20 apparently identical tests is obtained than by considering only the mean values of N_L, N_H and n_H.

To LEVY's principle and its application to test data two objections may be raised.

(1) It is thought to be incorrect to assume that a specimen will have the same probability of failure, regardless of the type of load program to which it is subjected. Probably it may be correct for conventional fatigue tests, but it will not hold for each type of cumulative damage test. An example may be a two-step test in which a strengthening effect of the pre-stress may be obtained, which is the more the higher the pre-stress cycle-ratio amounts. This involves that after applying a certain number of pre-stress cycles to a weak and a strong specimen, the original weaker one may have become the stronger one with the lower probability of failure. Also in spectrum tests with periodic high load cycles, the latter will level out the differences in weakness, thus affecting the probability of failure.

(2) The second reason is that LEVY's principle implies the assumption that weak and strong specimens endure cumulative damage in the same way. This can neither be proved nor disproved and only an experimental check may answer this question. The results of the present investigation do not offer conclusive test material. LEVY's treatment involves that the lower values of $\Sigma \frac{n}{N}$ become higher and the higher values become lower. For the present investigation this means that all results remain about unity. However applying the method to tests with results differing considerably from unity, such as the H-L tests on the notched specimens of ref. 33, showed that for these tests this principle can not be valid, as conflicting results were obtained.

However the value of ref. 26 is that it has drawn the attention to the fact that averaging the results in a way as done in table 5.1 and 5.2 (H-L and L-H tests) actually implies an averaging of results of specimens which received the same number of pre-stress load-cycles, however not the same degree of damage.

6 Comparison with the results of other investigations.

Several decades ago, realizing that many structural components in practice were subjected to stress amplitudes of variable magnitude, it became clear that normal fatigue tests did not provide any direct information on the service endurance of such components. The phenomenon, now called "cumulative damage in fatigue" was recognized at that moment and since then, numerous experiments have been performed to investigate this phenomenon. The first tests were conducted with steel specimens and things like training and coaxing were observed. Similar tests on light alloys showed that cumulative damage for this material may be quite different. Meanwhile the problem of fatigue in aircraft structures became more urgent and so at several laboratories investigations were started to establish general trends of cumulative damage in light alloys. These tests may be subdivided in three types. At first tests were performed to study the interaction of two different stress levels. Secondly there were tests, the main purpose of which was merely a checking of the linear cumulative damage hypothesis. The tests of the third type are spectrum tests in which a load spectrum was used that imitates the actual service loading. The first two types may be considered as having some basic significance. The latter one, supposing that no endurance in practice could be derived from the usual S-N curves, had a direct practical purpose.

The investigations yielded different trends. While one investigation showed that a life prediction with the linear cumulative damage rule was on the safe side $\left(\Sigma \frac{n_i}{N_i} > 1\right)$ the other one showed the opposite. Now it should be recognized that fatigue tests may be performed in quite different ways, thus introducing the possibility of different results. Two main points in this respect will be mentioned here. Some investigators use unnotched specimens, while others use notched specimens. Secondly a number of test programs has been conducted as rotating beam tests, while other ones were axial load tests with a mean stress unequal to zero. It therefore seems worthwile to compare the most important investigations, trying once more to reveal some general trends and to indicate the gaps of our knowledge. For this purpose a number of investigations will be summarized here. This implies a literature review and it may be quite possible that a number of investigations escaped the attention. This survey will be restricted to light alloys and more in particular to the precipitation hardening light alloys, which actually means alloys of the type Al-Cu-Mg (24 S-T) and Al-Zn-Mg (75 S-T). The nomenclature which will be used is given in chapter 2. Firstly the axial loading tests will be described, after that the rotating beam tests and finally the tests in which one high preload was applied. Moreover the investigations will be discussed in a more or less chronological order. However these sequences are not always maintained strictly.

Gassner has recommended the spectrum tests since 1939 (ref. 11 and 14) and he performed many of these tests. The results were not published in terms of $\Sigma \frac{n}{N}$. However, Gassner reports that in general the results disagree with this linear cumulative damage rule and that this rule may be on the unsafe side. Gassner's work will be discussed to some further extent in chapter 9.

Heyer *) (ref. 19) investigated the effect of cyclic pre-stressing on the S-N curve and more in particular on the fatigue limit. His results are summarized in figs. 6.1 to 6.5.

Fig. 6.1 illustrates the influence of cyclic pre-stressing at $R = 0$ and different cycle ratios of the pre-stress on the fatigue limit at $R = 0$ for two types of light alloys and for lugs and bars with a sharp circumferential groove. The trend of all these figures is the same, i. e. the fatigue limit is raised considerably by a high cyclic pre-stress. Moreover one figure shows that the rise is the higher for higher magnitudes of the pre-stress. One noteworthy feature in all these diagrams is that the maximum increase of the fatigue limit is not obtained after one pre-load cycle but a steady increase is found the longer the pre-stress lasted. The maximum effect is obtained at a pre-stress cycle-ratio of about 0.50.

The rise of the S-N curve after cyclic pre-loading is shown in terms of $\Sigma \frac{n}{N}$ in fig. 6.2. The tests of this type are actually two-step tests of the type H-L tests. Four cycle ratios were used, viz. $n_H = 1$ load cycle and $\frac{n_H}{N_H} = 0.05$, 0.50, and 0.80. All values of $\Sigma \frac{n}{N}$ are higher than unity but again the effect at $\frac{n_H}{N_H} = 0.50$ is much more pronounced than for $n_H = 1$ load cycle and $\frac{n_H}{N_H} = 0.05$. The increase in $\Sigma \frac{n}{N}$ is smaller for the higher test-stresses (smaller differences between pre-stress and test-stress) and larger for higher values of the pre-stress (larger differences between pre-stress and test-stress).

Fig. 6.3 illustrates how the fatigue limit is affected by cyclic pre-loading at a stress amplitude of $\pm$ 6 kg/mm² (8.53 kips) and different values of the mean stress. Also for the fatigue test a number of mean stresses were used and the results are presented as a fatigue diagram. It turned out that the higher the mean-stress of the pre-loading the more the fatigue limit was raised. This beneficial influence decreased at higher mean values of the test stress. Cyclic pre-loading with a negative mean stress (— 6 kg/mm² $\triangleq$ — 8.53 kips) hardly effected the fatigue limit.

Fig. 6.4 shows once more the rise of the fatigue limit at different mean stresses for lugs, caused by a high cyclic pre-stress. Three values for the pre-stress cycle ratio were applied, viz. 0.05, 0.50 and 0.80. The rise in the fatigue limit is maximum at $\frac{n_H}{N_H} = 0.50$. The rise decreases for higher values of S_m. The tension-compression side of the fatigue diagram does not allow a fair comparison as for this type of specimen the way in which the load is transferred then is different at S_{min} and S_{max}.

Fig. 6.5 gives the results of a number of spectrum tests on lugs. The test results were given in flying hours and were not evaluated in terms of $\Sigma \frac{n}{N}$. The spectra applied are schematically indicated. It may be seen that the first tests were conventional fatigue tests and in the following tests more stress amplitudes were added, which did not lead to a decrease of endurance but on the contrary an important increase in life was obtained. This clearly illustrates the beneficial

*) In general Heyer did not give detailed results. Also the number of tests performed was not mentioned.

influence of the higher stresses and $\Sigma \frac{n}{N} = 1$ would have underestimated the actual endurances here.

HEYER has also tested a riveted joint and a spot welded joint (one rivet or one spot weld in each specimen). It turned out that also for these types of specimens a high cyclic pre-stress caused a rise of the endurance limit. However the increase was somewhat less pronounced and there was a considerable scatter in these tests.

Results of MINER (ref. 28) of two-step tests on unnotched 24 S-T Alclad specimens are presented in fig. 6.6. Positive mean-stresses were used. Pre-stress cycle ratios ranged from 0.40 to 0.73. $\Sigma \frac{n}{N}$ did not deviate very much from unity and deviations to both sides of unity occurred. The same applies to some tests of MINER in which three or four stress levels were employed, the results of which are not presented here.

RUSSELL and co-workers (ref. 34), investigating the fatigue strength and related characteristics of aircraft joints, also performed a number of cumulative damage tests on unnotched 24 S-T Alclad specimens and riveted lapjoints of 24 S-T and 75 S-T Alclad with one and two rows of rivets. A positive mean-stress (0.212 S_u) was maintained. The number of tests was limited. The deviations of unity in the results of $\Sigma \frac{n}{N}$ could be explained by scatter in the S-N curve.

WÅLLGREN (ref. 45) performed two types of spectrum tests. For one type a gust spectrum with a constant mean stress and for the other type a manoeuvre load-spectrum with a constant minimum stress was applied, see fig. 6.7. Notched and unnotched specimens of 24 S-T Alclad and 75 S-T Alclad were tested and a number of mean stresses were employed, see fig. 6.7 and 6.8. In general, the results for the unnotched specimens are lower than for the notched specimens. Moreover, they do not deviate very much from unity. In the tables of fig. 6.7 and 6.8 the endurance at the highest stress amplitude applied is also given because this endurance indicates more or less the severity of the highest stress amplitude. As an average the results for notched specimens were higher than unity but values somewhat below unity occurred and sometimes rather high values of $\Sigma \frac{n}{N}$ were found.

In these spectrum tests one or more of the lowest stress amplitudes were below the endurance limit. To study their effect WÅLLGREN omitted these stress levels in a number of tests. For the 75 S-T specimens this resulted in somewhat larger endurances, whereas for the 24 S-T specimens this effect was not clear, as a lengthening as well as a shortening of the endurance was found. GASSNER (ref. 11) noticed that, omitting the lowest stress amplitudes in spectrum tests gave a considerable increase in life.

GROVER and co-workers (ref. 15) performed two-step tests of both the H-L and L-H type. A constant mean stress was maintained. Unnotched specimens of bare 24 S-T and 75 S-T were tested. The results are presented in fig. 6.9. Both materials show the beneficial effect of high cyclic pre-stressing and so far they are in agreement with the results of HEYER (ref. 19). However here the beneficial influence decreases more rapidly as the pre-stress cycle-ratio increases. Nevertheless, also here for 75 S-T the maximum benefit is not obtained after 10 load cycles but at a higher number of pre-stress cycles. The trend of the L-H tests is that $\Sigma \frac{n}{N}$ increases at increasing pre-stress cycle-ratio in such a way that it seems that the pre-stress was in-effective $\left(\Sigma \frac{n}{N} \approx 1 + \frac{n_1}{N_1}\right)$, this being more evident for 24 S-T than for 75 S-T.

HARTMAN (ref. 17) conducted some preliminary two-step tests on riveted lapjoints of 24 S-T Alclad, the same type of specimen as employed in the present investigation. His results are given in fig. 6.10. The results of the H-L tests are in good agreement with the results of HEYER (ref. 19) and GROVER and co-workers (ref. 15). Also here the beneficial effect of a pre-stress cycle ratio of 0.26 is much higher than for one pre-stress cycle. The L-H tests give a result slightly below unity.

A testprogram somewhat similar to the present investigation was conducted by the authors (ref. 33) on unnotched and notched 24 S-T Alclad sheet specimens, see fig. 6-11. An important difference was that in ref. 33 the tests were performed at $R = 0$, whereas now a constant mean stress is used. In the H-L tests the unnotched specimens showed a higher endurance the longer the pre-stress lasted, whereas in the L-H tests $\Sigma \frac{n}{N}$ was slightly below unity for this type of specimen for all values of the pre-stress cycle-ratio. These results are different from the results of GROVER and co-workers (ref. 15). However, these investigators used much higher stress amplitudes.

In the H-L tests on the notched specimens a considerable increase of endurance was obtained by pre-stress cycle-ratios of 0.02 up to 0.25. (The result for $\frac{n_H}{N_H} = 0.05$ is thought to be an exception which could not be explained). At $\frac{n_H}{N_H} = 0.50$ the increase in endurance is reduced again to a large extent. The L-H tests gave $\Sigma \frac{n}{N}$ values slightly beyond unity. Thus the results of the notched specimens agreed more or less with those of ref. 19, 15 and 17.

In the interval tests on the unnotched specimens the mean result for $\Sigma \frac{n}{N}$ was about unity whereas this was about 1.8 for the notched specimens. This shows that indeed the notched specimens experienced some beneficial effect of the high load or in other words, the high load caused the lower load to be more or less ineffective. In view of the H-L and L-H tests the results of the interval tests are not unexpected. It will be noted that it is quite unimportant whether the interval tests are started at the lower or the higher stress-amplitude.

SMITH and co-workers (ref. 39) performed numerous tests on unnotched specimens of 75 S-T Alclad and 24 S-T Alclad sheet specimens (fig. 6.12). The mean stress was zero but also a number of tests were performed at a positive mean stress (14.1 kg/mm² $\triangleq$ 20.0 kips). Most tests were of the interval-type. The $\Sigma \frac{n}{N}$ values were in general about unity or slightly below unity. Moreover, it turned out that also here there was no noticeable effect of starting with the high or the low stress amplitude which is in agreement with ref. 33. The cycle-ratios of the intervals at the high and the low stress amplitudes which were used in different tests ranged from high to low values. Moreover the ratio $\frac{n_H}{N_H} : \frac{n_L}{N_L}$ covered a large range of values. These variables did not affect the test results noticeably. One exception must be made for the tests with high values of $\frac{n_H}{N_H}$ and $\frac{n_L}{N_L}$ and thus a small number of intervals. For these tests starting at the higher stress amplitude leads to somewhat higher values of $\Sigma \frac{n}{N}$, giving a slight indication of the beneficial influence of the high stress amplitude. A number of H-L tests and L-H tests were performed only with relatively high values of the pre-stress cycle ratio. Also in these tests there were no large deviations of $\Sigma \frac{n}{N} = 1$, but again the H-L tests gave somewhat higher values than the L-H tests. In comparison to the investigation of GROVER and co-workers (ref. 15), it is noticeable that here no benefit of a very high stress, $S_a = 42.2$ kg/mm² (60 kips) was obtained whereas in ref. 15 somewhat smaller stress amplitude induced a marked increase in endurance. Two differences in test procedure may explain this. At first SMITH and co-workers (ref. 39) used for these tests a mean stress zero whereas GROVER and co-workers (ref. 15) used a positive mean stress. Secondly in ref. 39 clad material was used whereas in ref. 15 bare material was tested.

SMITH and co-workers did not find any noticeable influence of changing the mean stress from zero to 14.1 kg/mm² (20.0 kips). The most important trend of this extensive test program is that the deviations from $\Sigma \frac{n}{N} = 1$ were rather limited. To a certain extent there is some agreement with the tests on the unnotched specimens of ref. 33.

WÅLLGREN *) performed a number of spectrum tests at $R = 0$ on notched 75 S-T bars. In this spectrum he used fairly high stresses (0.75 S_u) and it was noticed that the experimentally determined endurances were much higher than the calculated ones. Introducing the statistical aspect WÅLLGREN calculated the endurance with S-N curves for three probabilities of failure, 0.1, 0.5 and 0.9. The three endurances calculated were compared with the experimental results of the same probability of failure. The results are given in fig. 6.13; the endurances were expressed in loading periods. Two conclusions are apparent from this figure. Firstly, the linear cumulative damage rule underestimated the endurance to a large extent. In the second place, the scatter in the test results is much lower than the linear cumulative damage rule predicts from the scatter of the conventional S-N curves. The latter conclusion was also reported by GASSNER (ref. 13).

For reasons of comparison the results of the present investigation are summarized in fig. 6.14. Some explanation is already given in chapter 5, which will only briefly be repeated here. In general, the difference between both mean stresses used was not important. For the H-L tests and the L-H tests the deviations of $\Sigma \frac{n}{N} = 1$ are not large. No appreciable strengthening effect of the high stress was found in the H-L tests, contrary to the results of previously discussed investigations.

Comparing the results of HARTMAN (ref. 17) with the present investigation (same type of specimens) it is noticeable that he found a strengthening effect in the H-L tests. However, the lower stress amplitude in ref. 17 was lower and so nearer the endurance limit, and a second reason which is thought to be even more important is that HARTMAN's tests were executed at $R = 0$. So changing over from the high to the low stress level also implies that the mean stress is lowered.

An important feature of the results of the present investigation is that the interval tests gave $\Sigma \frac{n}{N}$ values which were markedly higher than unity especially at $S_m = 7.2$ kg/mm² (10.2 kips).

In general, the axial loading fatigue tests were performed on sheet specimens. The rotating beam test specimens, however, were almost always taken from extruded bars.

STICKLEY (ref. 40) performed rotating beam tests on 25 S-T unnotched specimens. These were interval tests. Based on a limited number of experiments STICKLEY suggested that if a high and a low stress amplitude are applied alternately the stress-cycles at the lower stress-level do not affect noticeably the fatigue life at the higher stress-amplitude.

DOLAN and co-workers (ref. 4), conducting an extensive testprogram on different materials, also performed interval tests on unnotched 75 S-T specimens. The results are summarized in fig. 6.15. For a part of the tests, the lower stress amplitude was below the endurance limit. It can be seen that these tests do not suggest that the lower stress cycles are ineffective. It was not easy to derive some general trends of the results as they do not vary systematically. For $S_{a_L} = 4.1$ kg/mm² (5.88 kips) the highest values for $\Sigma \frac{n}{N}$ were obtained.

DOLAN and BROWN (ref. 5) performed rotating beam tests on the same unnotched specimen as used in the previously discussed testprogram. Two-step

*) Private communication.

tests with a test stress of 24.6 kg/mm² (35.0 kips) and three values of the pre-stress, 31.7, 28.1 and 21.1 kg/mm² (45.0, 40.0 and 30.0 kips) were executed for some values of the pre-stress cycle-ratio. The scatter in these tests was unexpectedly high, but a large number of tests allowed some qualitative conclusions.

In general, $\Sigma \frac{n}{N}$ was somewhat beyond unity in the L-H tests and somewhat below unity in the H-L tests. These results disagree slightly from the axial-loading tests on 24 S-T of SMITH and coworkers who also used a mean stress zero.

CORTEN, SINCLAIR and DOLAN (ref. 3) continued the previous testprograms also using unnotched specimens of 75 S-T 6. To be sure that scatter would not prevent conclusions, the normal fatigue tests were repeated many times whilst the interval tests, see fig. 6.16, were performed 20 times each. From the table in fig. 6.16 it may be seen that some values for the high and the low stress amplitude were used and moreover different values for the cycle-ratio's were chosen. Values of $\Sigma \frac{n}{N}$ well below unity and well beyond unity occur. The ratio of the cycle-ratio's of the high and the low stress seems to be quite important. This conclusion disagrees from the work of SMITH and co-workers (ref. 39).

NISHIHARA and YAMADA (ref. 30) conducted rotating beam tests on unnotched specimens (ø 9.0 or 10.0 mm) and specimens notched by a groove of 2 mm radius. Amongst the materials used was duralumin (the type was not specified). In these tests the stress amplitude was varied sinusoïdally. Various values for the minimum and maximum stress amplitude were used. No detailed results are given but it is reported that a good agreement with $\Sigma \frac{n}{N} = 1$ was obtained.

Similar tests on unnotched 24 S-T 4 specimens were performed by HARDRATH and UTLEY (ref. 16). They used two types of spectra, a sinusoïdal and an exponential one. Different values for the minimum and maximum stress amplitude were used. The results of $\Sigma \frac{n}{N}$ are given graphically in fig. 6.17. In general, the mean values were below unity which is somewhat more evident for the exponential spectrum. In these tests the overall mean of $\Sigma \frac{n}{N}$ was 0.62 as against 0.92 for the sinusoïdal spectrum.

FREUDENTHAL (ref. 9) also performing spectrum tests used a specially designed fatigue machine to apply the loads in a randomised sequence. Each stress amplitude was maintained constant for 10 load cycles. The next stress amplitude was chosen in some random way. Nevertheless the sumfrequencies of the six stress amplitudes, which were used, were in accordance with a planned load spectrum. FREUDENTHAL used four different load spectra, see fig. 6.18, in which the results of the spectrum tests are also given. For three spectra $\Sigma \frac{n}{N}$ is well below unity. Only for spectrum A, with relatively less high and many low loads $\Sigma \frac{n}{N} \simeq 1.25$, which is opposite to the results of HARDRATH and UTLEY, where the tests with relatively many high loads gave higher values of $\Sigma\, n/N$.

MARCO and STARKEY (ref. 27) performed rotating beam tests on unnotched specimens of 76 S-T 6 with stepwise increasing or decreasing stress amplitude. The results are given in fig. 6.19. The difference between both types of tests is evident. The first one gives values of $\Sigma\, n/N \sim 1.5$ whereas the second one gives values of $\Sigma\, n/N$ somewhat below unity. Among these tests there were also a number of two-step tests, and the results agreed qualitatively with the conclusions of DOLAN and BROWN (ref. 5).

It will have been noted that in almost all these rotating-beam test programs only unnotched specimens were used.

If one high pre-load is followed by a conventional fatigue test, it is more or less questionable whether this should be called a cumulative damage test. But as this type of test is thought to be informative in this respect it is still discussed here.

FORREST (ref. 6) studying the influence of internal stresses in rotating cantilever-beam specimens, pre-loaded specimens with a rather sharp notch to a very high stress and noticed a considerable increase in fatigue strength, see fig. 6.20. FORREST also investigated the effect of internal stresses formed by quenching and cold work by a sinking pass, the first giving compressive internal stresses and the second giving tensile internal stresses. The first treatment turned out to be beneficial whereas the second one was detrimental.

Similar results as obtained by FORREST were reported by ROSENTHAL and SINES (ref. 32) for 61 S-T and by TEMPLIN (ref. 43) for 75 S-T. Moreover, in these experiments the detrimental effect of residual tension stresses obtained by compression pre-loading was also shown.

BENNETT and BAKER (ref. 1) have tested unnotched sheet specimens in bending at $R = 0$. Positive as well as negative pre-loading was applied. The results are shown in fig. 6.21. At the higher test stresses the effect is not evident but at the lowest test stress the difference between positive and negative pre-loading is clear.

KEPERT and PAYNE (ref. 22) have tested a large number of complete wings. Some wings were preloaded before fatigue testing. The results are given in fig. 6.22, from which it can be seen that high pre-loads may give a considerable increase in life. The higher the maximum stress in the fatigue test the less is the increase in life.

An extensive study was reported by HEYWOOD (ref. 20 and 21). Fig. 6.23 gives the results for unnotched and notched sheet specimens. With the unnotched specimens no noticeable increase of life could be obtained, even by rather high pre-loads. For the sheet specimens with a transverse hole, a moderate increase in life was obtained. Also here this increase was less in fatigue tests with the higher maximum stress.

Fig. 6.24 shows the results for a number of different types of notched specimens. The effect of the pre-load on the endurance is illustrated by plotting horizontally the relative increase of the endurance and plotting vertically the pre-load stress divided by the yield stress ($S_{0.1}$). Also compressive pre-loading was employed. The general trend of these tests is clear and agrees with the results of the previously discussed test programs of this type. Also HEYWOOD found an important decrease in life, caused by compressive pre-loading.

To these pre-load tests HEYWOOD added a number of the following type of tests. A conventional fatigue test was interrupted at given moments for applying a high load, see fig. 6.25. In this figure the curve, representing the mean result of fig. 6.24 is also given. It turned out that a periodical application of high loads is much more effective than one high pre-load. This was also true for periodic high compressive stresses.

A limited number of tests was performed with 10 high pre-load cycles instead of one high pre-load. This seemed to be more effective than one high pre-load, which is in agreement with previously discussed axial-load tests.

7 Discussion of the reviewed test data.

In this chapter the discussion considers the mean results of fatigue tests and the scatter will be regarded only incidentally. In general the significance of a testprogram increases if each test is repeated many times. However also then inhomogeneity of the material tested may affect the results in some unknown way. Whereas inhomogeneity cannot always be avoided it should be recommended that sampling the specimens should occur in such a way that inhomogeneity may be recognized from the fatigue test results.

The experimental results presented in the previous chapter clearly show that the linear cumulative damage rule has no general validity and even in many cases does not provide a good approximation. Another striking feature of the previous chapter is the large variability of the testprograms which were performed by different investigators. The purpose of this chapter will be to evaluate the common characteristics.

Two affects are evident from the experimental results, viz.

(1) A high pre-load may have a considerable effect on the endurance at lower loads.

(2) Cyclic pre-loading can give a greater improvement of the endurance at lower loads than a single pre-load.

The first effect is rather evident for notched specimens and has been known for long. In general it is explained by internal stresses, caused by local yielding during the high pre-load (see ref. 6 and 20). These internal stresses can be beneficial or harmful, dependent on whether they lower or raise the mean stress. In redundant structures a high pre-load will also produce a load redistribution which may effect the fatigue resistance (ref. 20).

It is not so easy to understand why cyclic pre-loading may give a larger benefit than a single pre-load. In ref. 33 it was reasoned that cyclic pre-loading will cause cyclic slipping. This is not localized to the initial set of active slip planes but it will extend to adjacent slip planes. Microscopically a broadening of the slip regions has been observed (ref. 2). Therefore, the state of the crystal structure left after cyclic high pre-loading will be different from the state after one high pre-load. The cyclic strain-hardening may induce a higher fatigue resistance than a single deformation of a metal. It is quite remarkable that HEYER found that a cyclic pre-loading until 80 % of the endurance at the high pre-load still results in a marked improvement of the endurance at the lower test load, whereas at such a high pre-load cycle-ratio microcracks were certainly formed and probably small cracks might have been visible.

Another remarkable effect is that even unnotched specimens show an improvement in the fatigue endurance by high pre-loading. In this respect it may be noted that HEYWOOD did not find a noticeable benefit by one rather high pre-load (see fig. 6.23) whereas the present authors ((ref. 33) and GROVER and co-workers (ref. 15) found a beneficial influence of cyclic pre-loading of unnotched specimens. Also in unnotched specimens a high load may induce a stress redistribution on a microscopical scale, because a number of crystals will deform plastically, leaving the material after unloading in a state which is microscopically not stress-free. In ref. 33 the pre-load was not high ($N_H = 200.000$) and a moderate increase in endurance at the test-stress was found, see fig. 6.11. In ref. 15 the cyclic pre-load was much higher and the improvement of the endurance was considerable at $\frac{n_1}{N_1} = 0.10$, see fig. 6.9. At higher values of the pre-stress cycle-ratio the improvement decreased again.

FORREST (ref. 6) has shown that unfavourable internal stresses may be relieved by a high pre-load and this also applies to unnotched specimens. However for alleviating or building up internal stresses one pre-load should be sufficient and thus it remains to be explained why cyclic pre-loading may be more effective than one pre-load.

From the foregoing it will be clear that our knowledge of the fatigue phenomenon shows a gap here. The damaging effect has been identified by microcracks and cracks and the beneficial effect may partly be explained by the building up of internal stresses. But about the strain-hardening and the internal stresses which remain localized around the tip of the growing microcracks during the fatigue test little is known.

A number of interesting tests has been executed by HEYWOOD (ref. 20). He compared the effect of a single high pre-load with the effect of periodically applied high loads. It was noticed that the latter had a much better effect, see fig. 6.25. HEYWOOD gives two possible explanations (1) The internal stresses may decrease during the fatigue test and they are restored again by the periodic high loads (2) Microcracks may have been formed. Their growth will be retarded by the internal stresses built up around these cracks by the periodic high loads. Both reasons may be effective.

It is obvious that the benefit of high loads will depend on the test stress (S_a and S_m). From fig. 6.22 and 6.23 it is clear that the higher the load range of the fatigue test the less the benefit of the pre-load will be. The results do not allow to separate the effects of S_a and S_m but decreasing S_a as well as S_m will increase the effect. That this also holds for the cyclic pre-loading may be seen from fig. 6.1; 6.2 and 6.3 and by comparing fig. 6.10 with fig. 6.14. The beneficial effect was also obtained in the spectrum tests of HEYER (fig. 6.5) and WÅLLGREN (fig. 6.13). Both explain this by internal stresses formed at the highest stress amplitude. In these cases $\Sigma \frac{n}{N} = 1$ would have given a safe life estimate.

If now the results of the present investigations are studied as given in fig. 6.14 the following points may be noted. A rather high pre-load ($^2/_3$ S_u) gives a moderate increase of the endurance at 7.2 ± 3.2 kg/mm² (10.2 ± 4.6 kips). By cyclic pre-loading no noticeable beneficial effect is found. Nevertheless the interval tests showed $\Sigma \frac{n}{N}$ values well beyond unity. So there seems to be a difference in results between periodic cyclic overstressing and cyclic pre-stressing. The highest results in the interval tests are found if the high stress lasted relatively short and the worst results are obtained if the high stress lasted relatively long. This may be interpreted in such a way that the high stress cycles have some beneficial influence but if they are maintained longer, they also increase the depth of the (micro)cracks at a higher rate than this occurs at the low stress amplitude.

It would seem that in these interval tests some agreement is found with the results of HEYWOOD (fig. 6.25) who found that periodic high loads are more effective than one high pre-load. Now there is a difference in the way of loading, illustrated in fig. 7.1, which is self-explanatory. In the tests of HEYWOOD the high load may produce beneficial internal stresses whereas the effect on the internal stresses of a gradually increasing stress amplitude and afterwards gradually decreasing stress amplitude is difficult to predict.

It may be noted that FORREST (ref. 7) reports a series of preliminary tests in which no advantage of pre-loading riveted joints could be obtained. FORREST points out that riveted joints should not be considered to be simply notched specimens. The riveting will have induced compressive stresses around the hole. High pre-loads may loosen the rivets which is unfavourable. Moreover, in rivet-joints a part of the load is transmitted by friction which part may also be affected by high loads. Fretting corrosion which is no exception in loosened joints may thus be dependent on the load sequence.

Until now the discussion was related to the effect of a high pre-load, high cyclic pre-loading, periodic high loads and periodic high cyclic-loading. Now the attention will be turned to the L-H tests which are less numerous. For this type of test it is thought that internal stresses formed at the low pre-stress are quite unimportant with respect to the continuation of the fatigue process at the higher test stress. The same should be expected for strainhardening effects. At low stresses the micro-cracks are formed at a relatively later stage (higher n/N) than at high stresses. So for L-H test it should be expected that $\Sigma\, n/N$ values are somewhat above unity to a maximum of about $1 + \frac{n_1}{N_1}$ and a minimum of 1. This is more or less confirmed by the L-H tests of GROVER and co-workers, see fig. 6.9 and by the L-H tests on the notched specimens of ref. 33, see fig. 6.11. However the tests on the unnotched specimens of ref. 33 and to a certain extent the L-H tests of SMITH and co-workers (fig. 6.12) and of the present investigation (fig. 6.14) are in disagreement with this reasoning. They show values of $\Sigma \frac{n}{N}$ which are somewhat below unity. The results are never very much below unity. These somewhat unexpected results remain to be explained. Perhaps for the unnotched specimens of ref. 33 and 39 the fact that it concerns cladmaterial may have played a role.

The interval tests on unnotched specimens of ref. 33 and 39 agree very well. All values of $\Sigma \frac{n}{N}$ were about unity or a little lower. There seems to be little influence whether an interval test starts at the low or the high stress.

The results of the interval tests on the notched specimens of ref. 33 and the present investigation show $\Sigma\, n/N$ values which are beyond unity. In ref. 33 the high and the low stress amplitudes are applied alternately for 5 % of the corresponding endurances. As for these specimens the high pre-stress had a marked beneficial influence it might be expected that in such an interval test the low-stress cycles will be more or less ineffective which then should give $\Sigma \frac{n}{N} = 2$. Now in the tests $\Sigma \frac{n}{N} \approx 1.8$, because as soon as a macroscopical crack is formed the lower stress is no longer ineffective. This could be deduced from the oyster shell-markings on the surface of the failure. That the lower stresses become less effective is also suggested by the spectrum tests of HEYER (ref. 19) and WÅLLGREN (fig. 6.5 and 6.13), already discussed before. In the interval tests of the present investigation the high-stress cycles have some beneficial influence but the low-stress cycles are far from ineffective.

If now another program of WÅLLGREN (ref. 45), see fig. 6.7 and 6.8, also concerning spectrum tests, is studied it will be noted that here values of $\Sigma \frac{n}{N}$ below and beyond unity occur. The unnotched specimens (type a in fig. 6.7 and type d in fig. 6.8) give results for $\Sigma \frac{n}{N}$ which in general do not deviate very much from unity. The highest value, 1.64, was obtained for 75 S-T and a spectrum in which the highest stress amplitude was rather high ($N = 1{,}300$). To a certain extent the results of the unnotched specimens may be considered as exhibiting some agreement with the tests of ref. 15, 33 and 39.

The results of the notched specimens of fig. 6.7 and 6.8 are in general beyond unity. This was true for 75 S-T in all cases. For 24 S-T values below unity were found in those spectrum tests in which the highest stress amplitude was not very high. The seriousness of this stress is more or less characterized by its corresponding endurance which is also given in fig. 6.7 and 6.8. This fact illustrates once more the beneficial effect which high stresses may have.

An interesting feature of WÅLLGREN's test program is that in a number of tests he omitted the stress cycles which were below the fatigue limit. From the previous it will be clear that if any effect should be expected this should be an increase of $\Sigma\, n/N$. These low stresses do not contribute to $\Sigma \frac{n}{N}$ because $N = \infty$ but they will be effective during the macro-crack stage. So their effect should also be more important for the notched specimens than for the unnotched ones. This is confirmed by the 75 S-T specimens, see fig. 6.8, whereas the 24 S-T specimens in this respect do not behave in a distinct way (fig. 6.7). GASSNER (ref. 11) has noted an increase in endurance by omitting the lower stress amplitudes in spectrum tests.

The rotating beam tests were nearly all conducted with unnotched specimens. In the previous chapter the two-step tests of DOLAN and BROWN (ref. 5) were reported which showed that for H-L tests $\Sigma\, n/N$ was slightly below unity whereas for L-H tests $\Sigma \frac{n}{N}$ was somewhat beyond unity. These results may be thought to be confirmed by the tests of MARCO and STARKEY, see fig. 6.19. It was already discussed that these results are not unreasonable for tests in which the stress increases during the fatigue test. However in tests in which the stress decreases, a beneficial effect of the high stresses might have been expected but did not turn out. Comparable tests on sheet specimens also with $S_m = 0$ were performed by SMITH and co-workers (fig. 6.12) and concerning the effect of the stress sequence they found the opposite result.

The interval tests of DOLAN and co-workers (fig. 6.15) and CORTEN and co-workers (fig. 6.16) are difficult to interpret with respect to the interaction of the two applied stress amplitudes. Moreover, both test programs are not always in good agreement. CORTEN and co-workers conclude that the damage increase is mainly determined by the high stress amplitude which is not so strange as, in general, the periods of high stress cycles expressed in cycle ratio's were much longer than the periods of low stress cycles.

Rotating beam spectrum tests were performed by NISHIHARA and YAMADA (ref. 30), HARDRATH and UTLEY (fig. 6.17) and FREUDENTHAL (fig. 6.18). Whereas the first two investigators report a good fit of the results to $\Sigma \frac{n}{N} = 1$, the others find, in general, values of $\Sigma \frac{n}{N}$ below unity. It is noteworthy that FREUDENTHAL obtained the highest value of $\Sigma \frac{n}{N}$, viz. 1.25 in a test with the least number of high stress cycles. FREUDENTHAL's way of spectrum testing i.e. a randomized load sequence, will be discussed further in chapter 9.

It will be tried now to recapitulate the most important trends recorded in this chapter.

(1) There is a marked difference in the cumulative-damage behaviour of notched and unnotched specimens.

(2) For notched specimens a beneficial effect may be expected from positive high loads which cause local yielding. The effect may be obtained by one high pre-load but, in general, the benefit will increase by periodically applying high loads. The effect can be explained by the formation of internal stresses.

(3) Cyclic high pre-loading may give a higher benefit than a single high pre-load cycle. So apart from the internal stresses something else must be effective which probably will be a cyclic strainhardening effect.

(4) In spectrum tests on notched specimens at positive mean stresses $\Sigma \frac{n}{N} > 1$ is likely to occur if also high stresses are included in the spectrum. Values much above unity are possible. If too many high load-cycles are included the endurance will be lowered again.

(5) In spectrum tests on notched specimens stresses below the fatigue limit should not be omitted as these stresses are certainly effective as soon as the original fatigue limit is lowered by fatigue cracks. Including these stresses does not necessarily mean that $\Sigma\, n/N = 1$ will give an unsafe life estimate. Some available test results gave $\Sigma\, n/N$ beyond unity.

(6) Interval tests on notched specimens give results of $\Sigma \frac{n}{N}$ beyond unity.

(7) On axially loaded unnotched specimens the deviations of $\Sigma \frac{n}{N} = 1$ for all types of tests are noticeably smaller than for notched specimens. In many cases the deviations from unity are small. The beneficial effect of high pre-loads was obtained in some cases, but not in all cases.

(8) For interval tests and spectrum tests on unnotched sheet specimens $\Sigma \frac{n}{N}$ was about unity. For interval tests and spectrum tests on unnotched rotating beam specimens the results were less systematical but values well below unity were not seldom.

In this chapter 24 S-T, 75 S-T and some other materials were treated as if they were the same material. They are indeed of the same type in so far as they are precipitation-hardening light alloys and there are some indications in the testprograms discussed that they behave in a similar way in cumulative-damage tests. Nevertheless some disagreement in similar tests may have been introduced by using different alloys. Probably a better method for comparison might be to use non-dimensional stresses, for instance by dividing all stresses by the yield strength. However, for notched specimens it would be necessary for a good appreciation of the effect of stresses to know the stress distribution in the specimen. Since the purpose of this chapter was to obtain qualitative conclusions, this has not been done.

With repect to the type of material it was already noted that some investigators have used clad material whereas others used bare material. Probably this will not have affected noticeably the results for the notched specimens and perhaps this also holds for the unnotched specimens. SEBISTY and EDWARD (ref. 35) have shown that in unnotched specimens cracks penetrate through the cladding quite rapidly even at low stress amplitudes. They also showed that the transition of these cracks into the core material is retarded largely. In notched specimens of bare material microcracks will also be formed at an early stage and therefore the cladding will not have a marked effect on the results for notched specimens. But it is questionable whether this reasoning applies fully to the unnotched specimens.

8 The cumulative damage concept.

As early as 1924 PALMGREN (ref. 31) published the hypothesis which is now more generally known as the cumulative damage hypothesis. PALMGREN suggested that applying n_1 times a stress to which an endurance N_1 corresponds is equivalent to consuming $\frac{n_1}{N_1}$ of the fatigue resistance and thus failure should occur at the moment that

$$\frac{n_1}{N_1} + \frac{n_2}{N_2} + \frac{n_3}{N_3} + \ldots = 1$$

or

$$\Sigma \frac{n_i}{N_i} = 1. \tag{8.1}$$

Equation (8.1) will be called the linear cumulative damage rule. PALMGREN did not give any derivation for this rule. He needed it for ball-bearing life calculations.

PALMGREN's cumulative damage concept is illustrated by fig. 8.1a. Between the vertical stress axis and the S-N curve lines of equal damage can be drawn. They are determined by

$$\frac{n}{N} = \text{constant.}$$

LANGER (ref. 25) in 1937 introduced a refinement by dividing the fatigue phenomenon in two stages, viz. (1) a pre-crack stage and (2) a crack stage. He postulated that at different stress amplitudes the same state of damage was reached if the number of applied load cycles in the stage concerned had the same ratio to the endurance of that stage. This is illustrated by fig. 8.1b. If the crack starts at M load cycles and failure occurs at N load cycles, lines of constant damage are given by

$$\frac{n}{M} = \text{constant}, \quad n < M$$

and

$$\frac{n-M}{N-M} = \text{constant}, \quad n > M.$$

n is the number of load cycles. It will be clear that this implies that in cumulative tests the initiation of a crack occurs at the moment that

$$\Sigma \frac{n_i}{M_i} = 1$$

and that failure occurs if

$$\Sigma \frac{n_i'}{N_i - M_i} = 1$$

in which n_i' is the number of load cycles at a given load range ($Sm_i \pm Sa_i$) applied after the crack initiated.

Clearly, the concept of LANGER is identical to PALMGREN's concept if $\frac{M}{N} = \text{constant}$.

The difficulty introduced by LANGER's method is that it can only be used if M is known. So the moment at which the transition of the pre-crack stage to the crack stage occurs should be determined. However, the present state of knowledge about crack propagation is such that this moment depends on the refinement of the observation methods. It is believed that micro-cracks are initiated at a very early stage of the fatigue process. This gives a more or less arbitrary character to LANGER's hypothesis and it makes it difficult to apply.

MINER (ref. 28) in 1945 was the first to give a derivation of the linear cumulative damage rule. He assumed that the work that can be absorbed until failure is a constant W and the work w_i absorbed during n_i load cycles of the same load range is proportional to n_i. It then follows that

$$\frac{w_i}{W} = \frac{n_i}{N_i} \quad \text{or} \quad w_i = W \frac{n_i}{N_i} \tag{8.2}$$

$W = \Sigma w_i$ at the moment of failure.

$$W = \Sigma W \frac{n_i}{N_i}$$

or

$$\Sigma \frac{n_i}{N_i} = 1.$$

Equation (8.2) means that the energy absorbed in each load cycle of a fatigue test is a constant. It is generally recognized that this is not true, which implies that this derivation is not correct.

However, $\Sigma \frac{n_i}{N_i} = 1$ has been derived by NISHIHARA and YAMADA (ref. 30) on a completely different basis. They start from the relation

$$x = f(y) \tag{8.3}$$

in which x is the cycle ratio and y the degree of fatigue. This function should be valid for any loadrange which causes fatigue failure. In the notation of this report (8.3) becomes

$$\frac{n}{N} = f(y). \tag{8.4}$$

This relation means, that the fatigue phenomenon is exactly the same process at any load range, provided that one thinks in terms of cycle ratio's in stead of load cycles.

If two fatigue tests at stress amplitudes S_i and S' are performed, then the same degree of fatigue damage y is obtained if

$$\frac{n_i}{N_i} = \frac{n'}{N'}. \tag{8.5}$$

This follows from relation (8.4). For the degree of fatigue $y + \Delta y$ equation (8.5) becomes

$$\frac{n_i + \Delta n_i}{N_i} = \frac{n' + \Delta n'}{N'}. \tag{8.6}$$

This implies that Δn_i times S_i and $\Delta n'$ times S' added the same damage increment Δy.

(8.5) and (8.6) give

$$\frac{\Delta n_i}{N_i} = \frac{\Delta n'}{N'}. \tag{8.7}$$

(8.7) means that each cycle ratio increment Δn_i times S_i of an arbitrary spectrum may be replaced by $\Delta n'$ times S'

$$\Delta n' = N' \frac{\Delta n_i}{N_i}. \tag{8.8}$$

Failure will occur if

$$\Sigma \Delta n' = N'. \tag{8.9}$$

Combining (8.8) and (8.9) gives $\Sigma \frac{\Delta n_i}{N_i} = 1$ at failure. This is identical to $\Sigma \frac{n_i}{N_i} = 1$.

It will be noted that this derivation has been given without defining what damage actually is. According to NEWMARK (ref. 29) it is impossible to define fatigue damage in a simple way. Only stages of equal damage can be defined. NEWMARK considered two specimens tested at different stresses S_1 and S_2 as equally damaged if they had the same remaining endurance at a given test stress and he thought this concept to be applicable for interval tests in which only the stresses S_1 and S_2 were used. Still there are objections against this concept because also this definition implies that equal damage is qualified by one parameter ,i. e. the remaining endurance at the test stress. NEWMARK himself has already mentioned some objections against this concept, because different processes are going on during the progress of a fatigue test. For instance:

(1) Macroscopically some plastic yielding occurs depending on the stress level. Internal stresses built up by this yielding will, therefore, also depend on the stress level.
(2) Microscopical slip and strainhardening in slip regions will occur which is more severe at higher stress amplitudes.
(3) Weak points or microcracks are formed sooner and more frequently at high stresses.
For light alloys to these reasons may be added:
(4) The precipitation will proceed as a consequence of the alternating stress. The rate of this phenomenon will be stress-dependent.

More reasons may be possible.

The fact that the state of fatigue damage cannot be defined by one parameter also implies a rejection of the linear cumulative damage rule.

Much trouble is caused by the difficulty of defining fatigue damage. SHANLEY (ref. 36) has tried to eliminate this difficulty by identifying fatigue damage by depth of the fatigue crack. He interprets the fatigue phenomenon in terms of progressive unbonding of atoms as a result of reversed slip, caused by cyclic loading. An exponential law for the growth of the fatigue crack is assumed.

$$h = A\, e^{\alpha n} \tag{8.10}$$

h = crack depth, A = constant, α = factor depending on the stress amplitude, n = number of load cycles. The rate of crack propagation is given by

$$\frac{dh}{dn} = A\, \alpha\, e^{\alpha n} = \alpha h. \tag{8.11}$$

At a certain crack depth $\frac{dh}{dn}$ will be higher for higher stresses. For $S_m = 0$ and unnotched specimens SHANLEY derives

$$\alpha = C\, S^x$$

based on considerations in which the crack growth is related to the amount of slip.

$$h = A\, e^{CS^x n}. \tag{8.12}$$

Failure is assumed to occur at some constant crack depth h_0

$$h_0 = A\, e^{CS^x N}. \tag{8.13}$$

This relation actually represents the S-N curve.

It may be noted that $n = 0$ gives $h = A$ and so A is the initial depth of the crack. However, in SHANLEY's picture of fatigue initial cracks are not supposed to exist. An initial crack is formed during the first load cycle. The inconsistency of (8.12) could be removed by replacing n by $n - 1$ in all equations for crack depth. So A actually represents the crack depth after the first cycle. However, this is usually of no practical significance.

Combining (8.12) and (8.13) gives

$$h/h_0 = (h_0/A)^{\left(\frac{n}{N} - 1\right)}. \tag{8.14}$$

This equation means that the crack-growth curves for different stresses are affine, i. e. that plotting the crack depth as a percentage of the original unfailed cross-sectional area against the cycle ratio n/N will give the same curve for any stress. Relation (8.14) is a special type of relation (8.4) and it was already shown that then the linear cumulative damage rule may be derived.

SHANLEY has also given a second derivation by dropping the assumption that A in relation (8.12) and (8.13) is independent of the stress. He replaces A by $A'S^x$, also now reasoning that the crack depth formed in the first load cycle is related to the amount of slip. (8.12) and (8.13) now become:

$$h = A'S^x e^{CS^x n} \tag{8.15}$$

$$h_0 = A'S^x e^{CS^x N}. \tag{8.16}$$

(8.16) again represents the relation for the S-N curve. Now (8.15) and (8.16) give

$$\log h/h_0 = (1 - n/N) \log \frac{A'S^x}{h_0}. \qquad (8.17)$$

If $y = h/h_0$ is considered as the degree of fatigue (8.17) may be written as

$$\frac{n}{N} = f(y, S) \quad \text{or} \quad y = f\left(\frac{n}{N}, S\right). \qquad (8.18)$$

(8.18) implies non-affine damage curves, which is illustrated by fig. 8.2. From (8.17) it is clear that $\log h/h_0$ versus n/N gives a linear relation. This relation is shown for two different stresses in fig. 8.2a. In fig. 8.2b and c a graphical solution for the life calculation in H-L and L-H tests is given. For the first type of test $\Sigma\, n/N < 1$ and for the second $\Sigma\, n/N > 1$. That this cumulative damage concept is different from the linear cumulative damage rule is evident.

For spectrum tests SHANLEY derived a special formula. For this purpose a reduced stress amplitude S_R is introduced ($S_m = 0$!). This stress gives by definition the same endurance as the spectrum test $N_R = \Sigma\, n_i$.

The calculation of S_R will be illustrated by considering an interval test with intervals each consisting of $\Delta\, n_1$ times S_1 plus $\Delta\, n_2$ times S_2, such as shown in figure 6.11 *). The mean rate of crack growth during one interval is given by:

$$\left(\frac{dh}{dn}\right)_{\text{interval}} = \frac{\Delta\, n_1 \left(\frac{dh}{dn}\right)_1 + \Delta\, n_2 \left(\frac{dh}{dn}\right)_2}{\Delta\, n_1 + \Delta\, n_2}. \qquad (8.19)$$

According to the definition of S_R this rate must be equal to the rate at the reduced stress at the same crack depth

$$\left(\frac{dh}{dn}\right)_{\text{interval}} = \left(\frac{dh}{dn}\right)_R \qquad (8.20)$$

From (8.15) follows:

$$\frac{dh}{dn} = CS^x A'S^x e^{CS^x n} = CS^x h. \qquad (8.21)$$

Combining (8.19), (8.20) and (8.21) gives

$$\frac{\Delta\, n_1 CS_1{}^x h + \Delta\, n_2 CS_2{}^x h}{\Delta\, n_1 + \Delta\, n_2} = CS_R{}^x \,.\, h$$

or

$$S_R{}^x = \frac{\Delta\, n_1 S_1{}^x + \Delta\, n_2 S_2{}^x}{\Delta\, n_1 + \Delta\, n_2}. \qquad (8.22)$$

Generalization gives

$$S_R{}^x = \frac{\Sigma\, \Delta\, n_i S_i{}^x}{\Sigma\, \Delta\, n_i}. \ ^{*)} \qquad (8.23)$$

The value of x has to be derived from the S-N curve given by relation (8.16). This formula contains three parameters, viz. $\frac{h_0}{A'}$, C and x.

There is one objection against relation (8.19) on which (8.23) is based. Relation (8.19) is not valid for small crack sizes as will be clear from fig. 8.2a because the test at the high stress amplitude S_1 starts at a crack size which at the low stress amplitude is reached only after many load cycles. This inconsistency is inherent to the inconsistency already discussed before, which was eliminated by considering n to be the number of load cycles applied after the first load cycle.

A more serious objection is that this method is still a one-parameter method, although relation (8.18) might suggest a two-parameter concept. The only parameter for the state of fatigue is the depth of the fatigue crack and (8.18) only implies non-affine crack growth curves (damage curves). The state of the crystal structure at a certain crack depth will not be the same when this crack depth is reached at different stresses. Another shortcoming is that this damage concept does not allow the fatigue limit to be raised neither to be lowered.

Whereas thus the derivation of relation (8.23) is thought to lack sufficient physical background, this formula may still be appreciated merely as an empirical formula. It then is also no longer necessary to consider x as a parameter which is dependent on the S-N relation only, whilst, moreover, relation (8.23) may be applied to notched specimens and also for $S_m \neq 0$, x should then be chosen in such a way that relation (8.23) suits the test results. An evaluation of x-values for the available test-results may show its usefulness. Some more attention will be given to this relation in chapter 9.

Whereas the introduction of the fatigue-crack depth as a replacement of the vague term fatigue damage is considered to be an improvement, it will be clear that an urgent need is felt for parameters which will incorporate the effect of, for instance, the internal stress or the strainhardening ahead of the fatigue crack. However, it is evident that much basic research is necessary before this may be done in a reasonable way.

An experimental approach to this problem is to define the state of fatigue at a certain moment of a fatigue test by the remaining endurance at all possible load ranges. This means that a specimen in any state of fatigue may be considered to be a new specimen with its own fatigue diagram by which it is characterized. In ref. 18 HENRY treats the problem in such a way. He restricts himself to the interpretation of tests for which $S_m = 0$. Then each state of fatigue is characterized by one S-N curve. This S-N curve is obtained by

*) The formula (8.23) derived here differs from the "$2\,x$-formula" given in ref. 36. The derivation given in ref. 36 is incomplete and it must be assumed that it either contains an error or is based on some additional assumption which has not been mentioned.

*) Instead of $S_R^{2x} = \frac{\Sigma \Delta n_i S_i^{2x}}{\Sigma \Delta n_i}$ derived in ref. 36. Relation (8.23) is not identical to relation (16) of ref. 36 which is derived from (8.12).

dividing the stress ordinate of the S-N curve of the virgin specimens by a factor C, reasoning that fatigue damage may be identified with a notch effect. HENRY restricts this to stresses below the proportional limit. For two-step tests the value of C at the moment of changing from the pre-stress to the test stress is easily obtained. The endurance of the new S-N curve at the pre-load stress level is equal to the remaining endurance at that stress. So one point of the new S-N curve is known and the curve may be constructed then. This is illustrated in fig. 8.3. HENRY reports good results for some two-step tests on steel. An advantage of the method is that it allows a decrease of the endurance limit. A serious limitation, however, is that it is restricted to stresses below the proportional limit and a mean stress equal to zero. It is questionable whether this method could be developed for application in spectrum tests on notched specimens with $S_m \neq 0$.

9 Some remarks on fatigue testing of aircraft structures.

Fatigue may be considered to be a basic phenomenon from the viewpoint of metal physics. It is more questionable whether cumulative damage should be considered as such a problem. Many researchworkers would not tend to investigate this problem physically as long as they do not understand the basic fatigue phenomenon. Therefore, two questions seem worthwhile:

(1) What is the value of the previously discussed tests with respect to the basic fatigue phenomenon?
(2) What is their value with respect to practical questions such as fatigue testing of aircraft structures?

Concerning the first question only two-step tests, including tests with a high pre-load, are thought to be of some value. Something may be learned about the time-history of fatigue damage, internal stresses, strainhardening and so on. It may even be true that two-step tests are particularly suitable for such studies.

To answer the second question, the fatigue problem from the practical point of view will be outlined here briefly. In service, an aircraft encounters loads of different magnitudes. These loads were measured in several aircraft under different conditions. At the moment a fair estimate of the load spectrum of an aircraft which is in planned service is available. The problem is to base a life estimate for a certain aircraft structure on this load spectrum. The methods used for this purpose will be discussed now, after which an appraisal of these methods, based on the discussion in the previous chapter will be given.

GASSNER (ref. 11) has advised that the best thing that can be done is performing a test in which the service loads are simulated as nearly as possible. To this end he proposes the spectrum tests and he made an extensive study of this type of test. He used load spectra measured in flight. Once the type of spectrum has been chosen there are still two variables left, for which may be taken the mean stress S_m and the maximum stress of the spectrum S_{max}, see fig. 9.1a. If the endurance found in the spectrum test is called N' GASSNER gives his results plotting S_{max} versus N'. This is illustrated in fig. 9.1b in which the next step is also given, which involves the plotting of lines of constant endurances in an $S_{max} - S_m$ diagram (fig. 9.1c). It will be noted that apart from the way of loading the evaluation of test data is essentially the same as for conventional fatigue tests. The value of the diagram is possibly restricted to the type of load spectrum employed, but actually this also applies to the conventional fatigue tests and it may be worthwile to consider which type of fatigue diagram is the most valuable one for the aircraft designer.

As spectrum tests on complete structures would be very expensive GASSNER has tried to relate the results of spectrum tests to the results of conventional fatigue tests. He starts from a comparison of the spectrum fatigue diagram (fig. 9.1c) and the conventional fatigue diagram. The comparison is performed for some types of light-alloys and some types of notched specimens. Based on this comparison GASSNER gives a conversion method to derive the spectrum fatigue diagram from the conventional fatigue diagram. The conversion method was ascertained in such a way that it was independent of the type of light-alloy. The method actually involves that each point of the spectrum fatigue diagram is a conversion of a point of the conventional diagram. The method, moreover, implies that for corresponding points the same mean stress applies. GASSNER, reasoning that a desired life under a given spectrum represents one point of the spectrum fatigue diagram, advises to check the corresponding point of the conventional fatigue diagram. Thus, this implies a replacement of the spectrum test by a conventional fatigue test.

The conversion method is embodied in a diagram. Since this method is merely an empirical result, the physical meaning of which is difficult to judge, its value will not be under discussion here. It can only be verified by experiments. Its empirical value has to be considered as being an extrapolation of experience.

It would be very convenient if the linear cumulative damage rule could be adopted for a reliable life estimate, as it is such a simple method. However, the survey of available test data in chapter 6 has shown that in general this rule will not give a correct result. It should be noted that such a life estimate is in principle a calculation method. WÅLLGREN (ref. 45), considering that $\Sigma \frac{n}{N} = 1$ does not hold true, performed a test program in which spectrum tests were executed on simple structural elements. Two types of spectrum were used. The purpose of WÅLLGREN was to obtain a clear picture of how $\Sigma \frac{n}{N}$ may vary with the type of specimen, the type of material and the type of load spectrum. It was hoped that such variations would behave in some consistent way, as then the results could be extrapolated to other circumstances.

The variations of $\Sigma\, n/N$, found in the experiments were not as systematical as desirable. Nevertheless WÅLLGREN concludes that $\Sigma\, \frac{n}{N} = 1$ may be employed to obtain a provisional life estimate, whereas the deviations from these calculated results may be estimated with the aid of the results of his test program.

WÅLLGREN actually suggests an extrapolation of the results of spectrum tests. This is in agreement with GASSNER's method but a different extrapolation method is used.

SHANLEY (ref. 36) has proposed a nonlinear cumulative damage rule which was already discussed in chapter 8. His formula for spectrum tests is

$$S_R{}^x = \frac{\Sigma\, n_i S_i{}^x}{\Sigma\, n_i}. \qquad (9.1)$$

This method implies that all load cycles (at stresses of magnitude S_i and number n_i) are reduced to load cycles at stresses S_R (the reduced stress) in such a way that the endurance N_R at the reduced stress S_R should be the same as the endurance N' of the spectrum test. From formula (9.1) it will be clear that S_R depends on the value of x. SHANLEY has proposed to take a value equal to twice the inverse slope of the S-N curve if this curve is plotted on a log-log scale. If in (9.1) stresses below the fatigue limit are disregarded SHANLEY has shown (ref. 37) that relation (9.1) is much more conservative than $\Sigma\, \frac{n}{N} = 1$. It may be possible that it will always be on the safe side. However, quantitatively it is not known how safe it is and this is an important disadvantage. SHANLEY has pointed out that actually in a spectrum test stresses below the fatigue limit may not be neglected as they may contribute to the growth of the fatigue damage. This statement is confirmed by tests of GASSNER (ref. 11) and WÅLLGREN (ref. 45). However, it is difficult to decide which stress amplitudes should still be included. This once more indicates that relation (9.1) has to be considered as an empirical method. It is believed that its practical value can only be judged by applying the method to spectrum tests with a positive mean stress on typical structural elements.

WALKER analysed the fatigue problem for transport aircraft (ref. 44). Starting from gust frequency analysis and using the linear cumulative damage concept he concludes that the most damaging gust loads have an equivalent gust velocity of 8 feet/sec. This is illustrated in fig. 9.2. WALKER proposes to take a factor of safety of 1.25 and to test the complete structure at a load corresponding to 10 ft/sec. Each failure in the fatigue test should be repaired and the test continued until a survey of most critical components is obtained. From each critical component six samples should be tested separately at the same load which it carried in the fatigue test on the complete structure. Two-thirds of the lowest logarithmic mean endurance of the respective critical parts is considered to be a representative endurance for the complete structure. If this value is N^*, WALKER suggests that the number of safe flying hours may be given by

$$L = \frac{kN^*}{V}$$

in which L = life in flying hours
V = normal operating equivalent speed
k = constant, depending on the operational conditions.

Based on experience, (which is not published), WALKER takes $k = 2.5$ for normal transport aircraft flying at an operating height above 8000 ft.

From chapter 7 and 8 it will be clear that the damage distribution curve of fig. 9.2 cannot be considered as a realistic picture of the effect of different gust loads. Therefore, the choice of a load corresponding to a gust velocity of 10 ft/sec as a representative load range is more or less arbitrary. However WALKER did not use $\Sigma\, \frac{n}{N} = 1$, to obtain the life estimate.

In a later publication (ref. 44a) WALKER proposes to reduce all stresses to one representative stress level, which corresponds to a load induced by a gust with a velocity of 10 ft/sec. The number of greater and lesser gusts are corrected to this level by the linear cumulative-damage rule. The full-size test then gives a quantitative life estimate, thus dropping the empirical factor k. The method is then more or less similar to SHANLEY's method of using a reduced stress. However, this stress level is determined in another way, whereas the way of reducing the spectrum is also different.

An important feature of the full scale test on the entire structure is undoubtedly that a survey of the weakest components is obtained. Testing of six samples of each weak component offers the possibility of introducing the scatter into the life estimation. Since WALKER's first method is based on not-mentioned experience it is not possible to give an appraisal of its empirical value.

The second method incorporates fully the linear cumulative damage rule and thus lacks sufficiently rational background. However, from the results discussed in chapters 6 and 7, it may be expected that for gust spectra this method will be on the safe side.

The previously discussed methods to obtain a life estimate are of two different types:

(1) Extrapolation of spectrum tests in which similar spectra and notches are employed.
(2) Relating spectrum-test results to conventional fatigue-test results.

As to method (1) it can be noted that it is more or less similar to the problem of deriving S-N curves for a structure or structural element from the S-N curves of simply notched specimens. The difficulties affecting this problem are well recognized but not sufficiently solved. One needs only to think of the size effect, the effect of stress gradient in the notch, the effect of surface finish etcetera. All these difficulties also apply to method (1) and even more difficulties are introduced here, for instance the effect of the type of spectrum to be used. Thus it can be tried to obtain a life estimate with method (1) but it should be realized that errors are quite well possible.

Method (2) involves the use of a cumulative-damage rule (linear or non-linear). All the difficulties mentioned for method (1) also apply to method (2) whereas in method (2) an uncertainty is added by the use of the cumulative damage rule.

Whereas extrapolation of test results always will introduce an uncertainty it is evident that the uncertainty will be minimized by extrapolation of the most realistic test-data to be obtained. Thus an advantage of WALKER's method is that he extrapolates from test results of the entire structure. On the other hand it should be realized that conventional fatigue tests cannot represent the beneficial effect of high loads and the probably harmful effect of many low loads.

From the previous it will be clear that there is no reason to be optimistic concerning the value of simplified fatigue tests for a realistic life-estimate of an aircraft. Which simplified method will be the best method is a problem beyond the scope of this report. It has only been tried to discuss some proposed methods and to analyse their actual meaning in the light of the available test-data of cumulative-damage tests.

Because our knowledge of the cumulative-damage phenomenon is still insufficient, it seems logical to perform our tests as realistically as possible. This has been stressed by GASSNER (ref. 11) and later by SHANLEY (ref. 37).

Now a spectrum test seems to be rather realistic, but the discussion in chapter 7 allows some remarks in this respect. Replacing service loads by a spectrum test still incorporates some assumptions, at least for aircraft structures.

TEICHMANN and GASSNER (ref. 42 and 11) have pointed out that service loads are only indicated correctly by two parameters, for instance mean load and load amplitude. This means that load spectra should be given as three-dimensional plots, the frequency being the third variable. A determination of such a spectrum needs a complete graphical record of load versus time. As the evaluation of a spectrum in this way would be very laborious, only one parameter, the load amplitude, is measured. GASSNER (ref. 12) has pointed out that in this way only a rough approximation of the actual picture is obtained. TAYLOR (ref. 41) reports that in general a high positive load is not directly followed by a high negative load and vice versa. As it turned out that the number of positive and negative loads of equal magnitude is about the same, such loads are taken together to form complete load cycles. TAYLOR has pointed out that this is a conservative measure which is illustrated in fig. 9.3 by an extreme example. That this is indeed conservative will be clear if it is realized that in fatigue the stress amplitude is much more important than the mean stress.

An important question is how conservative this treatment of the load data actually is. There are at the moment no test data available which may answer this question and some preliminary research with simplified test programs seems desirable.

A second question with respect to spectrum tests is the load sequence, which is quite regular for spectrum tests. GASSNER (ref. 13) reports that spectrum tests with stepwise increasing loads and spectrum tests with stepwise decreasing loads (see fig. 9.4) will give about the same results, provided that the duration of one loading period is relatively short. This would suggest that the load sequence is not so important. FREUDENTHAL, being more sceptical in this respect, performed a number of rotating beam spectrum tests with a randomized load sequence. It is certainly advisable to conduct some ad-hoc research on some typical aircraft structural elements. Also for this purpose simplified test programs could be used.

It has already been stated that it may be difficult to apply the results of spectrum tests on simple specimens to the full-size structure for different reasons. One reason not yet mentioned is the load redistribution which occurs in redundant structures after high loads (ref. 20). In general, this effect will be favourable but it is difficult to obtain a quantitative idea about it.

10 Proposals for further investigation.

The discussion in the previous chapter suggests that it is rather difficult to obtain a quantitative life estimate of an aircraft structure with a reasonable accuracy.

The two main causes of this situation are briefly:

(a) Our knowledge of the fatigue phenomenon is insufficient and our knowledge of the fatigue process in cumulative-damage tests is even less.
(b) The quantitative meaning of practical life-estimation tests is insufficiently known.

To clarify these points some recommendations for research will be made here.

(1) The propagation of fatigue cracks should be carefully studied, in the micro-stage as well as in the macro-stage. The effect of the magnitudes of mean stress and of the stress amplitude, and of the type of notch should be studied. Such a study will offer experimental difficulties, but the results may lead to a better understanding of the time history of fatigue damage and of the fatigue phenomenon in general. Moreover, they may also give a better idea about the importance of S_m, S_a and the type of notch.
(2) In chapter 8 it has been mentioned that crack depth alone does not represent the state of fatigue. Thus, secondly, the research efforts should be directed to the study of the effect of internal stresses and strain-hardening. It is realized that such a study is even more difficult than the investigations mentioned under (1). Probably these factors may be investigated indirectly in two-step tests by studying the effect on the crack growth at the moment the stress-level is changed.

Items (1) and (2) may be considered as being of a basic nature and it is therefore advisable to perform these investigations as basically as possibly. This implies that a careful experimentation is thought necessary to avoid any effect of accessory circumstances.

For practical problems ad-hoc research will be a necessary condition. It has to be recommended to conduct such research as realistically as possible. In this respect axial-load tests on typical notched specimens at a positive mean stress should be strongly advised.

In chapter 9 a spectrum test was considered to be the best available simulation of aircraft conditions. Some points to investigate the interpretation of the results of such tests were mentioned, viz.

(3) It should be investigated whether spectrum tests involve a sufficient randomizing of the spectrum loads. Such tests are difficult to realize as it necesitates a machine in which axial loads can be applied in some arbitrary random sequence.

(4) The common spectrum test is based on the assumption that positive and negative loads of equal magnitude may be added to complete load cycles whereas in practice these loads do not occur in succession. The effect of this assumption will probably be small for moderate loads but it should be studied for the rather high loads which are relatively rare.

(5) In a spectrum test some assumed load spectrum is employed whereas in service a measured load spectrum may deviate from the assumed one. To interpret such deviations in terms of life, spectrum tests are recommended in which different types of spectra are employed.

In general, it will be impossible to perform spectrum tests on complete structures. It, therefore, is an urgent question to relate the results of spectrum tests to the results of conventional fatigue tests or some other simplified fatigue test. In chapter 8 it was pointed out that there is still no physical basis for such a relation and, therefore, recommendations (1) and (2) become rather important. Meanwhile it can be tried to establish such a relation as a merely empirical result based on the comparison of test results with the corresponding fatigue diagram or fatigue curve.

(6) For such a comparison no sufficient data are thought to be available and, therefore, spectrum tests on different type of structural elements using some types of spectra should be advised for this purpose.

(7) It may be recommended to study the influence of a cladding-layer on the fatigue behaviour of notched specimens. Whereas this influence probably will be small it is still advised to study the effect on the crack growth in the beginning of the fatigue process.

(8) In this report two aspects of the fatigue phenomenon were not considered ,viz. the effect of speed (number of loadcycles per minute) and the effect of rest periods. In general, it is believed that both do not affect the fatigue process in light alloys to a large extent. However, the effect of beneficial internal stresses may probably disappear after long periods or periods in which the specimen is loaded only by the mean stress. Some data may be found in the literature, which have not been reviewed in this respect. It seems worthwhile to pay some more attention to this subject.

11 Conclusions.

This report gives the results of cumulative damage tests on 24 S-T Alclad riveted joints. In all tests a constant mean stress was maintained. Two different mean-stresses were used, viz. $S_m = 7.2$ kg/mm^2 (10.2 kips) and $S_m = 9.0$ kg/mm^2 (12.8 kips). At each mean stress two different stress amplitudes were used viz. 7.2 kg/mm^2 and 3.2 kg/mm^2 (10.2 kips and 4.5 kips) for the mean stress of 9.0 kg/mm^2 and 7.0 kg/mm^2 and 3.2 kg/mm^2 (10.0 and 4.5 kips) for the mean stress of 7.2 kg/mm^2. The cumulative damage tests mainly consisted of three types of tests.

(1) A high pre-stress was followed by a low test stress (H-L tests).

(2) A low pre-stress was followed by a high test stress (L-H tests).

(3) The low and the high stress amplitudes were applied alternately (interval test).

In the first two types the stress amplitude was changed once, whereas in the interval tests this happened many times.

The test results are compared with available data from literature about cumulative damage tests on light alloy specimens. It was tried to reveal some general trends in the results of the reviewed test data.

After the discussion of the empirical results a review is given of different cumulative-damage conceptions.

Finally it was thought worthwhile to consider the significance of the discussed results for the testing of aircraft structures. As a consequence some proposals for further investigation could be made.

The main points of the report may be summarized in the following conclusions.

1. The distribution of the results of conventional fatigue tests could be approximated by a log-normal distribution.

2. The scatter found in the conventional fatigue tests as well as the cumulative damage tests was low.

3. The results of the H-L tests and the L-H tests agreed very well with the linear cumulative damage rule whereas in the interval tests the values of $\Sigma \frac{n}{N}$ ranged from about 1.3 to 1.9.

4. The assumption that a specimen would obtain the same probability of failure in any type of fatigue test seems not to be justified for all types of cumulative-damage tests.

5. As a consequence of a literature review it turned out that the number of studies on cumulative damage is steadily increasing. However, the

variety of the conducted test-programs is large. Some important variables are: (a) The type of material. In this report only precipitation hardening light alloys are studied . (b) The type of specimen. Unnotched and different types of notched specimens are used. (c) The type of loading. Axial loading and rotating beam tests are employed. (d) The type of cumulative-damage tests: two-step tests, interval tests, spectrum tests, conventional fatigue tests preceded by one high load are performed. This variety does not facilitate a comparison of the results of different test-programs.

6. Based on the reviewed data the following trends were found.

(a) In general $\Sigma \frac{n}{N} = 1$ is not valid, even not approximately. There is a marked difference in the cumulative-damage behaviour of notched and unnotched specimens.

(b) For notched specimens a beneficial effect may be expected from positive high loads which cause local yielding. The effect may be obtained by one high pre-load; in general, the benefit will increase by periodically applying high loads. The effect can be explained by the formation of internal stresses.

(c) Cyclic high pre-loading may give a higher benefit than a single high pre-load cycle. Apart from the favourable internal stresses a cyclic strain-hardening is thought to be effective.

(d) In spectrum tests on notched specimens at positive mean stresses $\Sigma \frac{n}{N} > 1$ is likely to occur if also high stresses are included in the spectrum. Values much above unity are possible. If too many high load-cycles are included the endurance will be lowered again.

(e) In spectrum tests on notched specimens stresses below the fatigue limit should not be omitted as these stresses are certainly effective as soon as the original fatigue limit is lowered by fatigue cracks. Including these stresses does not necessarily involve that $\Sigma\, n/N = 1$ will give an unsafe life estimate.

(f) Interval tests on notched specimens gave results of $\Sigma \frac{n}{N}$ beyond unity.

(g) On axially loaded unnotched specimens the deviations from $\Sigma \frac{n}{N} = 1$ for all types of tests are noticeably smaller than for notched specimens. In many cases the deviations are small. A beneficial effect of high pre-loads was obtained in some cases but not always.

(h) For interval tests and spectrum tests on unnotched sheet specimens $\Sigma \frac{n}{N}$ was about unity. For interval tests and spectrum tests on unnotched rotating beam specimens the results were less systematical and values well below unity were not seldom.

7. If the state of fatigue is represented by one parameter D, the fatigue process in a conventional fatigue test can be represented by a damage curve in which D is given as a function of the cycle ratio $\frac{n}{N}$. Without defining D it is then possible to derive $\Sigma \frac{n_i}{N_i} = 1$ on the assumption that the damage curves are the same for any loadrange (affine damage curves). However, it is thought to be an inadmissable oversimplification to represent the state of fatigue by one parameter.

8. The introduction of fatigue crack depth as a replacement of the vague term "fatigue damage" is considered to be an improvement. However, for a large part of the fatigue process the fatigue crack has micro-dimensions and thus is invisible.

The fatigue-crack depth alone does not sufficiently represent the state of fatigue. Other factors such as the internal stresses and the strain-hardening ahead of the fatigue crack and probably more factors should be included.

9. It is realized that at the moment no satisfactory method for the quantitative life-determination of an aircraft structure is available. The best method is thought to be a spectrum test, but some research on typical aircraft components concerning the relation of the spectrum-test result and the service life seems desirable.

12 List of references.

1. BENNETT, J. A. and BAKER, J. L. Effect of Prior Static and Dynamic Stresses on the Fatigue Strength of Aluminium Alloys. N.B.S., Journal of Research, Vol. 45, p. 449—457, 1950.
2. BULLEN, F. P., HEAD, A. K. and WOOD, W. A. Structural Changes During the Fatigue of Metals. Proc. of the Royal Soc. A, Vol. 216, p. 332—p. 343, 1953.
3. CORTEN, H. T., SINCLAIR, G. M. and DOLAN, T. J. An Experimental Study of the Influence of Fluctuating Stress Amplitude on Fatigue Life of 75 S-T 6 Aluminium. A.S.T.M. Preprint Nr. 70, 1954.
4. DOLAN, T. J. RICHART, F. E. and Work, C. E. The Influence of Fluctuations in Stress Amplitude on the Fatigue of Metals. Proc. A.S.T.M., Vol. 49, p. 646, 1949.
5. DOLAN, T. J. and BROWN, H. F. Effect of Prior Repeated Stressing on the Fatigue Life of 75 S-T Aluminum. Proc. A.S.T.M., Vol. 52, p. 733—742, 1952.
6. FORREST, G. Some Experiments on the Effects of Residual Stresses on the Fatigue of Aluminium Alloys. J. Inst. Metals. Vol. 72, Part I, p. 1—p. 17, Jan. 1946.
7. FORREST, G. Internal or Residual Stresses in Wrought Aluminium Alloys and their Structural Significance. J. Roy. Aero. Soc. Vol. 58, p. 261—p. 276, April 1954.
8. FREUDENTHAL, A. M. Planning and Interpretation of Fatigue Tests. Symp. on Statistical Aspects of Fatigue, Am. Soc. Met., p. 3, 1951.
9. FREUDENTHAL, A. M. A Random Fatigue, Testing Procedure and Machine. Proc. A.S.T.M. Vol. 53, p. 896—909, 1953.
10. FREUDENTHAL, A. M. and GUMBEL, E. J. Minimum Life in Fatigue. J. of the Am. Statistical Ass., Sept. 1954, Vol. 49, pp. 575—597.
11. GASSNER, E. Effect of Spectrum Loading on the Fatigue Strength of Aircraft Structural Elements. (in German.) Bericht der Deutschen Versuchsanstalt für Luftfahrt, Cf 407/5, Aug. 1941.
12. GASSNER, E. Results of Spectrum Tests on Steel and Light Alloy Structural Elements. (in German) Lilienthal, Gesellschaft für Luftfahrtforschung, Bericht 152, p. 1—p. 11, 1943.
13. GASSNER, E. A Method for the Determination of the Service Life of Structural Elements Subjected to Statistically Varying Loads. (in German) Konstruktion, Vol. 6, p. 97—p. 104, 1954.
14. GASSNER, E. A Study of the Fatigue Strength in Aircraft Design. (in German). Laboratorium für Betriebsfestigkeit — Bericht Nr. 281/53, Cat. 1954.

15. GROVER, H. J., BISHOP, S. M. and JACKSON, L. R. Fatigue Strength of Aircraft Materials; Axial-Load Fatigue Tests on Unnotched Sheet Specimens of 24 S-T 3 and 75 S-T 6 Aluminum Alloys and of SAE 4130 Steel. NACA T. N. 2324, March 1951.
16. HARDRATH, H. F. and UTLEY, E. C. An Experimental Investigation of 24 S-T 4 Aluminum Alloy Subjected to Repeated Stresses of Constant and Varying Amplitudes. NACA Tech. Note 2798, Oct. 1952.
17. HARTMAN, A. Preliminary Investigation to Verify the Cumulative Damage Hypothesis $\Sigma n/N = 1$ on Riveted Joints. (in Dutch). Nat. Aero. Res. Inst. Report M. 1923, 1953.
18. HENREY, D. L. A Theory of Fatigue-Damage Accumulation in Steel. Trans. A.S.M.E., Vol. 77, p. 913—p. 918, Aug. 1955.
19. HEYER, K. Mehrstufenversuche an Konstruktions-Elementen (Fatigue Tests at Varying Stressamplitudes on Structural Elements, in German). Lilienthal-Gesellschaft für Luftfahrtforschung, Bericht 152, 1943.
20. HEYWOOD, R. B. The Effect of High Loads on Fatigue. R.A.E. Internal Memorandum No. Structures 289, April 1955. To be published in Proceedings of International Colloquium on Fatigue in Stockholm, 25—27th May, 1955.
21. HEYWOOD, R. B. The Influence of Pre-Loading on the Fatigue Life of Aircraft Components and Structures. RAE Report Structures 182, June 1955.
22. KEPERT, J. L. and PAYNE, A. O. Interim Report on Fatigue Characteristics of a Typical Metal Wing. A.R.L. Department of Supply, Melbourne, Report SM. 207, Jan. 1955.
23. KERR, F. A., NICHOLS, J. and VINCENT, K. Cumulative Damage Fatigue Investigation. Saunders-Roe Report No. SR/S/762, Nov. 1952.
24. KLAASSEN, W. and HARTMAN, A. The Fatigue Diagram for Fluctuating Tension of Single Lap Joints of Clad 24 S-T and 75 S-T Aluminium Alloy with 2 Rows of 17 S Rivets. National Aeronautical Research Institute, Amsterdam. Report M. 1980, April 1955.
25. LANGER, B. F. Fatigue Failure from Stress Cycles of Varying Amplitude. J. Appl. Mech. Vol. 4, p. A 160—p. A 162, Dec. 1937.
26. LEVY, J. C. Cumulative Damage in Fatigue, A Method of Investigating, Economical in Specimens. Engineering, Vol. 179, p. 723—p. 725, June 10, 1955.
27. MARCO, S. M. and STARKEY, W. L. A Concept of Fatigue Damage. Trans. of the A.S.M.E. Vol. 76, May 1954 Nr. 4, pp. 627—632.
28. MINER, M. A. Cumulative Damage in Fatigue. J. Appl. Mech. Vol. 12, No. 3, p. A-159/—A-164. Sept. 1945.
29. NEWMARK, N. M. A Review of Cumulative Damage in Fatigue. Fatigue and Fracture of Metals, p. 197—p. 228. John Wiley and Sons, Inc., New York 1950.
30. NISHIHARA, T. and YAMADA, T. The Fatigue Strength of Metallic Materials under Alternating Stresses of Varying Amplitude. The Japan Science Review, Vol. 1 No. 3, p. 1—p. 6, 1950.
31. PALMGREN, A. The Endurance of Ball-Bearings (in German). Z.V.D.I. Vol. 68, p. 339—p. 341, April 5, 1924.
32. ROSENTHAL, D. and SINES, G. Effect of Residual Stress on the Fatigue Strength of Notched Specimens. Proc. A.S.T.M. Vol. 51; p. 593—608.
33. SCHIJVE, J. and JACOBS, F. A. Fatigue Tests on Notched and Unnotched Clad 24 S-T Sheet Specimens to Verify the Cumulative Damage Hypothesis. National Aeronautical Research Institute, Amsterdam, Report M. 1982, April 1955.
34. RUSSELL, H. W., JACKSON, L. R., GROVER, H. J. and BEAVER, W. W. Fatigue Strength and Related Characteristics of Aircraft Joints. II - Fatigue Characteristics of Sheet and Riveted Joints of 0.040 inch 24 S-T, 75 S-T and R 303—T 275 Aluminum Alloys. NACA T. N. 1485, 1948.
35. SEBISTY, J. J. and EDWARDS, J. O. Some Metallographic Observations on the Fatigue Failure of 24 S-T and Alclad 24 S-T Alloy Sheet. Dept. of Mines and Techn. Surveys, Mines Branch, Canada. Research Report No. PM 164, May, 1954.
36. SHANLEY, F. R. A Theory of Fatigue Based on Unbonding During Reversed Slip. The RAND Corporation Report No. P-350, 11 November 1952. Also Supplement, 1 May 1953.
37. SHANLEY, F. R. Fatigue Analysis of Aircraft Structures. Rand Paper No. RM-1127, July 1953.
38. SINCLAIR, G. M. and DOLAN, T. J. Effect of Stress Amplitude on Statistical Variability in Fatigue Life of 75 S-T 6 Al. Alloy. Trans. of the A.S.M.E. July 1953, Vol. 75 No. 5, p. 861.
39. SMITH, I., HOWARD, D. M. and SMITH, F. C. Cumulative Damage of Axially Loaded Alclad 75 S-T 6 and Alclad 24 S-T 3 Aluminum Alloy Sheet. NACA Tech. Note 3293, Sept. 1955.
40. STICKLEY, G. W. Effect of Alternating High and Low Repeated Stresses upon the Fatigue Strength of 25 S-T Aluminum Alloy. NACA Tech. Note 792, Jan. 1941.
41. TAYLOR, J. Measurements of Gust Loads in Aircraft. J. Roy. Aero. Soc. Vol. 57, p. 78—p. 88, Febr. 1953.
42. TEICHMANN, A. Some Basic Remarks on Spectrum Tests (in German). Jahrbuch 1941 der Deutschen Luftfahrtforschung, p. 1467—p. 1471, 1941.
43. TEMPLIN, R. L. Discussion to ref. (32). Proc. A.S.T.M. Vol. 51, 1951. p. 608, 1951.
44. WALKER, P. B. Estimation of the Fatigue Life of a Transport Aircraft. J. Roy. Aero. Soc. Vol. 57, p. 613—617, Oct. 1953.
44a. WALKER, P. B. Fatigue of Aircraft Pressure Cabins. Institute of the Aero. Sci. Preprint No. 562, June 1955.
45. WÄLLGREN, G. Fatigue Tests with Stress Cycles of Varying Amplitude. F.F.A. Report Nr. 28, June 1949.
46. WEIBULL, W. A Statistical Representation of Fatigue Failures in Solids. Acta Polytechnica No. 49, Mech. Eng. Series, Vol. 1 No. 9, 1949.
47. WEIBULL, W. Scatter in Fatigue Life of 24 S-T Alclad Specimens with Drilled Holes. SAAB T. N. 32, May 1955.

TABLE 4.1. Results of normal fatigue tests on 24 S-T Alclad riveted lap joints.

Mean Stress S_m	Stress amplitude S_a	Endurance N (10^3)	$\overline{\log N}$	Corresponding value of N	σ = standard deviation of $\log N$	$\sigma/\overline{\log N}$
9.0 kg/mm² (12.80 kips)	7.2 kg/mm² (10.24 kips)	87 96 100 104 105 105 106 112 115 115 121 121 122 123 124 126 128 130 139 157	5.06364	115 800	0.0587	0.0116
	3.2 kg/mm² (4.55 kips)	655 774 790 830 884 906 908 930 953 1 004 1 012 1 041 1 070 1 128 1 154 1 155 1 252 1 259 1 516 1 664	6.00806	1 018 800	0.0980	0.0163
7.2 kg/mm² (10.24 kips)	7.0 kg/mm² (9.96 kips)	90 114 115 119 124 124 128 131 133 135	5.0813	120 600	0.0487	0.0096
	3.2 kg/mm² (4.55 kips)	879 879 923 963 1 087 1 090 1 100 1 196 1 272 1 367	6.0270	1 064 000	0.0635	0.0105

TABLE 5.1. Results of H-L tests on 24 S-T Alclad riveted lap joints.

Type of test	$S_m = 9.0$ kg/mm² (12.8 kips)			$S_m = 7.2$ kg/mm² (10.24 kips)		
$\frac{n_1}{N_1}$	$\Sigma \frac{n}{N}$	Mean of $\Sigma \frac{n}{N}$	Standard deviation	$\Sigma \frac{n}{N}$	Mean of $\Sigma \frac{N}{n}$	Standard deviation
0.00001 (1 loadcycle)	0.56 0.80 1.00 1.05 1.10 1.13 1.13 1.19 1.24 1.27 1.34 1.88	1.14	0.35	1.12 1.16 1.19 1.27 1.50 1.81	1.34	0.27
0.0005 (60 loadcycles)	0.76 0.86 0.91 1.03 1.09	0.93	0.13	0.66 0.83 1.09 1.33 1.85	1.15	0.47
0.01	0.67 0.70 0.87 0.91 0.95 0.96 1.02 1.03 1.24 1.40	0.98	0.22	0.63 0.67 0.68 0.73 0.87 0.94 0.96 0.96 1.16 1.24	0.88	0.21
0.05	0.79 0.95 1.00 1.04 1.06 1.11 1.14 1.17 1.22 1.97	1.15	0.32	0.74 1.15 1.18 1.19 1.26 1.32 1.40 1.40 1.42 1.56	1.26	0.22
0.25	0.74 0.78 0.81 0.90 0.97 1.07 1.13 1.15 1.19 1.28	1.00	0.15	0.65 0.72 0.81 0.88 0.94 0.96 0.98 1.15 1.25 1.33	0.97	0.22
0.50	0.77 0.80 0.93 0.95 0.99	0.89	0.10	0.76 0.85 0.86 0.88 0.90	0.85	0.054

One high pre-load of 22.2 kg/mm² ($^2/_3$ S_u) followed by fatigue testing at 7.2 ± 3.2 kg/mm² ($N = 1\,064\,000$).

Endurance after pre-load (10³)	$\Sigma n/N$	$\overline{\Sigma n/N}$
1 212 1 622 1 679 1 971	1.14 1.52 1.58 1.85	1.52

TABLE 5.2. Results of L-H tests on 24 S-T Alclad riveted lap joints.

Type of test	$S_m = 9.0$ kg/mm² (12.8 kips)			$S_m = 7.2$ kg/mm² (10.24 kips)		
$\frac{n_1}{N_1}$	$\Sigma \frac{n}{N}$	Mean of $\Sigma \frac{n}{N}$	Standard deviation	$\Sigma \frac{n}{N}$	Mean of $\Sigma \frac{n}{N}$	Standard deviation
0.25	0.96 1.10 1.14 1.15 1.17 1.21 1.30 1.40 1.45 1.53	1.24	0.18	0.80 0.88 0.89 0.91 0.95 1.02 1.09 1.39 1.43 1.68	1.10	0.29
0.375	0.65 0.67 0.68 0.71 0.72 0.73 0.74 0.94 0.95 1.40	0.82	0.23	0.82 0.98 1.08 1.14 1.43	1.09	0.23
0.50	0.59 0.63 0.69 0.70 0.80 0.92 0.96 1.04 1.05 1.05 1.11 1.15 1.43	0.93	0.24	0.68 0.78 0.88 0.92 0.96 0.96 0.97 1.00 1.10 1.11	0.93	0.13
0.625	0.75 0.78 0.81 0.82 1.02	0.84	0.11	0.68 0.82 0.84 0.99 1.12	0.89	0.17

TABLE 5.3. Results of interval tests on 24 S-T Alclad riveted lap joints.

Type of test	$S_m = 9.0$ kg/mm² (12.8 kips)			$S_m = 7.2$ kg/mm² (10.24 kips)		
$\frac{n_L}{N_L} + \frac{n_H}{N_H} + \ldots$	$\Sigma \frac{n}{N}$	Mean of $\Sigma \frac{n}{N}$	Standard deviation	$\Sigma \frac{n}{N}$	Mean of $\Sigma \frac{n}{N}$	Standard deviation
0.05 + 0.05	0.81 1.11 1.18 1.21 1.21 1.30 1.33 1.53 1.61 1.86	1.31	0.29	0.87 0.88 1.14 1.19 1.19 1.21 1.28 1.36 1.53 1.55	1.22	0.23
0.10 + 0.03	0.78 0.82 0.84 0.85 0.91 0.96 1.24 1.32 1.49 1.58	1.08	0.30	0.89 1.21 1.27 1.47 1.64 1.74 1.92 2.01 2.05 2.08	1.63	0.41
0.10 + 0.01				1.26 1.34 1.35 1.44 1.54 1.76 2.04 2.04	1.60	0.31
0.20 + 0.01				1.07 1.34 2.07 2.10 3.23	1.96	0.84
0.05 + 0.01				1.22 1.26 1.98 2.26 2.41	1.83	0.56

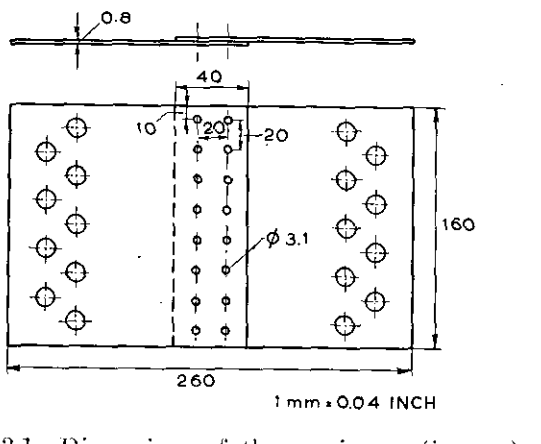

Fig. 3.1. Dimensions of the specimens (in mm).

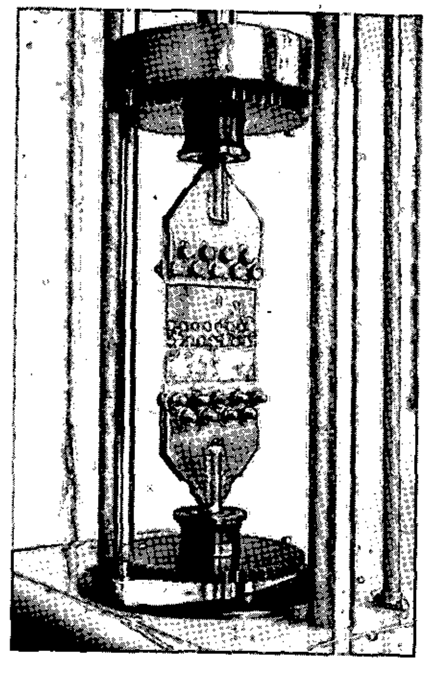

Fig. 3.2. Test set up in Amsler vibraphore.

The indicated scatterbands are twice the standard deviation. The curves are derived from the fatigue diagram of ref. 24 for the same type of specimen, tested on a Schenck pulsator, frequency 2000 c/min. The stress amplitudes of the present investigation are corrected for inertia forces of the clamping head between the specimen and the dynamometer, according to a diagram supplied by Amsler (corr. factor 1.75 %).

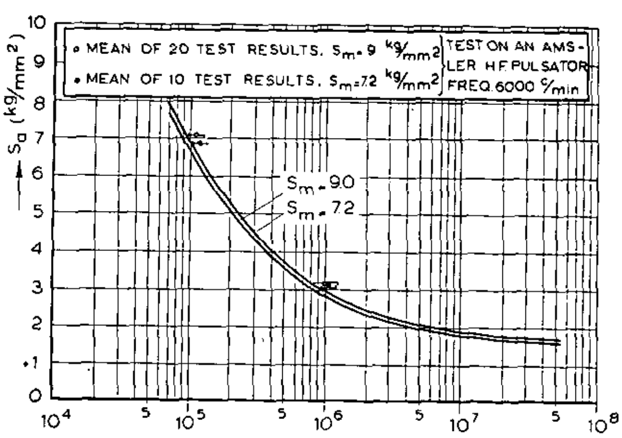

Fig. 4.1. Results of the normal fatigue tests on 24 S-T Alclad riveted lap joints. Comparison with the results of ref. 24.

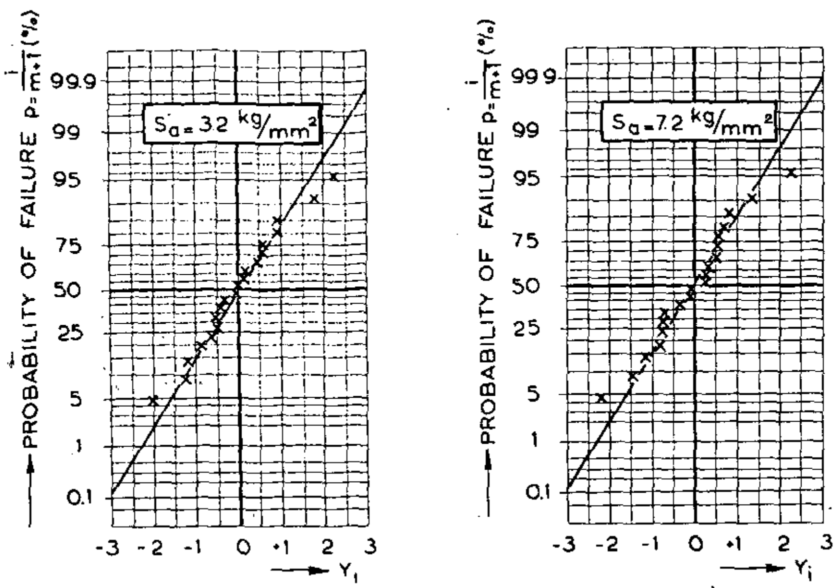

Fig. 4.2. Fatigue endurance distribution for riveted lap joints at $S_m = 9$ kg/mm² and $S_a = 7.2$ or 3.2 kg/mm².

$$y = \frac{\log N_i - \overline{\log N}}{\sigma}.$$

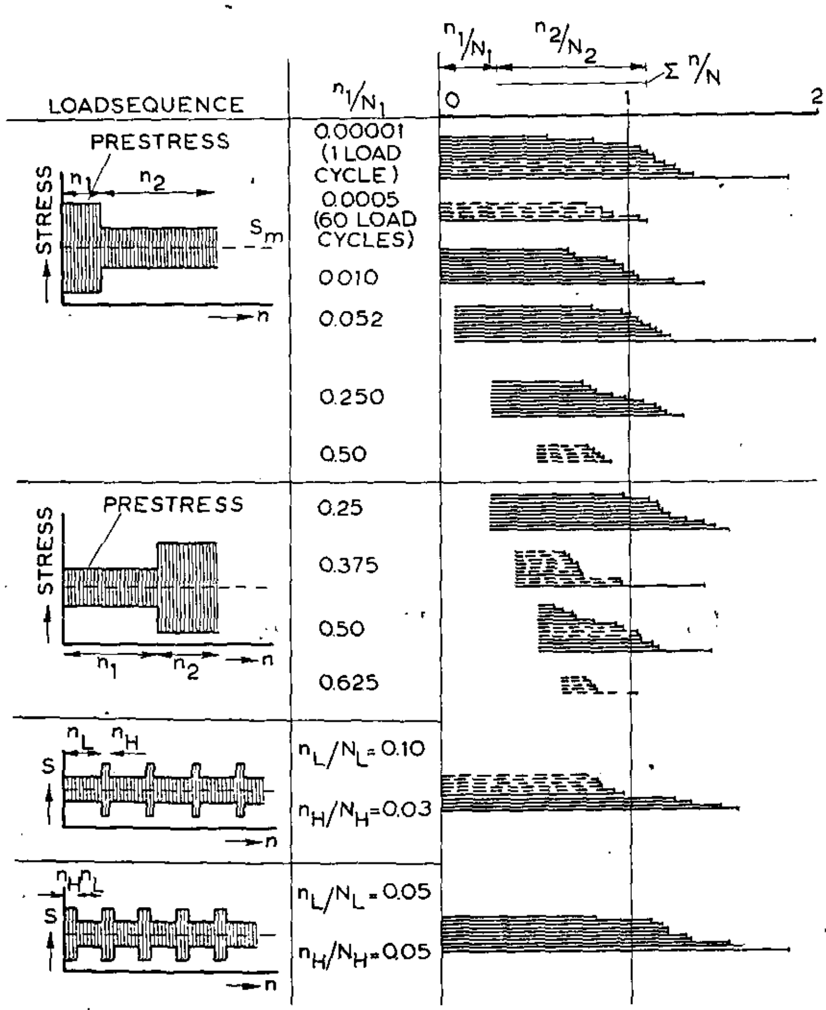

Fig. 5.1. Results of cumulative damage tests on riveted joints of 24 S-T Alclad at a mean stress of 9 kg/mm² (12.80 kips) and stress amplitudes of 7.2 and 3.2 kg/mm² (10.24 and 4.55 kips).
(Full lines give results of VLW material whereas dotted lines indicate the results of NAM material).

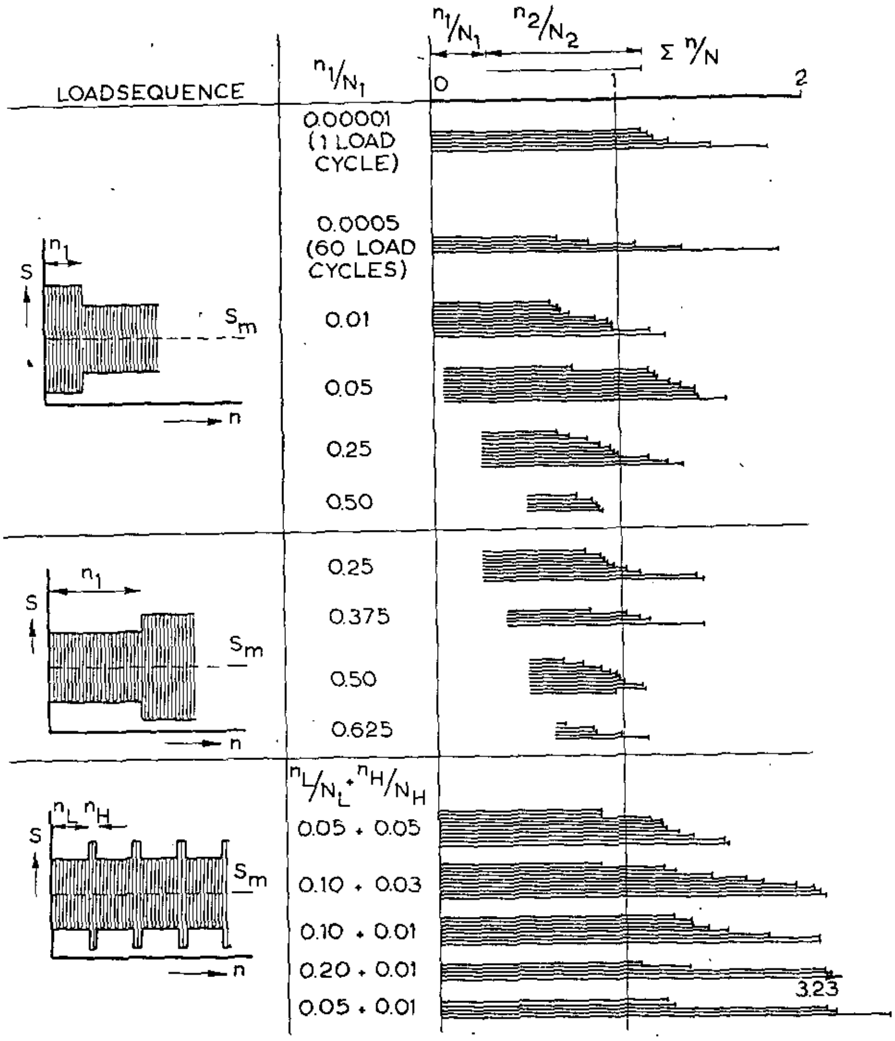

Fig. 5.2. Results of cumulative damage tests on 24 S-T Alclad riveted joints at a mean stress of 7.2 kg/mm² (10.24 kips) ($S_{a_H} = 7.0$ kg/mm² (9.96 kips) and $S_{a_L} = 3.2$ kg/mm² (4.55 kips).

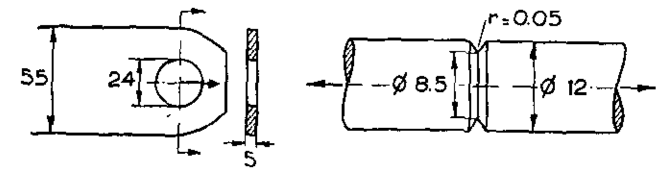

SPECIMEN A SPECIMEN B

Number	Type of duralumin.	Chemical composition							$S_{0.2}$ (kg/mm²)	S_u (kg/mm²)	δ_{10} (%)
		Cu	Mg	Si	Mn	Fe	Zn	V			
I	Al Cu Mg	3.05	1.72	0.43	0.92	0.51	—	—	30.9	44.3	19.0
II		3.91	0.66	0.51	0.71	0.40	—	—	30.6	43.8	21.4
III	Al Zn Mg	0.25	3.43	0.10	0.31	0.27	4.87	0.12	35.5	48.2	20.0
IV		0	2.48	0.28	0.88	0.33	5.92	—	48.5	59.3	10.0

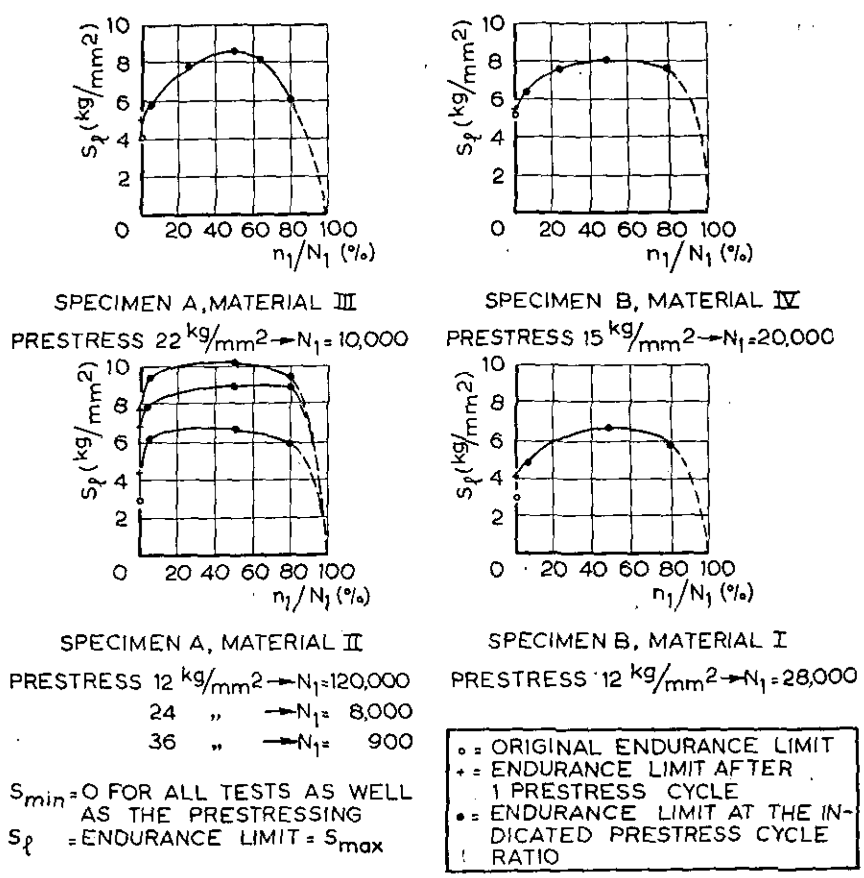

1 mm = 0.04 inch 1 kg/mm² = 1.422 kips

Fig. 6.1. The influence of cyclic pre-stressing (at $R = 0$) on the fatigue limit S_l (at $R = 0$) for two types of notched specimens and two types of duralumin. (ref. 19).

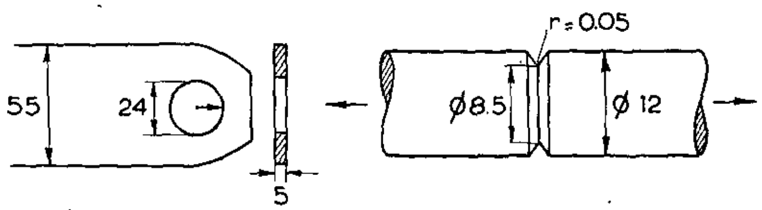

SPECIMEN A SPECIMEN B

TYPE OF TEST

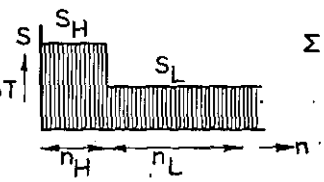

$$\Sigma \frac{n}{N} = n_H/N_H + n_L/N_L$$

Specimen	Type of dur-alumin *)	S_H (kg/mm²) (N_H)	S_L (kg/mm²) (N_L)	$\Sigma\, n/N$			
				$n_H =$ 1 cycle	$n_H/N_H =$ 0.05	$n_H/N_H =$ 0.50	$n_H/N_H =$ 0.80
A	Al-Zn-Mg (III)	22 (10 000)	5 (900 000)	> 10	∞	∞	∞
			8 (275 000)	1.41	1.90	∞	3.17
			12 (90 000)	1.11	1.33	2.44	1.91
	Al-Cu-Mg (II)	12 (120 000)	6 (800 000)	1.54	> 15	∞	> 15
			9 (300 000)	1.12	1.25	1.62	1.20
		24 (8 000)	6 (800 000)	∞	∞	∞	∞
			9 (300 000)	2.00	3.38	> 33.8	34.1
			13 (110 000)	1.00	1.05	1.24	1.04
		36 (900)	6 (800 000)	∞	∞	∞	∞
			9 (300 000)	3.33	∞	∞	∞
			13 (110 000)	1.18	1.41	3.87	2.03
B	Al-Zn-Mg (IV)	15 (20 000)	5 (1 000 000)	∞	∞	∞	∞
			7 (130 000)	1.38	1.97	∞	∞
			10 (54 000)	1.20	1.44	1.89	1.21
	Al-Cu-Mg (I)	12 (28 000)	4 (1 000 000)	10.0	∞	∞	∞
			6 (190 000)	2.53	5.31	∞	8.69
			9 (64 000)	1.33	1.38	1.83	1.13

*) Number in parentheses refers to fig. 6.1 in which material properties and chemical composition are given.

1 mm = 0.04 inch   1 kg/mm² = 1.422 kips

Fig. 6.2. Two-step tests on two types of notched dural specimens.

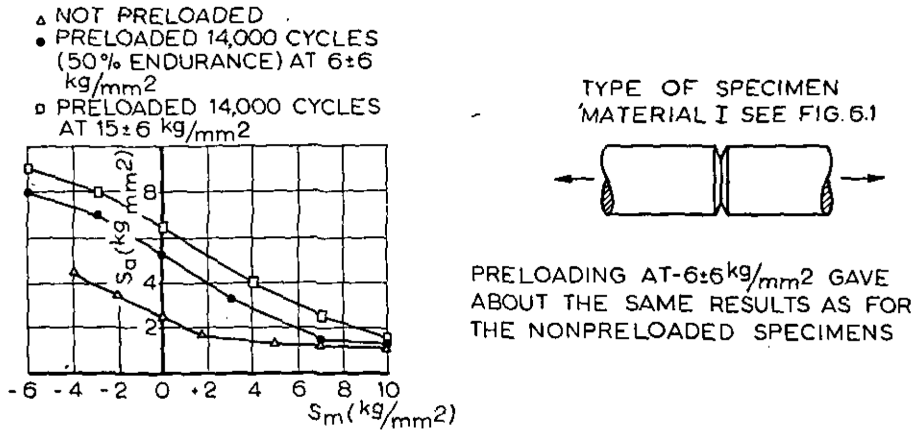

Fig. 6.3. Influence of cyclic pre-loading at different mean stresses on the fatigue limit ($N = \infty$) of a notched dural specimen.

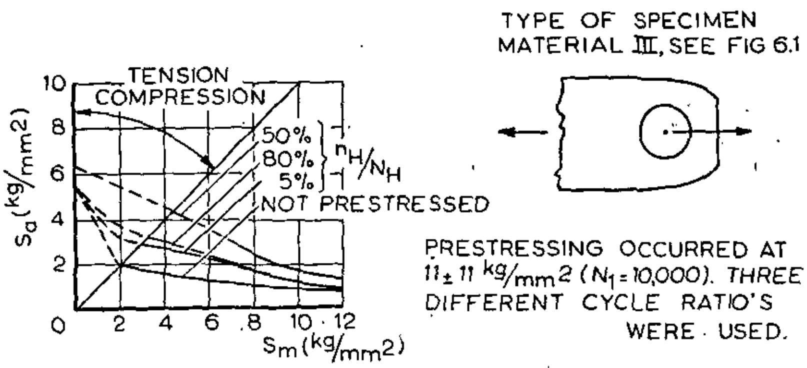

Fig. 6.4. Influence of cyclic pre-stressing on the fatigue limit ($N = \infty$) of a notched dural specimen.

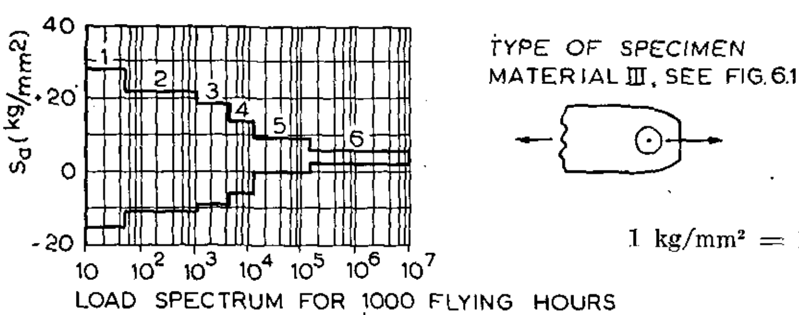

1 kg/mm² = 1.422 kips.

APPLIED LOAD STEPS *)	TEST RESULTS (FLYING HOURS)	MEAN
	RESULT IN S-N CURVE	750
	1200 - 1700	1450
	13000 - 19000 - 20000	17300
	31500 - 45500	38500
	10000 - 10000	10000
	5800 - 6000 - 7000 8000 - 8200 - 8200 9000 - 9800 - 12500	8300

*) ONLY LOAD RANGES INDICATED BLACK WERE APPLIED

Fig. 6.5. Spectrum tests on dural lugs. Some load steps were omitted.

SPECIMENS ARE AXIALLY LOADED

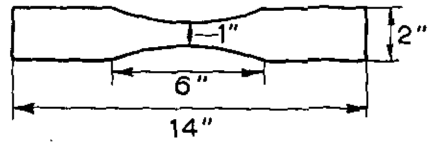

S_{a_1} (kg/mm²)	S_{m_1} (kg/mm²)	N_1 (10^3)	S_{a_2} (kg/mm²)	S_{m_2} (kg/mm²)	N_2 (10^3)	n_1/N_1	$\Sigma \frac{n}{N}$ [1]	Type of test
14.8	9.8	80	11.6	7.7	187	0.41	0.99	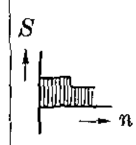
14.8	9.8	80	9.1	13.7	260	0.50	1.07	
9.4	14.1	243	8.4	12.5	330	0.55	0.98	
9.4	14.1	243	6.3	9.5	3000	0.55	0.99	
9.4	14.1	243	7.0	10.5	640	0.55	1.03	
15.8	10.5	63	7.0	$10.5 = S_{m_1}$	640	0.64	1.30	
16.9	11.3	48	7.5	$11.3 = S_{m_1}$	460	0.63	0.81	
16.9	11.3	48	7.5	$11.3 = S_{m_1}$	460	0.73	0.80	
8.4	12.7	320	14.1	21.1	85	0.40	0.75	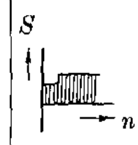
7.5	11.3	460	16.9	$11.3 = S_{m_1}$	48	0.43	1.49	
7.0	10.5	640	15.8	$10.5 = S_{m_1}$	63	0.49	1.39	
7.0	10.5	640	15.8	$10.5 = S_{m_1}$	63	0.55	0.93	
8.4	12.7	320	9.4	14.1	243	0.56	1.00	
11.6	7.7	187	16.9	11.3	48	0.68	0.81	

[1]) Each test was performed only once.

1 inch = 25.4 mm   1 kg/mm² = 1.422 kips

Fig. 6.6. Results of ref. 28. Two-step fatigue tests on unnotched specimens of 24 S-T Alclad.

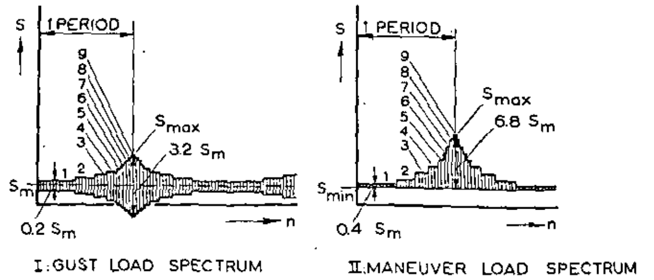

	Number of load cycles per period of the fatique test at stresslevel nr.								
	1	2	3	4	5	6	7	8	9
Spectrum I	281 000	65 700	11 500	1 440	432	131	50	16	10
Spectrum II	3 200	1 800	1 800	620	350	200	120	68	39

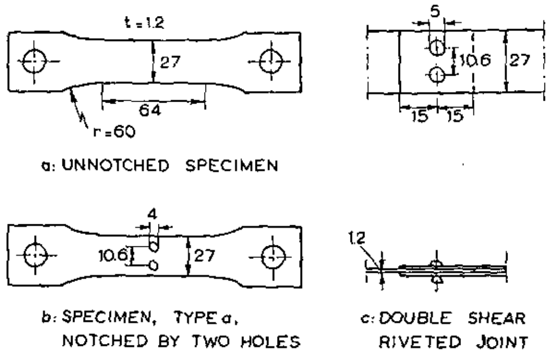

Type of load spectrum	Type of specimen	S_m (kg/mm²)	S_{max} (kg/mm²)	N at S_{max} (10^3)	Number of tests	$\overline{\Sigma\, n/N}$
I	a	15.2	40.4	4.8	5 2 *)	0.69 0.89
		13.0	34.7	13.0	4 2 *)	1.33 1.21
		10.9	29.0	30.5	5 2 *)	1.08 0.82
		8.7	23.1	78	4 2 *)	0.91 1.35
	b	13.0 10.9 8.7 6.5	34.7 29.0 23.1 17.3	1.5 5 16 45	3 3 3 3	1.33 2.28 3.00 0.90
	c	10.9 6.5 4.3	29.0 17.3 11.5	3.7 29 220	2 3 3	1.20 2.33 0.77
		3.5	9.3	220	2 4 *	0.64 0.69
II	c	S_{min} (kg/mm²) 3.6 2.7 2.2	28.0 21.1 16.8	6.0 16 35	2 2 2	2.34 1.45 1.20

*) Load amplitudes below the fatigue limit were omitted.
1 mm = 0.04 inch   1 kg/mm² = 1.422 kips

Fig. 6.7. Results of spectrum tests of ref. 45 on three types of 24 S-T Alclad specimens.

FOR LOAD SPECTRA SEE FIG.6.7

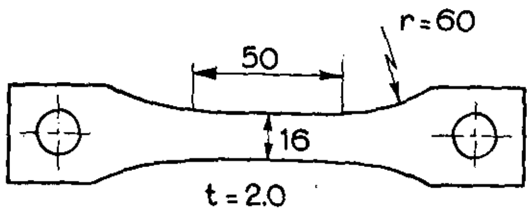

d: UNNOTCHED SPECIMEN

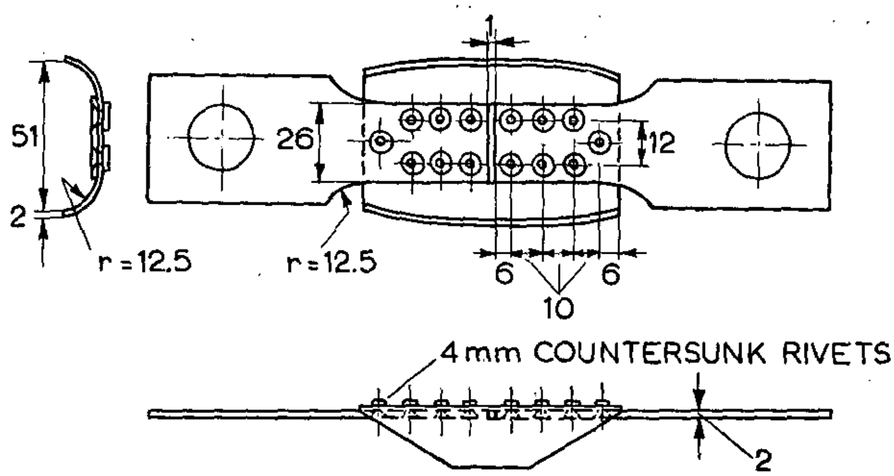

e: BUTT JOINT

Type of load spectrum	Type of specimen	S_m (kg/mm²)	S_{max} (kg/mm²)	N at S_{max} (10^3)	Number of test	$\overline{\Sigma\, n\, N}$
I	d	10.9 8.7	28.9 23.1	31.0 60.0	2 2	0.81 0.82
		7.8	19.3	85.0	2 2 *)	0.79 0.98
	e	9.3	24.8	1.4	4 2 *)	3.56 4.70
		6.2	16.5	14.5	2	2.25
		4.7	12.4	72.0	2 2 *)	1.33 2.16
II	d	S_{min} (kg/mm²) 6.75 5.40 4.50 3.37	 52.6 42.1 35.1 26.4	 1.3 20.0 41.0 92.0	 2 2 3 2	 1.64 1.29 0.93 0.82
	e	3.73 3.11 2.33	29.1 24.2 18.2	0.9 3.1 12.5	2 2 2	1.45 2.61 2.51

*) Load amplitudes below the fatigue limit were omitted.

1 mm = 0.04 inch   1 kg/mm² = 1.422 kips

Fig. 6.8. Results of spectrum tests of ref. 45 on two types of 75 S-T Alclad specimens.

TYPE OF SPECIMEN: 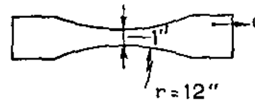

SHEET MATERIAL
24 S-T UNCLAD AND
75 S-T6 UNCLAD

TYPE OF FATIGUE MACHINE: KROUSE DIRECT REPEATED STRESS.
FREQUENCY 1100 c/min

TYPE OF LOADING: TWO-STEP TESTS

24 S-T $S_m = 12.8$ (kg/mm²)								75 S-T $S_m = 14.5$ (kg/mm²)							
Type of tests	S_{a1} (kg/mm²)	S_{a2} (kg/mm²)	N_1 (10^3)	N_2 (10^3)	n_1/N_1	$\overline{\Sigma\, n/N}$	No. of test	Type of tests	S_{a1} (kg/mm²)	S_{a2} (kg/mm²)	N_1 (10^3)	N_2 (10^3)	n_1/N_1	$\overline{\Sigma\, n/N}$	No. of test
	25.8	16.0	36	160.5	0.00025 *)	> 10.9	1	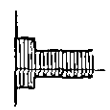	31.2	17.1	18	66.2	0.00055 *)	1.52	2
					0.10	> 22.8	2						0.10	14.76	3
					0.25	2.36	7						0.25	1.81	4
					0.50	1.35	3						0.50	1.09	3
					0.67	0.97	3						0.75	1.11	3
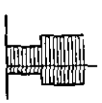	16.0	25.8	160.5	36	0.20	1.01	3		17.1	31.2	66.2	18	0.25	1.14	3
					0.35	1.35	3						0.50	1.25	4
					0.53	1.65	3						0.76	1.38	4
					0.75	1.87	5						0.85	1.44	3
					0.87	2.04	3								

*) $n_1 = 10$ load cycles.

1 inch = 25.4 mm   1 kg/mm² = 1.422 kips

Fig. 6.9. Results of axial load fatigue tests of ref. 15.

Type of specimens: A lapjoint with two rows of eight rivets in 0.8 mm sheet was used, similar to the specimen used in the present investigation, see fig. 3.1.

The specimens were axially loaded.

Type of tests: Two-step tests, resp. H-L and L-H tests.

High stress level: $S_m = 6.9$ kg/mm², $S_a = 6.0$ kg/mm² $\rightarrow N = 190\,000$.
Low stress level: $S_m = 3.65$ kg/mm², $S_a = 2.75$ kg/mm² $\rightarrow N = 2\,100\,000$.

Type of test	n_H/N_H	n_L/N_L	$\Sigma \overline{\frac{n}{N}}$	Number of tests
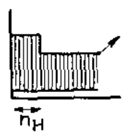	0.000005 [1]) 0.26		1.15 5.87	2 9
		0.24	0.86	9

[1]) This value corresponds to one loadcycle.

1 kg/mm² = 1.422 kips

Fig. 6.10. Two-step tests on riveted lapjoints of 24 S-T Alclad. (ref. 17).

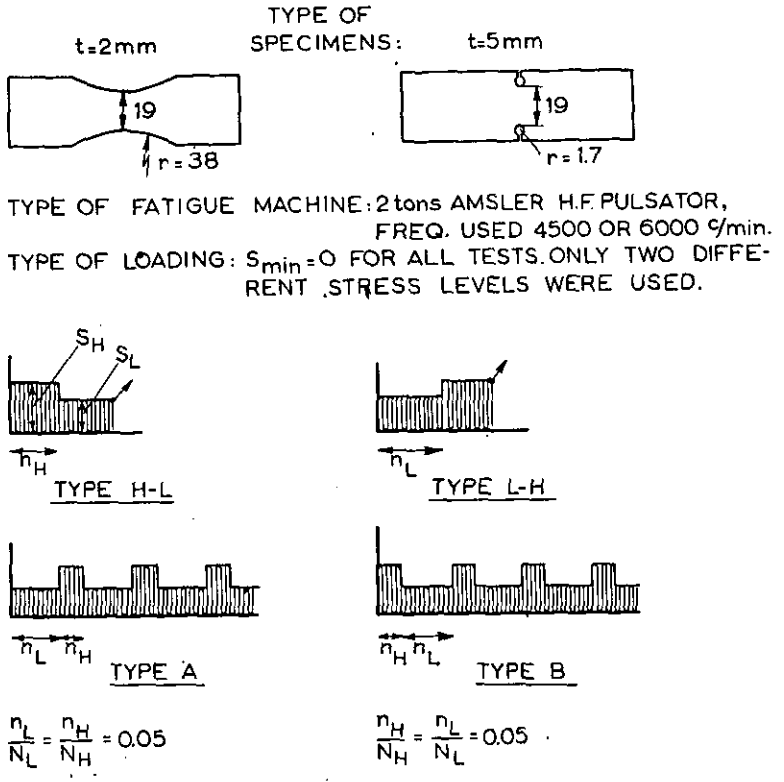

Unnotched specimens $S_H = 23$ kg/mm² $\rightarrow N_H = 200\,000$; $S_L = 16$ kg/mm² $\rightarrow N_L = 1\,300\,000$				*Notched specimens* $S_H = 10.5$ kg/mm² $\rightarrow N_H = 185\,000$; $S_L = 6.5$ kg/mm² $\rightarrow N_L = 1\,200\,000$			
Type of test	n_H/N_H	n_L/N_L	$\overline{\Sigma\, n/N}$	Type of test	n_H/N_H	n_L/N_L	$\overline{\Sigma\, n/N}$
H-L	0.05 0.10 0.25 0.50		1.38 1.37 1.65 2.36	H-L	0.02 0.05 0.10 0.25 0.50		> 6.50 1.77 5.10 5.35 1.67
L-H		0.05 0.10 0.25 0.50	0.84 0.75 0.75 0.85	L-H		0.05 0.10 0.25 0.50	1.10 1.27 1.21 1.15
A B	0.05 0.05	0.05 0.05	1.05 1.01	A B	0.05 0.05	0.05 0.05	1.81 1.77

Each type of test was repeated about 10 times.

1 mm = 0.04 inch 1 kg/mm² = 1.422 kips

Fig. 6.11. Axial loading fatigue tests on unnotched and notched 24 S-T Alclad sheet specimens. (ref. 33).

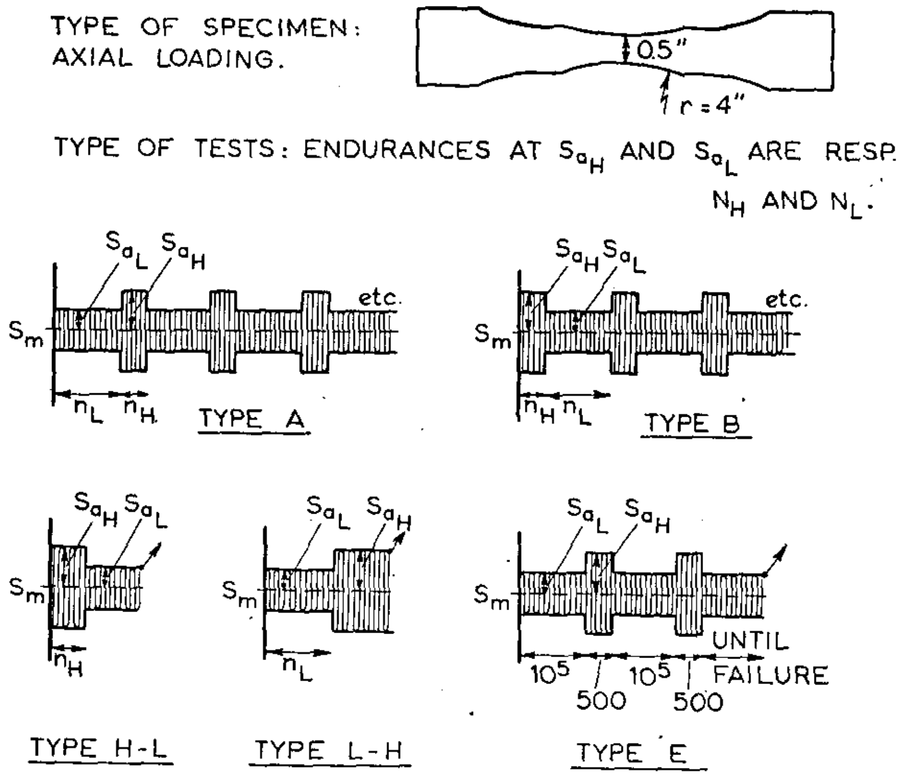

Material	S_m (kg/mm²)	S_{a_H} 1) (kg/mm²)	S_{a_L} 1) (kg/mm²)	N_H 2) (10^3)	N_L 2) (10^3)	Type of test	n_H/N_H	n_L/N_L	Number of tests	$\overline{\Sigma\, n/N}$
75 S-T6 (0.064″)	0.0	28.1	21.1	15	58	A and B	3)	3)	71	0.92
						H-L	0.68	—	4	1.01
						H-L	0.83	—	4	1.10
						L-H	—	0.89	4	1.04
		42.2	21.1	33	58	A and B	3)	3)	80	0.94
						H-L	0.37	—	4	1.07
						L-H	—	0.56	4	0.71
		21.1	11.2	58	1 650	A and B	3)	3)	94	0.87
						H-L	0.70	—	5	1.44
						H-L	0.56	—	4	1.42
						L-H	—	0.58	4	1.00
		42.2	11.2	33	1 650	A	0.034	0.052	4	0.66
						E	See above		4	0.81
75 S-T6 (0.032″)	0.0	21.1	11.2	41	1 280	A and B	4)	4)	14	0.94
						H-L	0.52	—	8	1.14
	14.1			30	460	A and B	4)	4)	24	1.03
						H-L	0.73	—	4	1.05
24 S-T3 (0.032″)	0.0	21.1	11.2	51	1 950	A and B	4)	4)	18	0.72
						H-L	0.60	—	4	1.10
	14.1			33	340	A and B	4)	4)	16	1.02
						H-L	0.61	—	4	1.04
						L-H	—	0.60	4	0.74

1) Nominal stresses. Actual stresses were slightly different.
2) Endurances were estimated from fig. 10 and 12 of ref. 39.
3) About 10 different values were used for both n_H/N_H and n_L/N_L, ranging from low to high. Moreover n_H/N_H: n_L/N_L covered a large range of values. Normally each type of tests was repeated four times.
4) 2 or 3 values were used for both n_H/N_H and n_L/N_L.

In general the results for type A- and type B-tests were the same.
Only for tests with high values of n/N type B-tests gave somewhat higher test results.

1 inch = 25.4 mm 1 kg/mm² = 1.422 kips

Fig. 6.12. Cumulative damage tests at two stress amplitudes on unnotched clad 75 S-T 6 and Alclad 24 S-T 3 sheet specimens. (ref. 39).

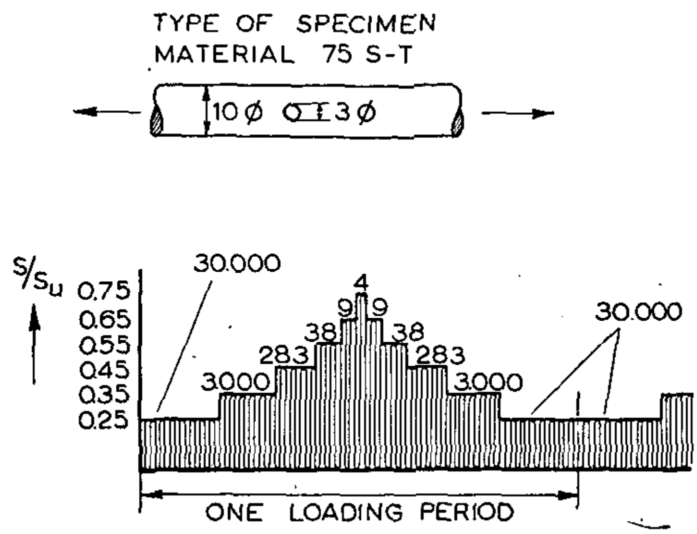

$S_{min} = 0$ $(R = 0)$ and $S_u = 66$ kg/mm².

Nine tests of this type were performed (more are planned).

The number of loading periods was calculated by means of $\Sigma \frac{n}{N} = 1$, N being based on S-N curves for 90, 50 and 10 % probability of failure.
The computed and the experimental values are given below.

Probability of failure (%)	Number of complete loading periods (T) to failure		$\frac{T_{exp.}}{T_{comp.}}$
	computed	experimental	
90	9.7	46	4.7
50	5.9	40	6.7
10	3.7	34	9.2

1 mm = 0.04 inch   1 kg/mm² = 1.422 kips

Fig. 6.13. Results of spectrum tests of Wållgren [1]) on notched 75 S-T specimens.

[1]) Test program carried out at FFA, Stockholm, not yet finished. The results given here were obtained by private communication. The permission for publication is acknowledged here.

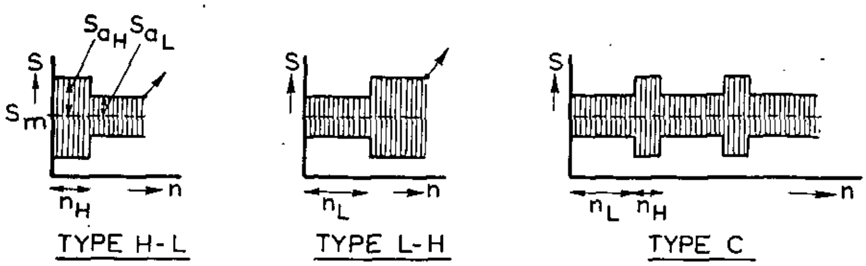

Type of specimen: Lapjoint of 24 S-T Alclad sheet with two rows of eight rivets, see fig. 3.1.
The specimens were axially loaded in an Amsler H. F. Pulsator at a frequency of 6000 cpm..
Type of loading: Two mean stresses were used. At each mean stress only two stress amplitudes were applied (S_{a_H} and S_{a_L}).

$S_m = 9$ kg/mm² $S_{a_H} = 7.2$ kg/mm² $\rightarrow N = 116.10^3$ $S_{a_L} = 3.2$ kg/mm² $\rightarrow N = 1\,019.10^3$			$S_m = 7.2$ kg/mm² $S_{a_H} = 7.0$ kg/mm² $\rightarrow N = 120.10^3$ $S_{a_L} = 3.2$ kg/mm² $\rightarrow N = 1\,064.10^3$	
Type of test	n_H/N_H	n_L/N_L	$S_m = 9$ kg/mm² $\Sigma\, n/N$	$S_m = 7.2$ kg/mm² $\Sigma\, n/N$
H-L test	0.00001 *) 0.0005 0.01 0.05 0.25 0.50		1.14 0.93 0.98 1.15 1.00 0.89	1.34 1.15 0.88 1.26 0.97 0.81
L-H test		0.25 0.375 0.50 0.625	1.24 0.82 0.91 0.84	1.10 1.12 0.93 0.89
Interval test	0.05 0.03 0.01 0.01 0.01	0.05 0.10 0.05 0.10 0.20	1.31 1.08 — — —	1.22 1.63 1.83 1.60 1.96
H-L test	One high pre-load of $S = 22.2$ kg/mm², ($^2/_3\, S_u$), followed by testing at 7.2 ± 3.2 kg/mm²			1.52

*) This value corresponds to one pre-load cycle.
Most tests were repeated about 10 times, some tests were only performed 5 times.

1 kg/mm² = 1.422 kips.

Fig. 6.14. Summary of the results of the present investigation.

TYPE OF SPECIMEN

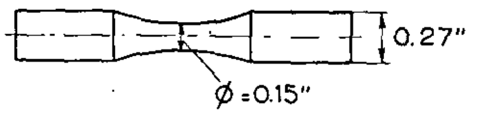

SPECIMENS WERE TAKEN FROM RODS
TYPE OF FATIGUE MACHINE: CANTILEVER ROTATING BEAM MACHINE, FREQ. 10,000 rpm.

TYPE OF LOADING:

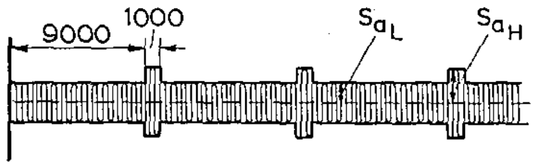

S_{a_L} above fatigue limit							S_{a_L} below fatigue limit (16.9 kg/mm²)					
S_{a_L} (kg/mm²)	S_{a_H} (kg/mm²)	N_L (10^3)	N_H (10^3)	$\Sigma\, n_H/N_H$	$\overline{\Sigma\, n/N}$	Num. of tests	S_{a_L} (kg/mm²)	S_{a_H} (kg/mm²)	N_L (10^3)	N_H (10^3)	$\overline{\Sigma\, n/N}$	Num. of tests
29.5	38.0	2.75	48	0.404	1.04	3	16.9	38.0	∞	48	1.49	3
	35.9		60	0.410	1.21	3		33.7		90	2.18	4
	33.7		90	0.694	2.73	7		29.5		275	2.36	4
	31.6		150	0.296	1.75	3		25.3		1 700	1.42	4
								23.2		6 000	0.72	4
								21.1		21 000	1.63	2
								19.7		60 000	1.07	1
25.3	38.0	1 700	48	0.575	0.72	4	12.7	38.0	∞	48	1.02	3
	33.7		90	0.647	0.96	3		33.7		90	1.63	3
	29.5		275	0.346	0.85	2		29.5		275	1.63	4
	27.4		600	0.330	1.38	3		25.3		1 700	1.51	3
								23.2		6 000	2.17	3
								21.1		21 000	1.10	2
								19.7		60 000	0.63	2
21.1	38.0	21 000	48	0.660	0.67	3	4.1	38.0	∞	48	1.96	2
	33.7		90	0.994	1.03	2		35.9		60	8.33	1
	29.5		275	1.64	1.83	3		35.2		68	5.80	2
	25.3		1 700	0.756	1.31	3		33.7		90	3.00	3
	23.2		6 000	0.283	1.01	3		29.5		275	2.36	3
								25.3		1 700	2.09	2
								21.1		21 000	1.67	1

1 inch = 25.4 mm   1 kg/mm² = 1.422 kips.

Fig. 6.15. Rotating beam tests on unnotched 75 S-T specimens (ref. 4).

TYPE OF SPECIMEN

SPECIMENS WERE TAKEN FROM RODS
TYPE OF FATIGUE MACHINE: CANTILEVER ROTATING BEAM MACHINE, FREQ. 10,000 rpm

TYPE OF LOADING

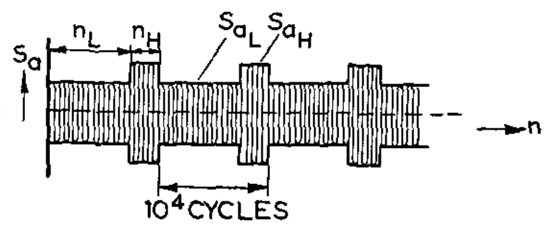

n_H = RESP. 500, 1000 OR 5000 CYCLES
$n_L = 10^4 - n_H$

S_{a_L} (kg/mm²)	S_{a_H} (kg/mm²)	n_L (10^3)	n_H (10^3)	n_L/N_L *) (%)	n_H/N_H *) (%)	$\overline{\Sigma\, n/N}$
21.1	28.2	5	5	0.02	1.9	0.843
,,	,,	9	1	0.04	0.4	0.466
21.1	35.2	5	5	0.02	9.1	0.889
,,	,,	9	1	0.04	1.8	0.510
,,	,,	9.5	0.5	0.04	0.9	1.96
28.2	35.2	5	5	1.9	9.1	0.612
,,	,,	9	1	3.4	1.8	1.15
24.0	28.0	9	1	0.4	0.4	0.789
24.0	32.0	9.5	0.5	0.4	0.8	3.44

*) data are rounded off.
Each type of test was repeated 20 times.

1 inch = 25.4 mm   1 kg/mm² = 1.422 kips

Fig. 6.16. Rotating beam tests on unnotched 75 S-T 6 specimens (ref. 3).

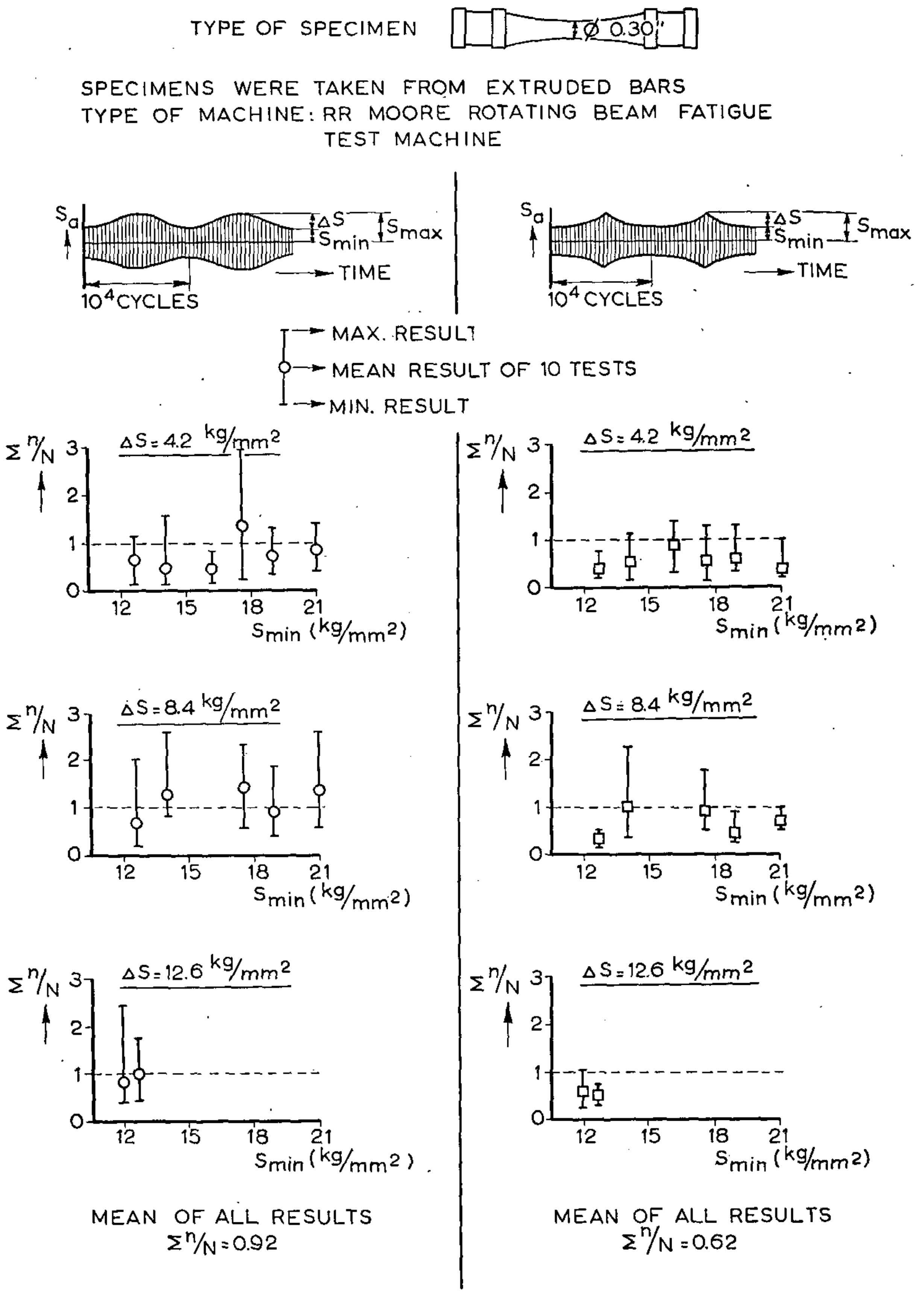

1 inch = 25.4 mm 1 kg/mm² = 1.422 kips

Fig. 6.17. Rotating beam tests on unnotched 24 S-T 4 specimens subjected to continuously varying amplitudes (ref. 16).

Rotating beam tests on unnotched 75 S-T specimens. The stress amplitude was constant for each ten load cycles. This amplitude followed a random sequence which was derived from a load spectrum. Four load spectra were used as given below. A special fatigue machine had been designed to apply the random load sequence. The test speed was 3600 rpm.

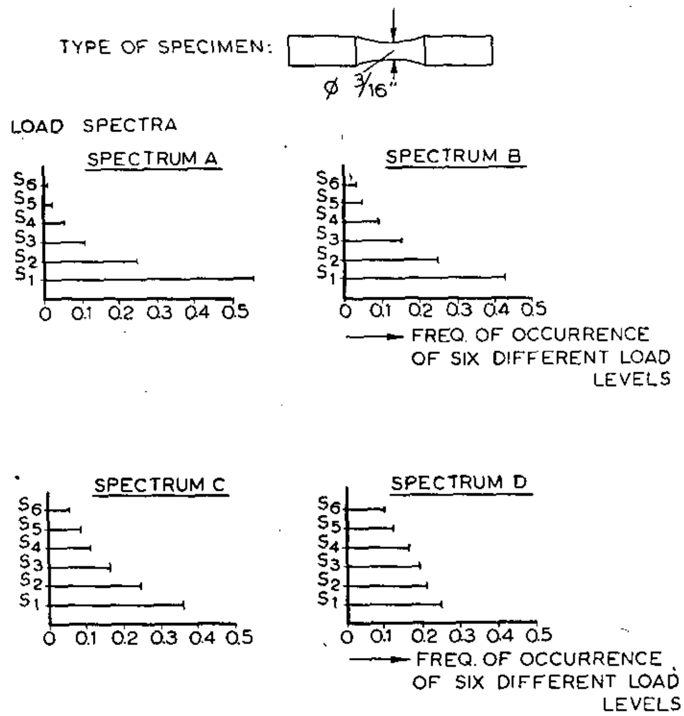

Load levels	Stress amplitude (kg/mm²)	Endurance (10^3)
S_6	41.4	50
S_5	37.6	70
S_4	33.7	120
S_3	29.9	300
S_2	26	900
S_1	22.1	5 000

Spectrum	$\overline{\Sigma\, n/N}$ *)
A	1.25
B	0.51
C	0.37
D	0.54

*) Each value is the mean of 12 test results.

1 inch = 25.4 mm 1 kg/mm² = 1.422 kips

Fig. 6.18. Results of spectrum tests of ref. 9 on unnotched 75 S-T specimens.

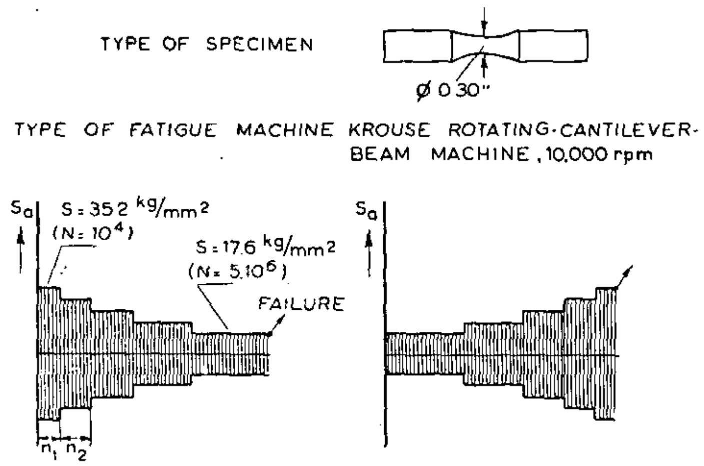

For all stress levels, except the last one, $\frac{N}{n} = m =$ number of stress-steps. At the last stress level the test is carried out until failure. (provided failure did not occur at a previous stress level, then $\Sigma\, n/N < \frac{m-1}{m}$). The difference between the stress amplitudes of two successive stress levels is constant and equal to $\frac{17.6}{m}$ kg/mm².
Tests with resp. 2, 4, 6 and 10 stress-steps were performed.

Decreasing stresslevel tests			Increasing stresslevel tests		
Number of steps (m)	Number of tests	$\overline{\Sigma\, n/N}$	Number of steps (m)	Number of tests	$\overline{\Sigma\, n/N}$
2	6	0.63	2	6	1.45
4	6	0.71	4	6	1.46
6	3	0.79	6	6	1.51
10	3	0.94	10	6	1.52

1 inch = 25.4 mm   1 kg/mm² = 1.422 kips

Fig. 6.19. Rotating beam tests on unnotched 76 S-T 6 specimens (ref. 27).

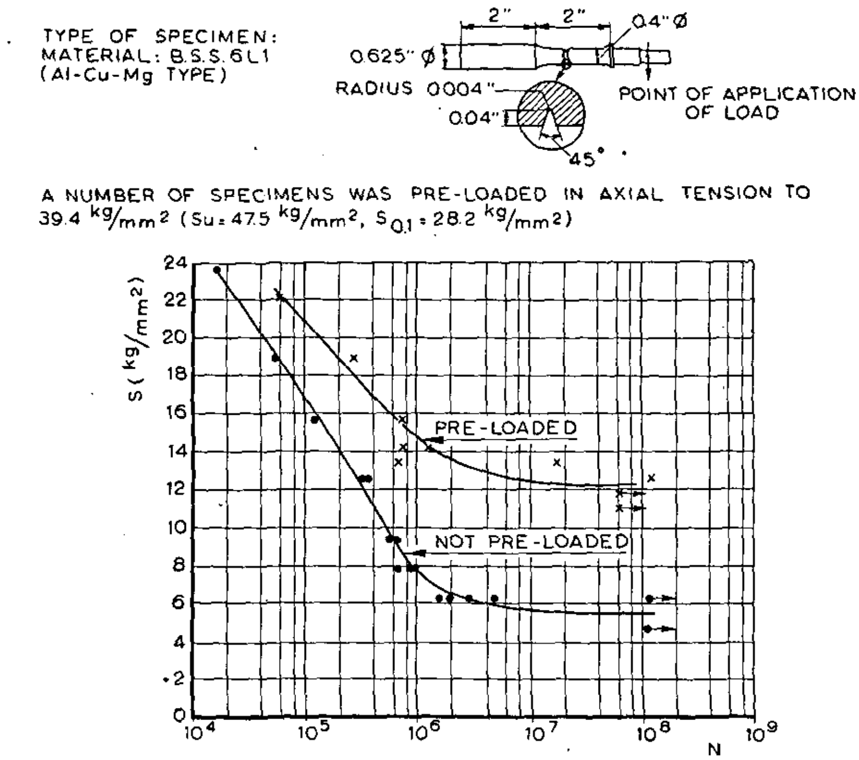

1 inch = 25.4 mm 1 kg/mm² = 1.422 kips

Fig. 6.20. Results of rotating cantilever beam tests of ref. 6.

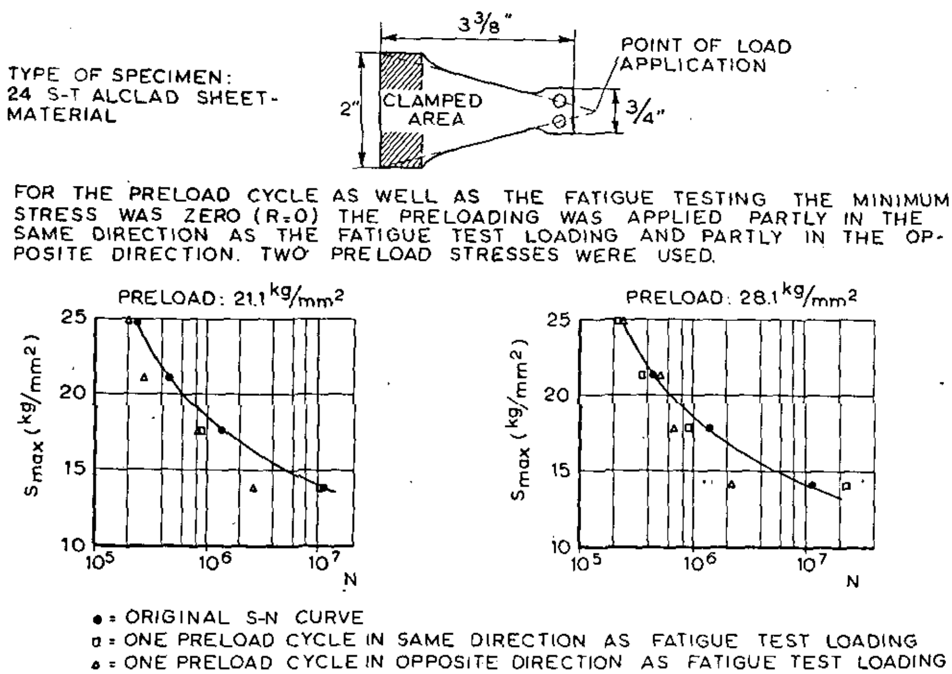

Preload (kg/mm²)	Direction of loading	$\bar{N}$ (10^3) at teststresses							
		Number of tests	14.1 kg/mm²	Number of tests	17.6 kg/mm²	Number of tests	21.1 kg/mm²	Number of tests	24.6 kg/mm²
None	—	6	11 723	4	1 489	8	461	6	253
21.1	Same	4	10 763	1	927	—	—	—	—
28.1	„	2	23 660	2	920	2	367	3	222
21.1	Opposite	3	2 788	2	878	2	286	1	207
28.1	„	2	2 166	2	677	2	508	2	255

1 inch = 25.4 mm 1 kg/mm² = 1.422 kips

Fig. 6.21. Effect of pre-loading on the S-N curve at $R=0$ (ref. 1).

Type of specimens: P 51 D "Mustang" mainplanes.
Material mainly 24 S-T Alclad sheet and 24 S-T extruded sections.
All loads are expressed in percentage of the "ultimate failing load". (U.F.L.)

Magnitude of pre-load (% U.F.L.)	Load range (% U.F.L.)	Meanlife (cycles)		$\frac{N_p}{N}$
		virgin specimen (N)	pre-loaded specimen (N_p)	
85 95	6 ± 10.6	1 238 000	4 769 000 4 561 000	3.85 3.68
70 85 90 95	6 ± 28	17 500	68 100 78 700 67 500 43 800	3.89 4.50 3.86 2.50
85 95	26.9 ± 16.1	31 460	63 820 57 410	2.03 1.82
103	32.3 ± 21.5	7 950	12 971	1.63
85.6	37.7 ± 26.9	4 139	4 975	1.20

Fig. 6.22. Effect of pre-loading on fatigue life of a typical metal wing. (ref. 22).

TYPE OF SPECIMEN:

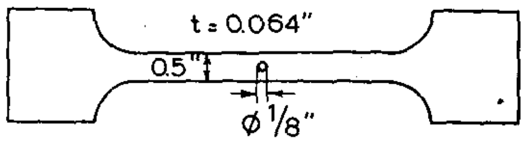

FOR THE UNNOTCHED SPECIMENS THE TRANSVERSE HOLE WAS OMITTED THE SPECIMENS WERE AXIALLY LOADED.

Type of specimen	Pre-load stress (kg/mm²)	Load range in fatigue test (kg/mm²)	Mean endurance (10^3)	Number of tests
Unnotched	No pre-load	15.7 ± 7.9	280	3
	28.3		314	1
	31.5		265	1
	34.6		370	1
	37.8		294	1
	40.9		271	1
	44.1		396	1
Notched	No pre-load	15.7 ± 7.9	62	5
	28.3		114	1
	31.5		56	3
	34.6		78	3
	37.8		77	3
	40.9		98	3
	44.1		65	2
	No pre-load	10.5 ± 10.5	33.3	3
	42.9		105.1	3
	No pre-load	14.1 ± 14.1	10.0	3
	42.9		16.8	3
	No pre-load	17.6 ± 17.6	3.8	3
	42.9		5.2	3

1 inch = 25.4 mm   1 kg/mm² = 1.422 kips

Fig. 6.23. Effect of pre-loading on the fatigue strength of unnotched and notched sheet specimens of D.T.D. 546 B. (Al Cu Mg type) (ref. 21).

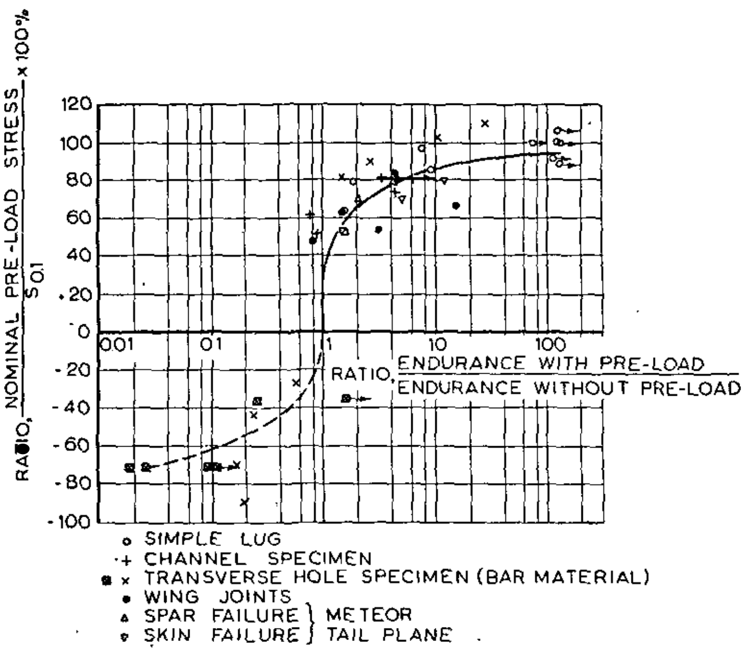

All specimens were tested in fluctuating tension, except for Meteor tailplanes which were tested in bending at resonance. The mean stress was positive in all fatigue tests and varied in the range of 8.4—14.2 kg/mm². The stressamplitudes were in the range of 2.7—5.4 kg/mm². The corresponding endurances for the not pre-loaded specimens varied from 79 000 to 850 000 except for six transverse hole specimens, indicated with ⊠ for which N was 7 700 000.

1 kg/mm² = 1.422 kips

Fig. 6.24. Influence of one high pre-load on the endurance of different types of light alloy specimens. (ref. 20 and 21).

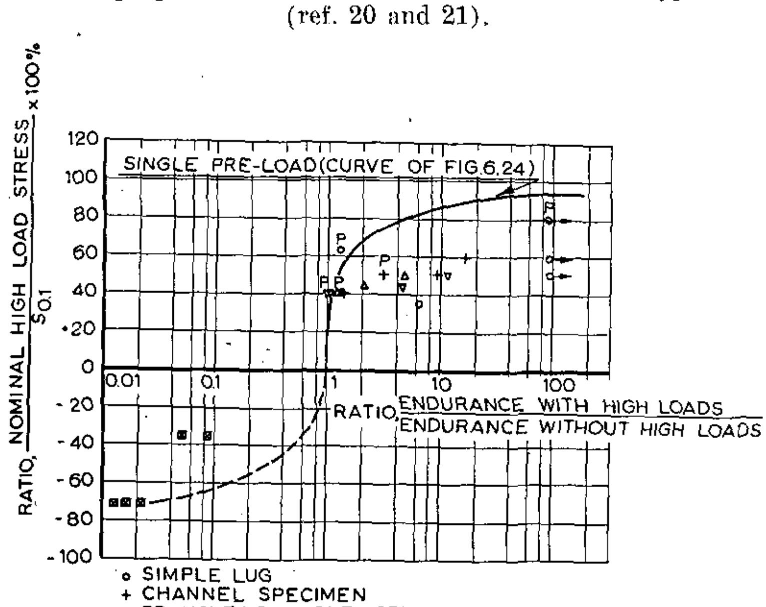

For some details on the testprocedure see fig. 6.24.
Letter P near a point denotes that specimen had received ten high pre-loads.
All other points represent specimens which were subjected to periodic high loads, which were applied at intervals during the fatigue test, the load turning to the mean of the fatigue test after each application. The intervals of high loading were as follows:
At commencement of test, and every 20.000 cycles to 500 000 cycles.
Then every 50 000 cycles to 1 000 000 cycles.
Then every 100 000 cycles to 2 000 000 cycles.
Then every 200 000 cycles to 4 000 000 cycles.
Then test continued to failure without further overloads.

Fig. 6.25. Effect of 10 pre-loads and of periodic high loads on the endurance of different types of light alloy specimens. (ref. 20).

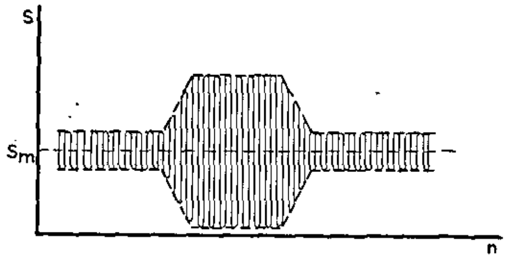

a. WAY OF PERIODIC CYCLIC OVER-STRESSING IN THE PRESENT INVESTIGATION

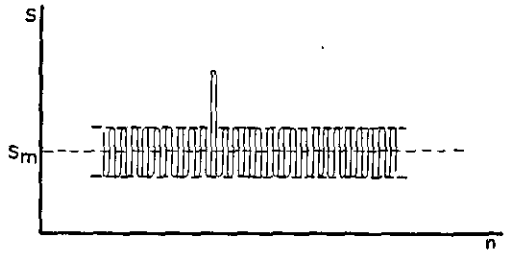

b. WAY OF PERIODIC HIGH LOADING IN THE TESTS OF HEYWOOD (REF 20)

Fig. 7.1. Different ways of overstressing.

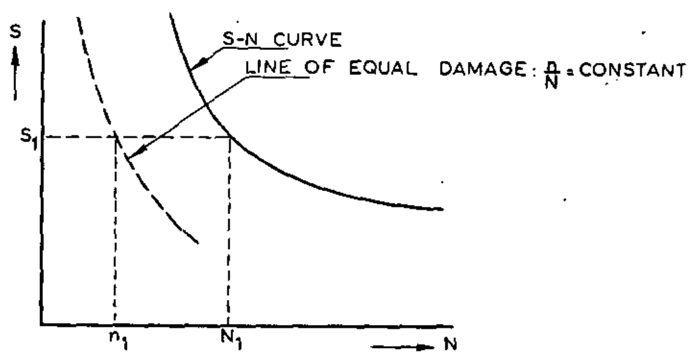

a. CONCEPT OF PALMGREN (REF 31)

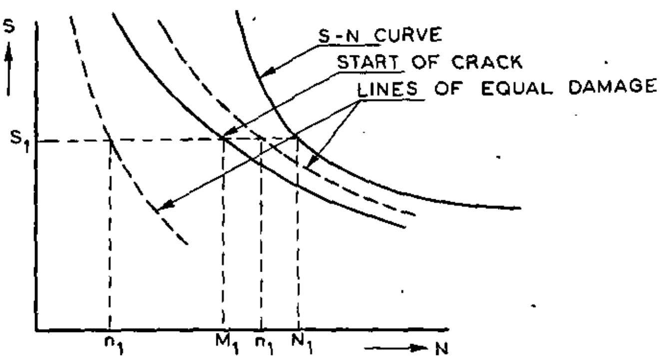

b. CONCEPT OF LANGER (REF.25)
LINES OF CONSTANT DAMAGE ARE DEFINED BY
$\frac{n}{N}$ = CONSTANT (n<M) AND $\frac{n-M}{N-M}$ = CONSTANT (n>M)

Fig. 8.1. Lines of constant damage according to Palmgren and Langer.

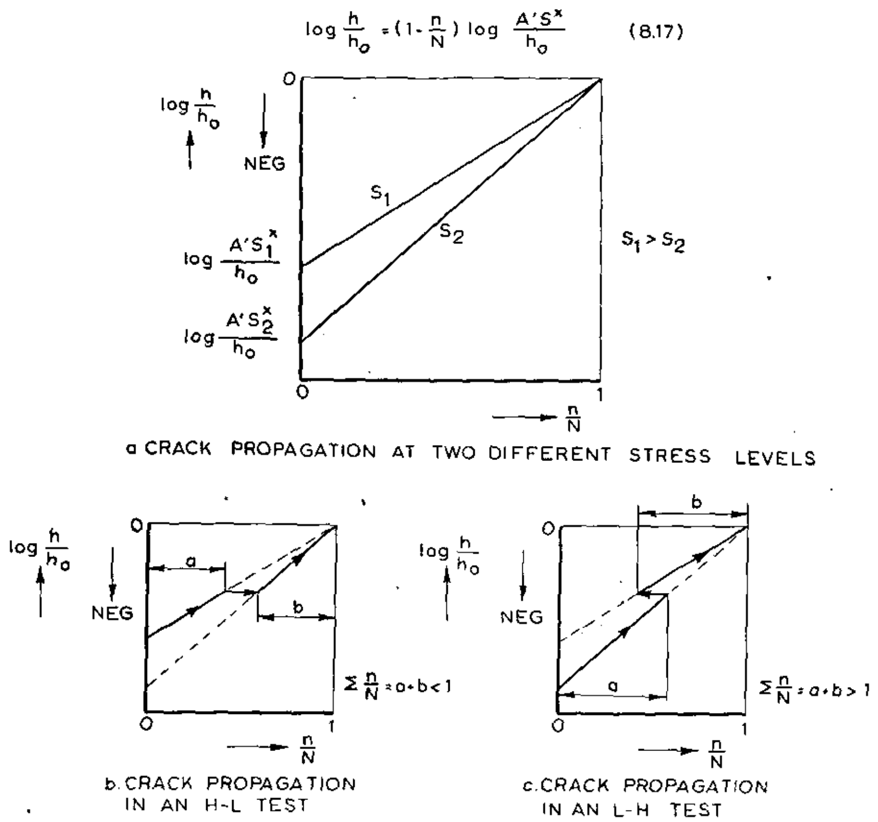

Fig. 8.2. Crack propagation according to SHANLEY.

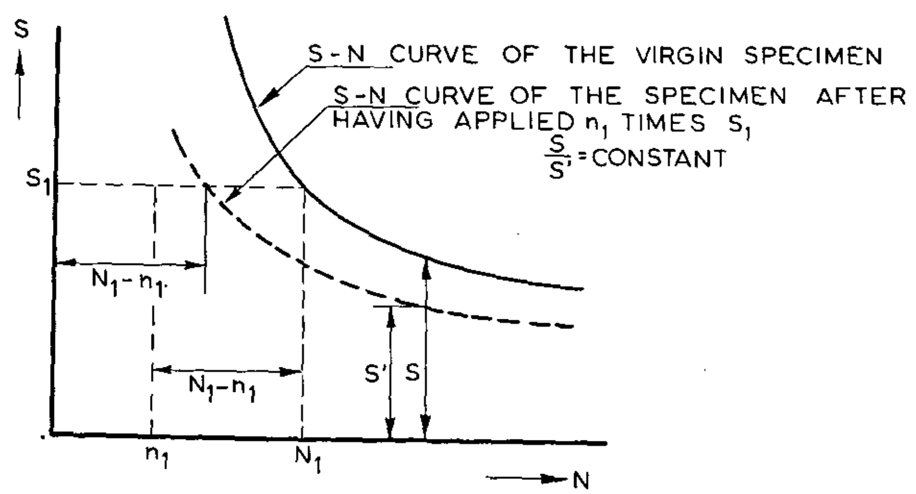

Fig. 8.3. HENRY's concept of fatigue damage in two step tests at $S_m = 0$.

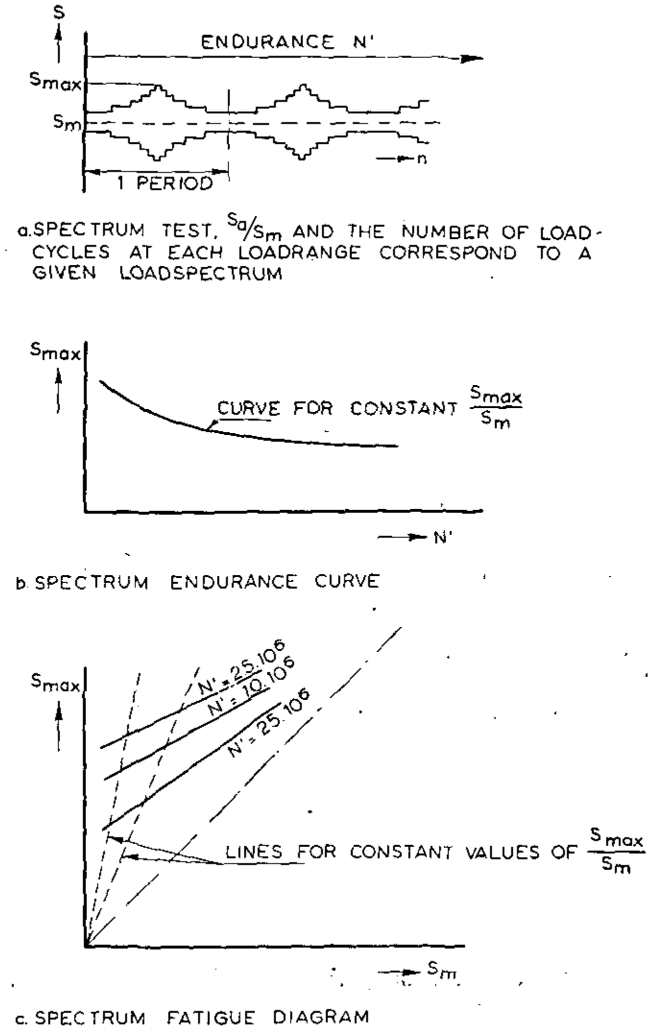

Fig. 9.1. GASSNER's method of spectrum tests.

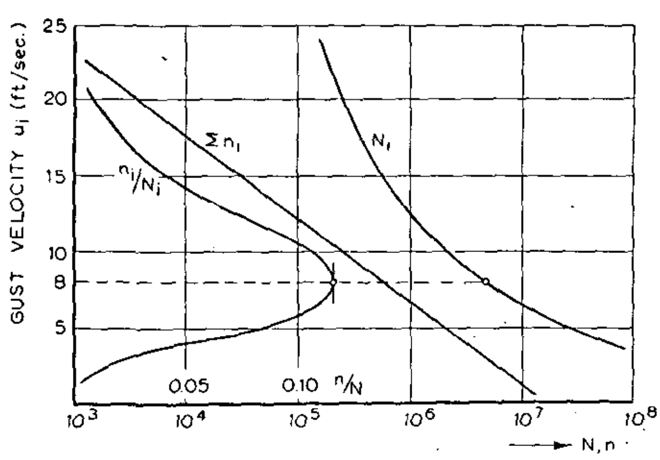

The gust load spectrum is given by Σn_i as a function of the gust load velocity u_i. Σn_i is the number of gust loads with velocity $\geqslant u_i$, encountered in a given number of flying hours. Thus the number of gust loads in the interval $u_i - \frac{1}{2}\Delta u$ until $u_i + \frac{1}{2}\Delta u$ is given by $\frac{d(\Sigma u_i)}{du_i} \cdot \Delta u$.
$N_i(u_i)$ denotes the S-N curve.
The curve $n_i/N_i(u_i)$ is the damage distribution curve according to the linear cumulative damage concept.

Fig. 9.2. Damage distribution curve for a gust load spectrum according to the linear cumulative damage concept.

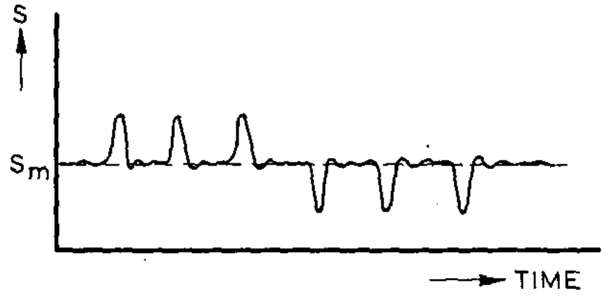

PART OF A LOAD-TIME RECORD.

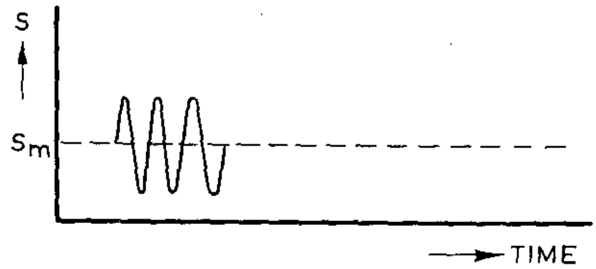

REPLACEMENT OF ABOVE GIVEN PART OF LOAD-TIME RECORD.

Part 9.3. Illustration of a conservative assumption by establishing load spectra.

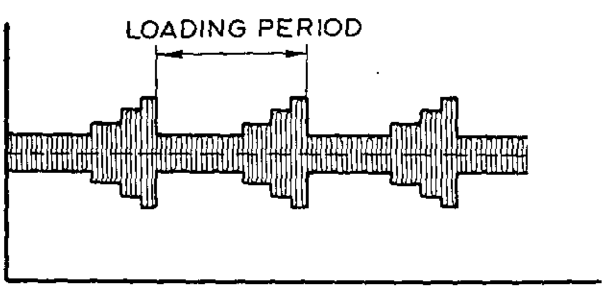

a. SPECTRUM TESTS WITH STEPWISE INCREASING LOADAMPLITUDES.

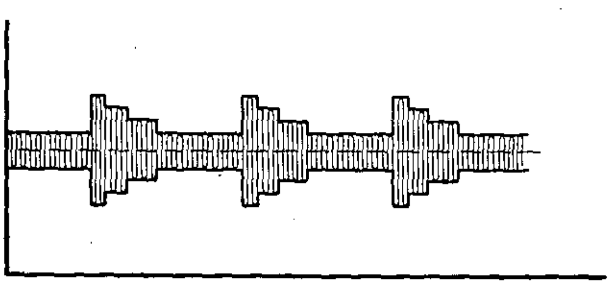

b. SPECTRUM TESTS WITH STEPWISE DECREASING LOADAMPLITUDES.

Fig. 9.4. Two types of spectrum tests.

C. C. L. Class. C 473-1

REPORT S. 476

Buckling and Post-Buckling Behaviour of a Cylindrical Panel under Axial Compression

by

W. T. KOITER *)

Summary.

The post-buckling behaviour of narrow cylindrical panels, such as occur in stiffened cylindrical shells, is investigated by means of the general theory of ref. 8 for one set of boundary conditions along the longitudinal edges. It appears that the initial post-buckling stage is stable only for very narrow panels. A program for further research is outlined with respect to other boundary conditions, to the more advanced post-buckling stage, and to an experimental verification. It is conjectured that the behaviour of a narrow curved panel in the advanced post-buckling stage will approach the behaviour of a flat panel of the same width.

Contents.

List of symbols.

a	amplitude of buckling mode.
b	width of panel.
a_0^*, a_n^*, b_n, b_n^*, c_0, c_n, c_n^*	FOURIER coefficients defined by (A 25).
h	sheet thickness, (also: a subscript for 1, 2, 3, ... in sec. A 3).
$k=\dfrac{h^2}{3R^2}$	(see (A 8)).
l	length of panel.
m	defined by (2.3).
p	wave number parameter in axial direction.
q	wave number parameter in circumferential direction.
u	axial displacement of middle surface.
v	tangential displacement of middle surface.
w	radial displacement of middle surface.
u_1, v_1, w_1	buckling mode.
$\bar{u}$, $\bar{v}$, $\bar{w}$	modification of buckling mode in post-buckling stage.
x	axial coordinate.
B	flexural rigidity of stiffener in tangential bending.
E	YOUNG's modulus.
G	shear modulus.
N	compressive load on panel.
P	potential energy; a subscript n denotes the degree of the energy expression (see (A 3)).
Q_1'	correction term to energy expression due to initial imperfections (see (A 57)).
R	radius of panel.
S	defined by (4.2).
T_h	defined by (A 41).
U, V, W	displacements in fundamental state.
$\alpha=x/R$	nondimensional axial coordinate.
β	circumferential angle (fig. 2).
β_0	circumferential angle between two stiffeners (fig. 2).
ε	overall compressive strain.

*) Chairman of the Scientific Advisory Committee NLL-NIV.

ε_1	buckling strain.
$\bar{\varepsilon}$	contribution to ε due to modification of buckling mode $\bar{u}, \bar{v}, \bar{w}$.
$\lambda = \dfrac{N}{E\beta_0 Rh}$	nondimensional load.
λ_1	nondimensional buckling load.
λ^*	nondimensional buckling load for imperfect panel.
μh	amplitude of initial waves in imperfect panel.
ν	POISSON's ratio.
θ	total curvature parameter, defined by (2.7).

1 Introduction.

The buckling and post-buckling behaviour of flat panels and of cylindrical shells under axial compression have already been investigated extensively (see e.g. refs. 1—8), and the fundamental difference in behaviour between these two types of structural elements is now fairly well understood. Much less is known about the behaviour of curved panels, such as occur in stiffened cylindrical shells. Several investigations on the classical buckling stress of such panels have been published (refs. 9, 10, 11) but little or no information seems to be available on their post-buckling behaviour.

It has of course been conjectured that the behaviour of a cylindrical panel will be similar to the behaviour of a flat panel if the panel is very narrow, i.e. if its curvature is very small. On the other hand, a cylindrical panel may be expected to show similar behaviour as a complete unstiffened cylindrical shell when the circumferential angle is sufficiently large. This conjecture may be illustrated schematically by fig. 1, where the ratio

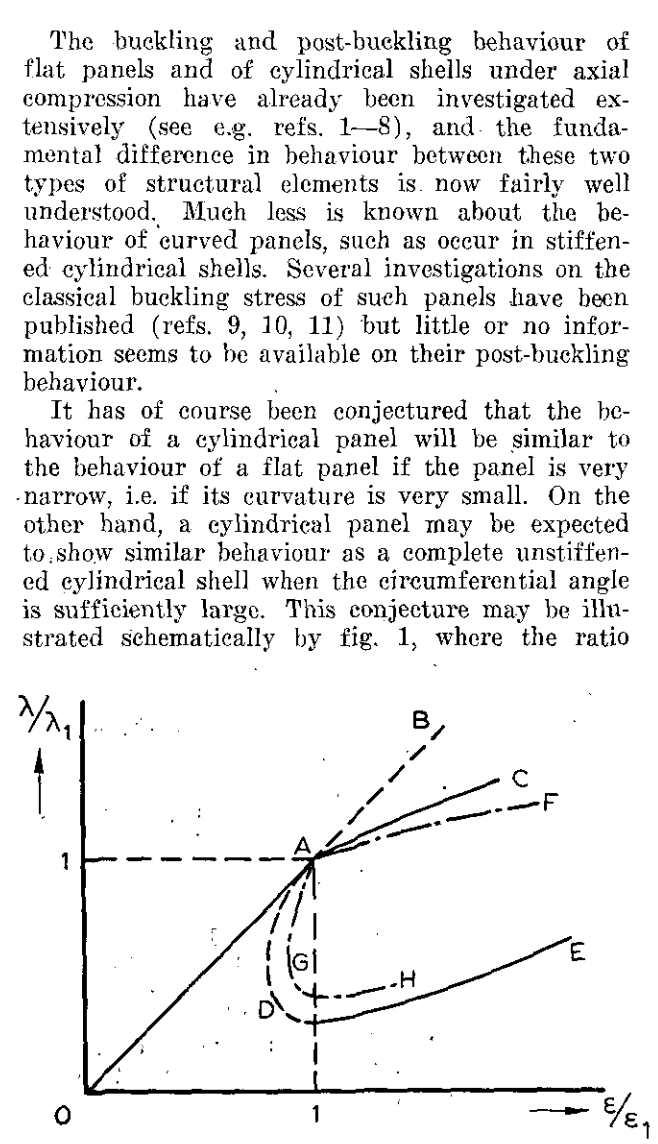

Fig. 1.

λ/λ_1 of the compressive load to the classical buckling load has been plotted as a function of the ratio $\varepsilon/\varepsilon_1$ of the overall compressive strain to the classical buckling strain. The straight line OAB represents the fundamental state of equilibrium (simple axial compression) which becomes unstable when the buckling load λ_1 is exceeded. Curve AC represents the stable post-buckling behaviour of a flat panel whereas the (initially unstable) behaviour of a cylindrical shell is described by curve ADE. Curve AF depicts the conjectured stable behaviour of a very narrow cylindrical panel and curve AGH the (initially unstable) behaviour of a wide cylindrical panel.

The initially highly unstable post-buckling behaviour of an unstiffened cylindrical shell and a wide cylindrical panel has several undesirable features. First of all the load and/or compressive strain change abruptly when the buckling load (point A in fig. 1) is reached and this jump is accompanied by comparatively large amplitudes of the waves in which the shell or panel buckles. Apart from the danger of exceeding the yield limit (or fatigue limit) of the material due to high bending stresses, such deep waves are objectionable in airplane structures from an aerodynamic point of view. Moreover, the actual buckling load is usually much lower than the theoretical buckling load due to unavoidable irregularities in the actual structure, and the decrease in buckling load is highly unpredictable because it is very sensitive to the magnitude of the deviations of the actual structure from a perfectly cylindrical shell or panel. Therefore we believe that the load-carrying capacity in the post-buckling stage is of little practical importance for a complete unstiffened cylindrical shell or wide panel. In a structure of this type the loads should be kept well below the classical buckling load.

The *type* of post-buckling behaviour is governed completely by the *tangent* to and the curvature of the post-buckling curve at the point A in fig. 1. Hence our primary interest in the investigation of curved panels is directed towards their *initial* post-buckling behaviour, i.e. for loads in the neighbourhood of the buckling load. A general method for the investigation of this type of problem has been described elsewhere (ref. 8, ch. 3). Its application to the problem of a cylindrical panel is straight-forward although somewhat laborious, once the boundary conditions of the panel and the buckling mode have been established. These basic data for a *narrow* panel are discussed in sec. 2 and the general method of analysis is outlined in sec. 3; details of the analysis for one set of boundary conditions and the corresponding buckling mode are given in appendix A. The main results are discussed in sec. 4. It appears that the initial post-buckling behaviour is *stable only for very narrow panels*. A program for further research is suggested in sec. 5.

2 Boundary conditions and buckling mode for a narrow panel.

A complete unstiffened cylindrical shell of length l, simply supported at its ends, has a large number of buckling modes at the same critical axial stress (refs. 1, 2, 8)

$$\sigma_{cr} = \frac{E}{\sqrt{3\,(1-\nu^2)}}\,\frac{h}{R}, \qquad (2.1)$$

where E is YOUNG's modulus, ν is POISSON's ratio, h is the thickness and R is the radius of the shell.

These buckling modes are described by the axial, tangential and radial displacements u_1, v_1, w_1 (ref. 8)

$$\left.\begin{aligned} u_1 &= \frac{p(\nu p^2 - q^2)}{(p^2+q^2)^2}\cos p\alpha \sin q\beta, \\ v_1 &= \frac{q[(2+\nu)p^2+q^2]}{(p^2+q^2)^2}\sin p\alpha \cos q\beta, \\ w_1 &= \sin p\alpha \sin q\beta, \end{aligned}\right\} \quad (2.2)$$

where $\alpha = x/R$ is the nondimensional axial coordinate, β is the circumferential angle, q is any integer satisfying the inequality

$$q \leqq m = \frac{1}{2}\sqrt[4]{12(1-\nu^2)}\sqrt{\frac{R}{h}}, \quad (2.3)$$

and p is a root of the equation

$$p^2 - 2mp + q^2 = 0, \quad (2.4)$$

subject to the conditions that p^2 is large and pl/R is a multiple of π. Obviously a long, thin shell has a substantial number of these buckling modes. Moreover in a long shell the boundary conditions at the ends have no appreciable effect, and additional buckling modes appear which are obtained by replacing α and/or β by $\alpha + \pi/2$ and $\beta + \pi/2$ respectively.

The most important constraint due to the stiffeners in a reinforced shell (fig. 2) is the *suppression of radial deflection waves along the stiffeners.* If we neglect all other constraining effects of the stiffeners, the buckling mode (2.2) is again possible at the *same* critical stress (2.1) as for the unstiffened shell, provided that the stiffeners are equally spaced and do not exceed $2m$ in number. In other words the circumferential angle β_0 between two stiffeners (cf. fig. 2) should not be less than π/m in order that the critical stress for the reinforced shell be the same as for an unstiffened shell.

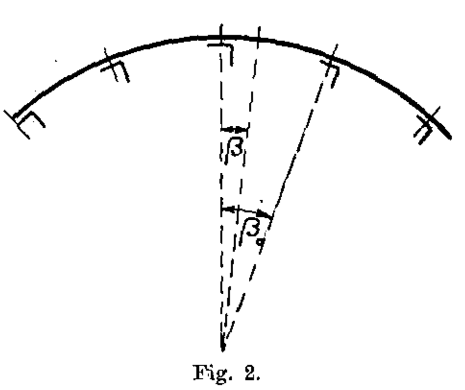

Fig. 2.

Part of cross-section of stiffened cylindrical shell.

The panels into which the cylindrical shell is divided by the stiffeners will be called *narrow* if their circumferential angle β_0 is *smaller* than π/m. The buckling mode is then again given by (2.2), where now $q = \pi/\beta_0$. The corresponding buckling stress is given by (ref. 1, art. 84; ref. 8, art. 74)

$$\sigma = E\left[\frac{p^2}{(p^2+q^2)^2} + \frac{h^2}{12(1-\nu^2)R^2}\frac{(p^2+q^2)^2}{p^2}\right], \quad (2.5)$$

where $q = \pi/\beta_0$. The critical buckling stress σ_{cr} is now given by the minimum value of (2.5) as a function of p. This minimum is attained for $p = q\ (= \pi/\beta_0)$; its value is

$$\sigma_{cr} = E\left[\frac{1}{4q^2} + \frac{h^2}{3(1-\nu^2)R^2}q^2\right] = E\,\frac{\pi^2 h^2}{3(1-\nu^2)b^2}(1+\theta^4), \quad (2.6)$$

where

$$\theta = \frac{m\beta_0}{\pi} = \frac{1}{2\pi}\sqrt[4]{12(1-\nu^2)}\frac{b}{\sqrt{Rh}} \quad (2.7)$$

is a measure for the *total curvature* of the panel and $b = R\beta_0$ is the width of the panel; a *narrow* panel is defined by $\theta \leqq 1$. The first factor in (2.6) is the well-known critical stress of a flat panel, simply supported along its longitudinal edges.

So far we have ignored all constraining effects of the stiffeners apart from the suppression of *radial* deflection waves along their lines of attachment. The corresponding buckling mode (2.2) induces *bending* of the stiffeners in a tangential plane to the shell with a curvature given by

$$\frac{1}{R^2}\left(\frac{\partial^2 v_1}{\partial\alpha^2}\right)_{\beta=0} = -\frac{p^2 q[(2+\nu)p^2+q^2]}{(p^2+q^2)^2 R^2}\sin p\alpha \quad (2.8)$$

and *torsion* of these stiffeners with a twist

$$\frac{1}{R^2}\left(\frac{\partial^2 w}{\partial\alpha\partial\beta}\right)_{\beta=0} = \frac{pq}{R^2}\cos p\alpha. \quad (2.9)$$

In most conventional stiffened shell structures the *flexural* strain energy in the stiffeners, due to tangential bending with curvature (2.8), is small compared to the extensional energy in the panel in the buckling mode (2.2) (cf. appendix B). The tangential constraint due to the stiffeners may then indeed be ignored. If the flexural rigidity of the stiffeners in bending in the tangential plane is comparatively large, the tangential constraint may become more important, resulting in a modification of the buckling mode and an increase in critical stress. However, even for completely rigid stiffeners this increase in critical stress is at most 25 per cent (ref. 11).

On the other hand, the *torsional* strain energy in the stiffeners corresponding to a twist given by (2.9) usually has a magnitude comparable to the flexural strain energy in the panel, and the torsional constraint of the stiffeners may result in an appreciable modification of the buckling mode (2.2) and a corresponding increase in critical stress. In the present report we shall neglect this effect.

The investigation of post-buckling behaviour will be simplified if we also assume that the stiffeners have no *constraining effect on the axial displacements* u along their lines of attachment. It is well-known that this assumption involves no serious error in the corresponding flat plate problem (ref. 3, secs. V and VI; ref. 8, art. 632). In our buckling mode we have $u_1 = 0$ at the attachment to the stiffeners. Hence our assumption of no constraint can only affect the modification of the displacement pattern in the post-buckling stage, exactly as in the corresponding flat plate problem, and it may be expected with some confidence that it will not involve appreciable errors.

It may be observed that it is always possible to estimate a posteriori the errors introduced by the neglection of the tangential, torsional and axial constraints by calculating the strain energy in the stiffeners corresponding with the deflection pattern without these constraints. If the resulting increase in strain energy is sufficiently small compared to the strain energy in the panel itself, the approximation is certainly sufficiently accurate. It may also be noted that our results should always be conservative.

Our final assumption is that the boundary conditions at the transverse frames of a stiffened shell may be replaced by a condition of *periodicity*. It is well known that this assumption is justified both for a flat plate and for an unstiffened shell if the length of the plate or shell is not less than several times (say 2 to 4 times) the half wave length. This assumption should therefore also be justified in our panel problem if the panel length l is not less than several times its width $b = R\beta_0$.

3 Method of analysis of initial post-buckling behaviour.

The general theory of the initial stage of post-buckling behaviour (ref. 8, ch. 3) starts from the assumption that for loads in the neighbourhood of the buckling load a *neighbouring state of equilibrium* exists, i.e. *a state of equilibrium that is obtained from the fundamental state at the same load by small (although finite) additional displacements.* Next it is observed that these additional displacements may be written in the form

$$u = au_1 + \bar{u},\quad v = av_1 + \bar{v},\quad w = aw_1 + \bar{w},\quad (3.1)$$

where u_1, v_1, w_1 is the buckling mode, a is the (as yet unknown) amplitude of the buckling mode, and $\bar{u}$, $\bar{v}$ and $\bar{w}$ are in some sense orthogonal to the buckling mode. It is assumed that $\bar{u}$, $\bar{v}$ and $\bar{w}$ are *small compared to the buckling mode contribution* to the additional displacements au_1, av_1, aw_1.

The conditions of equilibrium may be expressed by the requirement that the potential energy (the sum of the elastic strain energy and the potential energy of the external loads) has a stationary value. This requirement is applied in two steps. In the first step the stationary value of the potential energy as a functional of $\bar{u}$, $\bar{v}$, $\bar{w}$ is obtained for a *fixed* value of a. It can be proved (ref. 8) that this stationary value is a minimum and that in its evaluation only terms of the first and second degree in $\bar{u}$, $\bar{v}$ and $\bar{w}$ need be retained; the terms of the first degree are (for small values of a) proportional to a^2. Hence the differential equations for $\bar{u}$, $\bar{v}$ and $\bar{w}$, obtained as the EULER equations of the variational problem, are *linear* in $\bar{u}$, $\bar{v}$ and $\bar{w}$, and the right-hand members are proportional to a^2, and the assumption regarding the smallness of $\bar{u}$, $\bar{v}$, $\bar{w}$ has been proved. Upon substitution of the solution for $\bar{u}$, $\bar{v}$ and $\bar{w}$ into the potential energy we obtain an expression for this energy as a function of the amplitude a of the buckling mode that is accurate (for small values of a) up to terms of the *fourth* degree in a.

The equilibrium values of a are now obtained by equating to zero the derivative of the energy with respect to a, and the sign of the second derivative with respect to a decides whether the state of equilibrium is stable or unstable. It depends on the actual form of the expression of the potential energy as a function of a whether neighbouring states of equilibrium exist both for loads above and below the buckling load or only for loads either above or below the buckling load. *Usually* neighbouring states of equilibrium at loads *above* the buckling load are *stable* (if they exist), whereas neighbouring states of equilibrium at loads *below* the buckling load (if existing) are *always unstable.*

The detailed analysis for our problem of a narrow panel in a stiffened cylindrical shell (with the boundary conditions discussed in sec. 2) is given in appendix A. The results are discussed in the next paragraph.

4 The initial post-buckling behaviour of a narrow panel.

The results of our analysis in appendix A may be summarized as follows. After buckling the initial relation between the overall compressive strain ε and the (nondimensional) load λ, i.e. the tangent to the post-buckling curve, is given by (A 54)

$$\varepsilon = \lambda + \frac{\lambda - \lambda_1}{1 - 2\,\theta^4 - 9\,S}\,, \qquad (4.1)$$

where θ $(0 \leqq \theta \leqq 1)$ is defined by (7) and S is the sum of the series

$$S = \sum_{n=1}^{\infty} \left[\frac{1}{(n^2+1)^2} + \theta^{-4}\,(n^2+1)^2 - 1 - \theta^{-4} \right]^{-1}. \qquad (4.2)$$

We have a real solution only for $\lambda \geqq \lambda_1$ if the denominator in (4.1) is positive, and for $\lambda \leqq \lambda_1$ if the denominator is negative. The results of our numerical calculations are presented in table 1, and the tangents to the post-buckling curves are pictured in fig. 3, where the straight line $\lambda = \varepsilon$ represents the fundamental state of equilibrium which is unstable for $\lambda > \lambda_1$.

First of all we note that for a *very narrow* panel $(\theta \ll 1)$ our formula (4.1) is simplified into

$$\varepsilon = 2\,\lambda - \lambda_1 \qquad (4.3)$$

in complete agreement with the well-known result for a flat panel (ref. 3.4 and ref. 8, art. 633, eq. (63.45)). This simplified formula is approximately valid for values of θ up to about 0.3. The slope of the tangent of the post-buckling curve in fig. 3 decreases slowly for values of θ up to about

TABLE 1

θ	S	$1-2\theta^4-9S$
0	0	1.000
0.3	0.0032	0.955
0.5	0.0248	0.652
0.6	0.0523	0.270
0.7	0.0993	— 0.374
0.8	0.1764	— 1.407
0.9	0.3008	— 3.019
1.0	0.5049	— 5.544

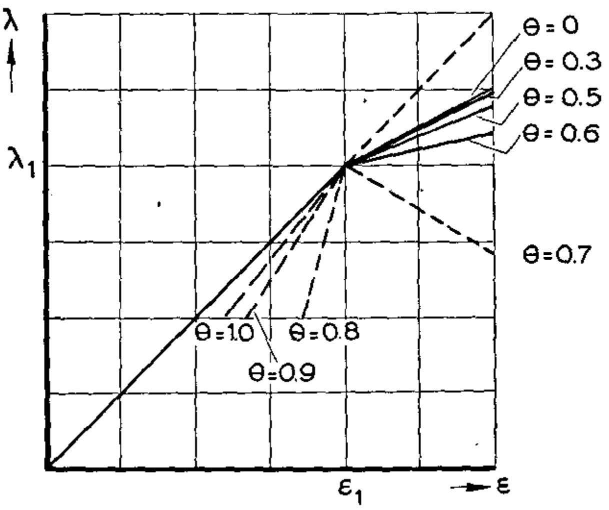

Fig. 3

Tangents to post-buckling curve for several values of total curvature θ.

$\theta = 0.5$. A rapid change occurs for values of θ between 0.6 and 0.8. The post-buckling tangent is *horizontal* for $\theta = \sim 0.64$, and *vertical* and directed *downwards* for $\theta = \sim 0.77$. The horizontal tangent represents the limiting case of a stable post-buckling behaviour for a *prescribed load*, whereas the vertical tangent represents the limiting case of stability for *prescribed overall strain* ε. *Evidently the complete change from the stable behaviour of a flat panel to the unstable behaviour of a shell occurs within the range of a narrow panel* $0 < \theta < 1$.

It may be interesting to compare these results to the values of θ which occur in modern airplane structures. In *wing panels* the values of θ are usually considerably smaller than 0.5. In *fuselage panels* the values of θ range from approximately 0.4 to about 2.0 [1]), and an initially unstable post-buckling behaviour should therefore be expected in most cases if the assumed boundary conditions would apply. However, it should be borne in mind that the torsional constraint of the stiffeners is usually important. The boundary conditions along the longitudinal edges then approach more those of "clamped" edges, and it may be expected that the post-buckling behaviour with clamped edges will be stable up to higher values of θ. Further research in this direction is highly desirable.

The effect of *initial imperfections* in the panel is easily taken into account by means of the general theory of ref. 8 (ch. 4). We have investigated in appendix A deviations from the true cylindrical form in the shape of the buckling mode, i.e. we have assumed that the imperfect panel may be obtained from the perfect panel by means of radial "displacements" given by

$$w_0 = \mu h \sin q\alpha \sin q\beta, \tag{4.4}$$

where μ is a nondimensional parameter for the magnitude of the initial waves. The resulting load *vs* strain curves are given in figs. 4 and 5 for $\theta = 1$, $\mu = 0.1$ and $\theta = 0.7$, $\mu = 0.1$ respectively; the tangents to the post-buckling curves for perfect cylindrical panels (fig. 3) have also been drawn in these figures.

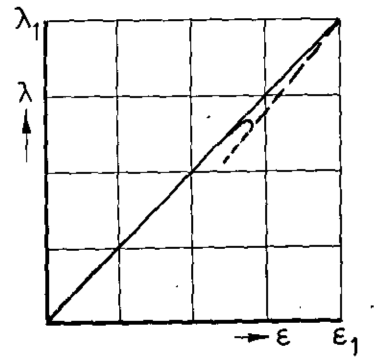

Fig. 4

Load *vs* strain curve for $\theta = 1$ and $\mu = 0.1$

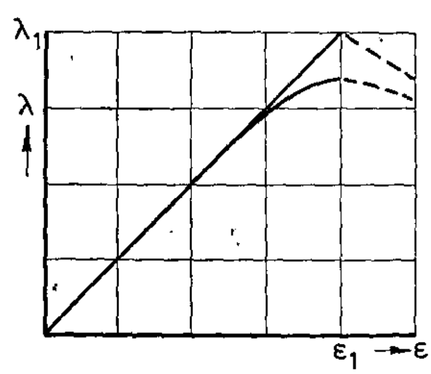

Fig. 5

Load *vs* strain curve for $\theta = 0.7$ and $\mu = 0.1$.

It will be noted that the critical load λ^* *for these imperfect panels is considerably smaller than the buckling load for a perfect panel.* This effect always occurs if the denominator in the second term of (4.1) is negative (see eq. A (64)). The drop in buckling load as a function of the amplitude of the initial waves is illustrated in fig. 6 for two values of the total curvature θ.

It may be emphasized here that our analysis is only valid if the deflections from the fundamental state are sufficiently small, i.e. if the amplitude a of the buckling mode is sufficiently small. How-

[1]) The author is indebted to Mr. E. J. van Beek of the Fokker Aircraft Company for these data on current designs.

ever, our most important result, i.e. the initial unstable behaviour of panels for which $\theta > \sim 0.64$ for a prescribed load or $\theta > \sim 0.77$ for a prescribed overall strain, is entirely rigorous for the

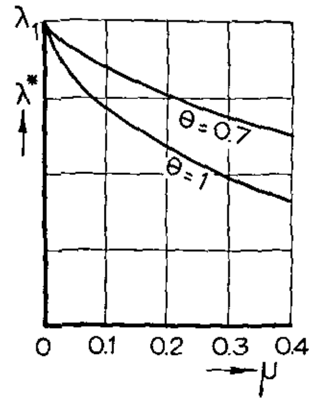

Fig. 6

Buckling loads for imperfect panels.

assumed boundary conditions. Moreover, it does not seem too audacious to offer a conjecture on the behaviour of a narrow panel in the more advanced post-buckling stage (see sec. 5.2).

5 Suggested program for further research.

Further research on the post-buckling behaviour of curved panels seems desirable in several directions.

5.1 First of all the effect of other *boundary conditions* along the longitudinal edges should be investigated.

The most simple (although not the most important) extension of our analysis is the investigation of complete *longitudinal constraint* along the stiffener attachments. For this purpose it is sufficient to add a term

$$-(a_0{}^* + \sum_{n=1}^{\infty} a_n{}^*) \sin 2\, q\alpha$$

to our expression for $\bar{u}$ (A 27), and to analyse the corresponding modified equations for the FOURIER coefficients.

The most important modification of the boundary conditions is the suppression of transverse deflection slopes along the stiffeners if their *torsional rigidity is high.* It may be expected that a panel with clamped edges will show a stable post-buckling behaviour up to higher values of the total curvature parameter θ. It will be convenient to obtain first a sufficiently simple and accurate approximation to the buckling mode corresponding to clamped longitudinal edges, because the rigorous buckling mode (ref. 11) would probably require excessive analytical work even in the *initial* post-buckling stage.

In view of the fact that the critical stress is not very sensitive to *tangential constraint* by the stiffeners (cf. sec. 3), while the modification of the buckling mode $(\bar{u}, \bar{v}, \bar{w})$ does not involve additional tangential displacements (cf. (A 27)), it does not seem worthwhile to investigate the effect of such constraint.

5.2 Next, it should be remembered that our analysis has been restricted to the initial post-buckling stage. In order to extend the theory to the more advanced post-buckling stage a convenient first step may be to retain the displacement pattern, calculated for the initial stage, but now taking into account *all* energy terms, i.e. up to the fourth degree in $\bar{u}$, $\bar{v}$, $\bar{w}$. A more refined analysis of the advanced post-buckling stage would require a careful examination of appropriate wave patterns in order to achieve adequate results without excessive analytical labour.

However, *it would appear to be not too bold a conjecture that the behaviour of a narrow curved panel in the advanced post-buckling stage approaches the behaviour of a flat panel of equal width.* This conjecture is indeed fairly plausible for the initially already stable very narrow panels ($\theta < \sim 0.64$) because their critical stress is at most 17 percent above the critical stress of a flat panel. The conjecture is illustrated in fig. 7 for panels

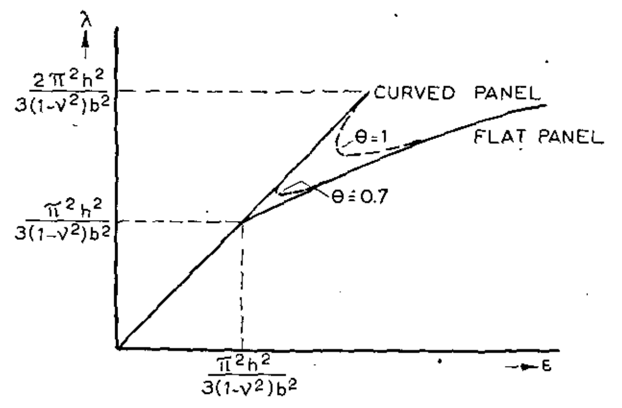

Fig. 7

Conjectured post-buckling curves in advanced stage for narrow cylindrical panels.

with a total curvature θ up to unity. If our conjecture were confirmed by analysis it would seem that a detailed knowledge of the complete post-buckling curve for narrow panels is of minor practical interest because the part of the curve that would lie substantially above the curve for a flat panel is highly sensitive to initial imperfections (see figs. 4 and 5).

5.3 Finally, an experimental verification of the theoretical results seems desirable. It is suggested that the boundary conditions which were assumed in the present report might be obtained in a test set-up similar to the set-up for the investigation of flat panels (ref. 13). However, it may be better to await the results of a theoretical investigation of other boundary conditions before a decision on experimental verification is made.

6 References.

1. Timoshenko, S. Theory of elastic stability, New York (1936), arts. 63, 72, 81, 84.
2. Flügge, W. Statik und Dynamik der Schalen, Berlin, Kap. IX.
3. Marguerre, K. und Trefftz, E. Ueber die Tragfähigkeit eines Plattenstreifens nach Ueberschreiten der Beullast. Z.A.M.M. 17 (1937), 85.
4. Marguerre, K. Die mittragende Breite der gedrückten Platte ‚Luftfahrtforschung 14 (1937), 121.
5. Koiter, W. T. De meedragende breedte bij grote overschrijding van de knikspanning voor verschillende inklemming der plaatranden (The equivalent width at loads far above the buckling load for various boundary conditions along the plate edges). NLL report S. 287 (1943).
6. Von Kármán, T. and Tsien, H. S. The buckling of thin cylindrical shells under axial compression. J. Aero. Sci. 8 (1941), 303.
7. Leggett, D. M. A. and Jones, R. P. N. The behaviour of a cylindrical shell under axial compression when the buckling load has been exceeded. Aeronautical Research Council, R. & M. 2190, London (1942).
8. Koiter, W. T. Over de stabiliteit van het elastisch evenwicht (*On the stability of elastic equilibrium*). Proefschrift Delft (1945).
9. Redshaw, S. C. Elastic instability of a thin curved panel. Aeronautical Research Council, R. & M. 1565, London (1933).
10. Redshaw, S. C. The elastic instability of a curved plate under axial thrusts. J. Roy. Aero. Soc. 42 (1938), 536.
11. Leggett, D. M. A. The buckling of a long curved panel under axial compression. Aeronautical Research Council, R. & M. 1899, London (1942).
12. Whittaker, E. T. and Watson, G. N. A course of modern analysis, 4th ed., Cambridge (1927).
13. Botman, M. and Besseling, J. F. The effective width in the plastic range of flat plates under compression. NLL report S. 445, Sept. 1954.

APPENDIX A.

Analysis of initial post-buckling behaviour of a narrow cylindrical panel.

A 1. *The basic energy expressions.*

The fundamental state of equilibrium of a panel under axial compression is given by

$$U = -\lambda R\alpha,\ V = 0,\ W = \nu\lambda R, \tag{A 1}$$

where

$$\lambda = \frac{N}{\beta_0 RhE} = \frac{\sigma}{E} \tag{A 2}$$

is a nondimensional parameter for the total load on the panel. The increase in potential energy on passing from the fundamental state to a neighbouring state $U+u$, $V+v$, $W+w$ is (ref. 8, art. 72 with the simplifications indicated in arts. 75 and 76)

$$\frac{Gh}{4(1-\nu)}\ \{P_2^{\,0}[u] + \lambda P_2'[u] + P_3[u] + P_4[u]\}, \tag{A 3}$$

where the various terms are given by

$$P_2^{\,0}[u] = \int_0^{l/R} d\alpha \int_0^{\beta_0} d\beta\,\{4u'^2 + 4(v^{\cdot} + w)^2 + 8\nu u'(v^{\cdot} + w) + 2(1-\nu)(u^{\cdot} + v')^2 + \\ + k\,[w''^2 + w^{\cdot\cdot 2} + 2\nu w'' w^{\cdot\cdot} + 2(1-\nu)w'^{\cdot 2}]\}, \tag{A 4}$$

$$P_2'[u] = -4(1-\nu^2)\int_0^{l/R} d\alpha \int_0^{\beta_0} d\beta w'^2, \tag{A 5}$$

$$P_3[u] = \frac{4}{R}\int_0^{l/R} d\alpha \int_0^{\beta_0} d\beta\,\{[u' + \nu(v^{\cdot} + w)]w'^2 + [\nu u' + v^{\cdot} + w]w^{\cdot 2} + (1-\nu)(u^{\cdot} + v')w'w^{\cdot}\}, \tag{A 6}$$

$$P_4[u] = \frac{1}{R^2}\int_0^{l/R} d\alpha \int_0^{\beta_0} d\beta (w'^2 + w^{\cdot 2})^2, \tag{A 7}$$

G is the shear modulus, k is defined by

$$k = \frac{h^2}{3R^2}, \tag{A 8}$$

and primes and dots denote differentiations with respect to α and β.

The buckling mode for the assumed boundary conditions of a narrow panel, defined by

$$\theta = \frac{m\beta_0}{\pi} = \frac{1}{2\pi} \sqrt[4]{12(1-\nu^2)}\ \frac{b}{\sqrt{Rh}} \leqq 1, \tag{A 9}$$

is given by (2.2), where $p = q = \pi/\beta_0$

$$\left.\begin{aligned} u_1 &= -\frac{1-\nu}{4q} \cos q\alpha \sin q\beta, \\ v_1 &= \frac{3+\nu}{4q} \sin q\alpha \cos q\beta, \\ w_1 &= \sin q\alpha \sin q\beta. \end{aligned}\right\} \tag{A 10}$$

We assume our additional displacements on passing from the fundamental state (A 1) to a neighbouring state in the form

$$u = au_1 + \bar{u},\ v = av_1 + \bar{v},\ w = aw_1 + \bar{w}, \tag{A 11}$$

where $\bar{u}$, $\bar{v}$ and $\bar{w}$ are supposed to be small compared to au_1, av_1, and aw_1. Moreover we impose the orthogonality condition

$$P_{11}'[u_1, \bar{u}] = -4(1-\nu^2) \int_0^{l/R} d\alpha \int_0^{\beta_0} d\beta \,.\, 2\, w_1' \bar{w}' = 0. \tag{A 12}$$

We may now rewrite the energy expression between brackets in (A 3) (ref. 8, ch. 3)

$$P_2^0[u] + \lambda P_2'[u] + P_3[u] + P_4[u] = a^2 \{ P_2^0[u_1] + \lambda P_2'[u_1] \} + a^3 P_3[u_1] + a^4 P_4[u_1] + P_2^0[\bar{u}] + \\ + \lambda P_2'[\bar{u}] + a^2 P_{21}[u_1, \bar{u}] + \ldots\ldots, \tag{A 13}$$

where all terms which have not been written down explicitly may be neglected. Substituting (A 10) into (A 13), and performing the integrations as far as possible, we obtain for a *long* panel, $l \gg R\beta_0$ (cf. ref. 8, arts. 74, 75)

$$P_2^0[u_1] + \lambda P_2'[u_1] = \frac{\beta_0 l}{R} (1-\nu^2) q^2 (\lambda_1 - \lambda), \tag{A 14}$$

$$P_3[u_1] = 0, \tag{A 15}$$

$$P_4[u_1] = \frac{\beta_0 l}{R^3}\ \frac{5}{16} q^4, \tag{A 16}$$

where

$$\lambda_1 = \frac{1}{4q^2} + \frac{k}{1-\nu^2} q^2 = \frac{\pi^2 h^2}{3(1-\nu^2) b^2} (1 + \theta^4) \tag{A 17}$$

is the critical load parameter (cf. (2.6)). We also have

$$P_{21}[u_1, \bar{u}] = \frac{4}{R} \int_0^{l/R} d\alpha \int_0^{\beta_0} d\beta\, \{ (w_1'^2 + \nu w_1^{\cdot 2}) \bar{u}' + (1-\nu) w_1' w_1^{\cdot} \bar{u}^{\cdot} + (\nu w_1'^2 + w_1^{\cdot 2}) \bar{v}^{\cdot} + (1-\nu) w_1' w_1^{\cdot} \bar{v}' + \\ + (\nu w_1'^2 + w_1^{\cdot 2}) \bar{w} + [2\{ u_1' + \nu (v_1^{\cdot} + w_1) \} w_1' + (1-\nu)(u_1^{\cdot} + v_1') w_1^{\cdot}] \bar{w}' + \\ + [2 \{ \nu u_1' + v_1^{\cdot} + w_1 \} w_1^{\cdot} + (1-\nu)(u_1^{\cdot} + v_1') w_1'] \bar{w}^{\cdot} \} = \\ = \frac{1}{R} \int_0^{l/R} d\alpha \int_0^{\beta_0} d\beta\, \{ q^2 [1 + \nu + (1-\nu) \cos 2q\alpha - (1-\nu) \cos 2q\beta - (1+\nu) \cos 2q\alpha \cos 2q\beta]\, \bar{u}' + \\ + q^2 [(1-\nu) \sin 2q\alpha \sin 2q\beta]\, \bar{u}^{\cdot} + q^2 [1 + \nu - (1-\nu) \cos 2q\alpha + (1-\nu) \cos 2q\beta + \\ - (1+\nu) \cos 2q\alpha \cos 2q\beta]\, \bar{v}^{\cdot} + q^2 [(1-\nu) \sin 2q\alpha \sin 2q\beta]\, \bar{v}' + q^2 [1 + \nu - (1-\nu) \cos 2q\alpha + \\ + (1-\nu) \cos 2q\beta - (1+\nu) \cos 2q\alpha \cos 2q\beta]\, \bar{w} + q [(1-\nu^2) \sin 2q\alpha]\, \bar{w}' + q [(1-\nu^2) \sin 2q\beta]\, \bar{w}^{\cdot} \} \tag{A 18}$$

A 2. *The equations for $\bar{u}$, $\bar{v}$, $\bar{w}$.*

It should now be remembered that our panel is only one out of a number $2\pi/\beta_0$ equal panels in the stiffened cylindrical shell (see fig. 2 in sec. 2). It is immediately obvious from (A 13) to (A 18) that all panels have the same energy expressions. Hence the condition of equilibrium, expressed by the requirement that the potential energy has a stationary value, may be applied to a single panel if due account is taken of the fact that the displacements $\bar{u}$, $\bar{v}$, $\bar{w}$ and the derivative $\bar{w}^{\cdot}$ are continuous across the line of attachment of a stiffener, and that these displacements are the same in all panels. We also remember our requirement that the displacements are periodic functions of the axial coordinate and that no radial deflection waves occur along the line of attachment of a stiffener. We may summarize these *geometric* boundary conditions

$$\left.\begin{array}{ll} \text{a)} & \bar{u},\ \bar{v},\ \bar{w} \text{ are periodic in } \alpha; \\ \text{b)} & (\bar{u})_{\beta=\beta_0} = (\bar{u})_{\beta=0},\ (\bar{v})_{\beta=\beta_0} = (\bar{v})_{\beta=0}, \\ & (\bar{w})_{\beta=\beta_0} = (\bar{w})_{\beta=0},\ (\bar{w}^{\cdot})_{\beta=\beta_0} = (\bar{w}^{\cdot})_{\beta=0}; \\ \text{c)} & \beta = 0 : \bar{w}' = 0. \end{array}\right\} \tag{A 19}$$

As a first step we determine the minimum value of (A 13) for a *fixed* value of the amplitude a of the buckling mode, i.e. we determine $\bar{u}$, $\bar{v}$, $\bar{w}$ from the condition that

$$P_2^0[\bar{u}] + \lambda P_2'[\bar{u}] + a^2 P_{21}[u_1, \bar{u}] \tag{A 20}$$

is a minimum (cf. ref. 8, ch. 3). The EULER equations of this variational problem are

$$\left.\begin{array}{l} 8\bar{u}'' + 4(1-\nu)\bar{u}^{\cdot\cdot} + 4(1+\nu)\bar{v}'^{\cdot} + 8\nu\bar{w}' = q^3 \dfrac{a^2}{R}[2(1-\nu)\sin 2q\alpha - 4\sin 2q\alpha\cos 2q\beta], \\ 4(1+\nu)\bar{u}'^{\cdot} + 8\bar{v}^{\cdot\cdot} + 4(1-\nu)\bar{v}'' + 8\bar{w}^{\cdot} = q^3 \dfrac{a^2}{R}[2(1-\nu)\sin 2q\beta - 4\cos 2q\alpha\sin 2q\beta], \\ 8\nu\bar{u}' + 8\bar{v}^{\cdot} + 8\bar{w} + 2k[\bar{w}'''' + 2\bar{w}''^{\cdot\cdot} + \bar{w}^{\cdot\cdot\cdot\cdot}] + 8(1-\nu^2)\lambda\bar{w}'' = \\ \quad = q^2 \dfrac{a^2}{R}\{-(1+\nu) + (1-\nu)(3+2\nu)\cos 2q\alpha + (1-\nu)(1+2\nu)\cos 2q\beta + \\ \qquad + (1+\nu)\cos 2q\alpha\cos 2q\beta\}, \end{array}\right\} \tag{A 21}$$

and the "natural" or *dynamic* boundary conditions of the variational problem are

$$\left.\begin{array}{ll} \text{d)} & (\bar{u}^{\cdot})_{\beta=\beta_0} = (\bar{u}^{\cdot})_{\beta=0},\ (\bar{v}^{\cdot})_{\beta=\beta_0} = (\bar{v}^{\cdot})_{\beta=0},\ (\bar{w}^{\cdot\cdot})_{\beta=\beta_0} = (\bar{w}^{\cdot\cdot})_{\beta=0}; \\ \text{e)} & \displaystyle\int_0^{l/R} [(\bar{w}^{\cdot\cdot\cdot})_{\beta=\beta_0} - (\bar{w}^{\cdot\cdot\cdot})_{\beta=0}]\, d\alpha = 0; \\ \text{f)} & \displaystyle\int_0^{\beta_0} \{8[\bar{u}' + \nu(\bar{v}^{\cdot} + \bar{w})] + \frac{4a^2}{R}(w_1'^2 + \nu w_1^{\cdot 2})\}\, d\beta = 0. \end{array}\right\} \tag{A 22}$$

The boundary conditions (A 19) and (A 22) may be simplified by observing that the righthand members of (A 21) represent a *symmetric* "loading" of the shell with respect to $\beta = \frac{1}{2}\beta_0$ Hence we may write instead of (A 19 b and c) (A 22 d and e)

$$\beta = 0 \text{ and } \beta = \beta_0:\ \bar{u}^{\cdot} = \bar{v} = \bar{w}^{\cdot} = \bar{w}' = 0, \tag{A 23}$$

$$\beta = 0 \text{ and } \beta = \beta_0:\ \int_0^{l/R} \bar{w}^{\cdot\cdot\cdot}\, d\alpha = 0. \tag{A 24}$$

Conditions (A 19 a) and (A 22 f) remain unchanged.

A 3. *Direct solution of the variational problem.*

The variational problem involved in minimizing (A 20) may be solved directly by the RAYLEIGH-RITZ method by assuming suitable series representations for $\bar{u}$, $\bar{v}$, $\bar{w}$ and minimizing with respect to the coefficients in these series. This method is completely rigorous if the series assumed are sufficiently complete. The right-hand members in (A 21) and the boundary conditions (A 22) suggest that suitable series for $\bar{u}$, $\bar{v}$, $\bar{w}$ are [1])

---

[1]) It might be objected that the assumed expressions (A 25) may not be sufficiently general; our analysis would then not yield the required minimum but only an upper bound. However, it may be shown that an alternative approach, i.e. the solution of the differential equations and boundary conditions by FOURIER-transforms, yields the same result.

$$\left.\begin{aligned}
\bar{u} &= -\bar{\varepsilon}\alpha R + \left[a_0^* + \sum_{n=1}^{\infty} a_n^* \cos 2\,nq\beta\right] \sin 2\,q\alpha \\
\bar{v} &= \sum_{n=1}^{\infty} b_n \sin 2\,nq\beta + \sum_{n=1}^{\infty} b_n^* \sin 2\,nq\beta \cos 2\,q\alpha \\
\bar{w} &= c_0 + \sum_{n=1}^{\infty} c_n \cos 2\,nq\beta + \left[-\sum_{n=1}^{\infty} c_n^* + \sum_{n=1}^{\infty} c_n^* \cos 2\,nq\beta\right] \cos 2\,q\alpha
\end{aligned}\right\} \tag{A 25}$$

Evaluating the expressions (A 4), (A 5) and (A 18) we now obtain by some elementary algebra

$$\begin{aligned}
P_2^{0}[\bar{u}] = \frac{\beta_0 l}{R} \Big\{ & 4\,\bar{\varepsilon}^2 R^2 - 8\,\nu\,\bar{\varepsilon}\,Rc_0 + 4\,c_0^2 + 8\,q^2 a_0^{*2} - 8\,\nu q a_0^* \sum_{n=1}^{\infty} c_n^* + (2 + 8\,kq^4) \left[\sum_{n=1}^{\infty} c_n^*\right]^2 + \\
& + \sum_{n=1}^{\infty} \Big[2(c_n + 2\,nqb_n)^2 + 8\,kq^4 n^4 c_n^2 + 4\,q^2 a_n^{*2} + (c_n^* + 2\,nqb_n^*)^2 + 4\,\nu q a_n^* (c_n^* + 2\,nqb_n^*) + \\
& + 2\,(1-\nu) q^2 (na_n^* + b_n^*)^2 + 4\,kq^4 (1+n^2)^2 c_n^{*2} \Big] \Big\},
\end{aligned} \tag{A 26}$$

$$P_2'[\bar{u}] = -\frac{\beta_0 l}{R}(1-\nu^2) \left\{ 4\,q^2 \sum_{n=1}^{\infty} c_n^{*2} + 8\,q^2 \left[\sum_{n=1}^{\infty} c_n^*\right]^2 \right\}, \tag{A 27}$$

$$\begin{aligned}
P_{21}[u_1, \bar{u}] = \frac{\beta_0 l}{R^2} q^2 \Big\{ & -(1+\nu)\,\bar{\varepsilon} R + (1+\nu) c_0 + (1-\nu) q b_1 - \tfrac{1}{2}(1-\nu)(1+2\,\nu) c_1 + \\
& + (1-\nu) q a_0^* - q a_1^* - q b_1^* - \tfrac{1}{4}(1+\nu) c_1^* + \tfrac{1}{2}(1-\nu)(3+2\,\nu) \sum_{n=1}^{\infty} c_n^* \Big\}.
\end{aligned} \tag{A 28}$$

Substituting (A 26) to (A 28) into (A 20) and minimizing the resulting expression with respect to the parameters $\bar{\varepsilon}$, c_0; b_1, c_1; b_h, c_h $(h > 1)$; a_0^*; a_1^*, b_1^*, c_1^*; a_h^*, b_h^*, c_h^* $(h > 1)$, we derive the equations

$$\left.\begin{aligned}
& 8\,\bar{\varepsilon} R^2 - 8\,\nu R c_0 - (1+\nu) q^2 a^2 = 0, \\
& -8\,\nu\,\bar{\varepsilon} R + 8\,c_0 + (1+\nu) q^2 \frac{a^2}{R} = 0;
\end{aligned}\right\} \tag{A 29}$$

$$\left.\begin{aligned}
& 8\,q(2\,qb_1 + c_1) + (1-\nu) q^3 \frac{a^2}{R} = 0, \\
& 4(2\,qb_1 + c_1) + 16\,kq^4 c_1 - \tfrac{1}{2}(1-\nu)(1+2\,\nu) q^2 \frac{a^2}{R} = 0;
\end{aligned}\right\} \tag{A 30}$$

$$\left.\begin{aligned}
& 8\,hq(2\,hqb_h + c_h) = 0, \\
& 4(2\,hqb_h + c_h) + 16\,kh^4 q^4 c_h = 0;
\end{aligned}\right\} \tag{A 31}$$

$$16\,q^2 a_0^* - 8\,\nu q \sum_{n=1}^{\infty} c_n^* + (1-\nu) q^3 \frac{a^2}{R} = 0; \tag{A 32}$$

$$\left.\begin{aligned}
& 4(3-\nu) q^2 a_1^* + 4(1+\nu) q^2 b_1^* + 4\,\nu q c_1^* - q^3 \frac{a^2}{R} = 0, \\
& 4(1+\nu) q^2 a_1^* + 4(3-\nu) q^2 b_1^* + 4\,q c_1^* - q^3 \frac{a^2}{R} = 0, \\
& 4\,\nu q a_1^* + 4\,q b_1^* + [2 + 32\,kq^4 - 8(1-\nu^2)\lambda q^2]\, c_1^* - 8\,\nu q a_0^* + \\
& \quad + 4[1 + 4\,kq^4 - 4(1-\nu^2)\lambda q^2] \sum_{n=1}^{\infty} c_n^* - \tfrac{1}{4}(1+\nu) q^2 \frac{a^2}{R} + \tfrac{1}{2}(1-\nu)(3+2\,\nu) q^2 \frac{a^2}{R} = 0;
\end{aligned}\right\} \tag{A 33}$$

$$\left.\begin{aligned}
& 4[2 + (1-\nu) h^2] q^2 a_h^* + 4(1+\nu) h q^2 b_h^* + 4\,\nu q c_h^* = 0, \\
& 4(1+\nu) h q^2 a_h^* + 4[2\,h^2 + 1 - \nu] q^2 b_h^* + 4\,hq c_h^* = 0, \\
& 4\,\nu q a_h^* + 4\,hq b_h^* + [2 + 8\,k(1+h^2)^2 q^4 - 8(1-\nu^2)\lambda q^2]\, c_h^* + \\
& \quad - 8\nu q a_0^* + 4[1 + 4\,kq^4 - 4(1-\nu^2)\lambda q^2] \sum_{n=1}^{\infty} c_n^* + \tfrac{1}{2}(1-\nu)(3+2\,\nu) q^2 \frac{a^2}{R} = 0.
\end{aligned}\right\} \tag{A 34}$$

The equations (A 29) to (A 31) are readily solved. Their solution is given by

$$\bar{\varepsilon} = \frac{q^2 a^2}{8\,R^2}, \quad c_0 = -\frac{q^2 a^2}{8\,R}; \tag{A 35}$$

$$b_1 = -\frac{1-\nu^2}{32}\,\frac{1}{kq^3}\,\frac{a^2}{R} - \frac{1-\nu}{16}\,q\,\frac{a^2}{R}, \quad c_1 = \frac{1-\nu^2}{16}\,\frac{1}{kq^2}\,\frac{a^2}{R}; \tag{A 36}$$

$$b_h = c_h = 0 \ (h > 1). \tag{A 37}$$

The first pairs of equations (A 33) and (A 34) are solved for a_1^*, b_1^*; a_h^*, b_h^*

$$a_1^* = \frac{1-\nu}{8q}\,c_1^* + \frac{1}{16}\,q\,\frac{a^2}{R}, \quad b_1^* = -\frac{3+\nu}{8q}\,c_1^* + \frac{1}{16}\,q\,\frac{a^2}{R}; \tag{A 38}$$

$$a_h^* = \frac{h^2-\nu}{2(h^2+1)^2 q}\,c_h^*, \quad b_h^* = -\frac{h[h^2+2+\nu]}{2(h^2+1)^2 q}\,c_h^*. \tag{A 39}$$

Substituting these results and the value of a_0^* given by (A 32) into the last equations (A 33) and (A 34), we obtain both for $h=1$ and $h>1$

$$c_h^* = -\left\{\frac{3}{4}\,q^2\,\frac{a^2}{R} + 2\left[1 + \frac{4\,kq^4}{1-\nu^2} - 4\,\lambda q^2\right]\sum_{n=1}^{\infty} c_n^*\right\} T_h, \tag{A 40}$$

where T_h is defined by

$$T_h = \left[\frac{1}{(h^2+1)^2} + \frac{4\,kq^4}{1-\nu^2}\,(h^2+1)^2 - 4\,\lambda q^2\right]^{-1}. \tag{A 41}$$

By summing (A 40) from $h=1$ to $h=\infty$ we finally obtain an equation for $\sum\limits_{n=1}^{\infty} c_n^*$. Putting

$$S = \sum_{h=1}^{\infty} T_h, \tag{A 42}$$

and remembering (A 9) and (A 17), we obtain

$$\sum_{n=1}^{\infty} c_n^* = -\frac{3}{4}\,q^2\,\frac{a^2}{R}\,\frac{S}{1+2(1+\theta^{-4})(1-\lambda/\lambda_1)S}, \tag{A 43}$$

$$c_h^* = -\frac{3}{4}\,q^2\,\frac{a^2}{R}\,\frac{1}{1+2(1+\theta^{-4})(1-\lambda/\lambda_1)S}\,T_h. \tag{A 44}$$

We may now calculate the minimum value of (A 20) for a *fixed* value of the amplitude a of the buckling mode. This calculation is simplified by observing that this minimum is equal to $\frac{1}{2}\,a^2 P_{21}[u_1, \bar{u}]$ where $\bar{u}$ is our solution of the variational problem (ref. 8, art. 25). The result is

Minimum of $\{P_2{}^0[\bar{u}] + \lambda P_2{}'[\bar{u}] + a^2 P_{21}[u_1, \bar{u}]\} =$

$$= -\frac{\beta_0 l}{R^3}\,q^4 a^4\left\{\frac{4+\nu^2}{16} + \frac{1-\nu^2}{8}\,\theta^4 + \frac{9(1-\nu^2)}{16}\,\frac{S}{1+2(1+\theta^{-4})(1-\lambda/\lambda_1)S}\right\} \tag{A 45}$$

In order to facilitate the numerical evaluation of our result it should be remembered that our attention is focussed on the *initial* stage of post-buckling behaviour. In fact, our neglections of the terms in (A 13) which have not been written down explicitly is only justified if the amplitude a of the buckling mode is small. It was shown in ref. 8 that (A 45) may then be simplified by putting $\lambda = \lambda_1$. Our final result is therefore

$$\text{Minimum of } \{P_2{}^0[\bar{u}] + \lambda P_2{}'[\bar{u}] + a^2 P_{21}[u_1, \bar{u}]\} = -\frac{\beta_0 l}{R^3}\,q^4 a^4\left\{\frac{4+\nu^2}{16} + \frac{1-\nu^2}{8}\theta^4 + \frac{9(1-\nu^2)}{16}\,S\right\}, \tag{A 46}$$

$$S = \sum_{h=1}^{\infty}\left[\frac{1}{(h^2+1)^2} + \theta^{-4}(h^2+1)^2 - 1 - \theta^{-4}\right]^{-1}. \tag{A 47}$$

A 4. *The neighbouring states of equilibrium.*

The minimum value of (A 13) for a fixed value of the amplitude a of the buckling mode may now be written down from (A 14), (A 15), (A 16) and (A 46)

$$P(a) = \frac{\beta_0 l}{R}(1-\nu^2)q^2\left\{(\lambda_1 - \lambda)a^2 + \left[\frac{1}{16} - \frac{1}{8}\theta^4 - \frac{9}{16}S\right] q^2\,\frac{a^4}{R^2}\right\}. \tag{A 48}$$

The positions of equilibrium are characterized by a stationary value of (A 48) with respect to its single variable a, i. e. by

$$2(\lambda_1 - \lambda)a + \tfrac{1}{4}\,[1 - 2\,\theta^4 - 9\,S]q^2\,\frac{a^3}{R^2} = 0. \tag{A 49}$$

The solution $a = 0$ corresponds to the fundamental state of equilibrium. The neighbouring positions of equilibrium are described by

$$\frac{a^2}{R^2} = \frac{8(\lambda - \lambda_1)}{q^2[1 - 2\,\theta^4 - 9\,S]}; \tag{A 50}$$

whether a position of equilibrium is stable or unstable is decided by the sign (positive for stable equilibrium) of the second derivative of (A 49), i.e. by the sign of

$$2(\lambda_1 - \lambda) + \tfrac{3}{4}\,[1 - 2\,\theta^4 - 9\,S]q^2\,\frac{a^2}{R^2}. \tag{A 51}$$

Obviously only stable neighbouring states of equilibrium exist for $\lambda > \lambda_1$ if

$$1 - 2\,\theta^4 - 9\,S \tag{A 52}$$

is positive, whereas only unstable neighbouring positions of equilibrium can occur for $\lambda < \lambda_1$ if (A 52) is negative.

The corresponding overall compressive strain of the panel is given by

$$\varepsilon = \lambda + \bar{\varepsilon}\,; \tag{A 53}$$

substituting (A 35) and (A 50), we have

$$\varepsilon = \lambda + \frac{\lambda - \lambda_1}{1 - 2\,\theta^4 - 9\,S} \tag{A 54}$$

where $\lambda \geqq \lambda_1$ if (A 52) is positive and $\lambda \leqq \lambda_1$ if (A 52) is negative.

Hence the result of our analysis is contained in the single expression (A 52) which has been evaluated numerically for several values of θ in the range $0 \leqq \theta \leqq 1$ to which our analysis applies (table 1 in sec. 4). The numerical work is negligible because no more than 4 terms of the series (A 47) need to be calculated, the remainder being approximated with adequate accuracy by the remainder of the series

$$\theta^4 \sum_{h=1}^{\infty} \frac{1}{(h^2+1)^2}, \tag{A 55}$$

which may be summed by means of the formula

$$\sum_{h=1}^{\infty} \frac{1}{(h^2+1)^2} = \frac{\pi}{4}\coth\pi + \frac{\pi^2}{4}\,\frac{1}{\sinh^2\pi} - \tfrac{1}{2} = 0.3068, \tag{A 56}$$

obtained from ref. 12, p. 136, Ex. 7 by differentiation.

A 5. *The effect of initial imperfections.*

The effect of *small* deviations of our panel from the true cylindrical form may again be examined by means of the general theory of ref. 8 (art. 47). These imperfections are taken into account to a first approximation by adding a term

$$\mu\lambda Q_1'\,[u] \tag{A 57}$$

to the expressions between brackets in (A 3), where μ is a parameter [1]) which is a measure for the magnitude of the imperfections.

Denoting the radial "displacements" by means of which the imperfect panel may be obtained from a true cylindrical panel by $w_0(\alpha, \beta)$, we have (ref. 8, eq. (77,3) with the simplification discussed on p. 198)

$$\mu\lambda Q_1'[u] = 8(1-\nu^2)\lambda \int_0^{l/R} d\alpha \int_0^{\beta_0} d\beta\,.\,w_0 w''. \tag{A 58}$$

In our first approximation, expression (A 13) is now modified by adding the term

$$\mu\lambda a Q_1'[u_1] = 8(1-\nu^2)\lambda a \int_0^{l/R} d\alpha \int_0^{\beta_0} d\beta\,.\,w_0 w_1''. \tag{A 59}$$

If we assume *initial imperfections* w_0 *in the form of the buckling mode*

$$w_0 = \mu h \sin q\alpha \sin q\beta, \tag{A 60}$$

where h is the sheet thickness, we obtain

---

[1]) We have replaced the symbol ε for this parameter in ref. 8 by μ here in order to avoid confusion with the overall compressive strain.

$$Q_1'[u_1] = -8(1-\nu^2)q^2h \int_0^{l/R} d\alpha \int_0^{\beta_0} d\beta \, . \, \sin^2 q\alpha \sin^2 q\beta = -\frac{\beta_0 l}{R} 2(1-\nu^2)q^2 h. \tag{A 61}$$

Adding the term (A 59) to (A 48), equilibrium of our imperfect panel requires a stationary value of the expression

$$\frac{\beta_0 l}{R}(1-\nu^2)q^2 \left\{ -2\,\mu\lambda h a + (\lambda_1 - \lambda)a^2 + \frac{1}{16}[1-2\,\theta^4 - 9\,S]q^2 \frac{a^4}{R^2} \right\}. \tag{A 62}$$

Hence we obtain

$$-2\,\mu\lambda h + 2(\lambda_1 - \lambda)a + \tfrac{1}{4}[1-2\,\theta^4 - 9\,S]q^2 \frac{a^3}{R^2} = 0.$$

Remembering $q = \pi/\beta_0$, (A 9) and (A 17): this result may be rewritten in the final form

$$-\mu \frac{\lambda}{\lambda_1} + \left(1 - \frac{\lambda}{\lambda_1}\right)\frac{a}{h} + \frac{3(1-\nu^2)}{8(1+\theta^4)}[1-2\,\theta^4 - 9\,S]\frac{a^3}{h^3} = 0. \tag{A 63}$$

The equilibrium is stable if the second derivative of (A 62) with respect to a is positive, i.e. if (A 51) is positive. Obviously no instability can occur for $\lambda < \lambda_1$ if (A 52) is positive. On the other hand, the imperfect panel will become unstable at a load $\lambda^* < \lambda_1$ if (A 52) is negative. The buckling load λ^* of the imperfect panel is obtained when (A 52) is zero. Elimination of a between this condition and (A 63) yields the equation for the buckling load λ^*

$$-2\,|\mu|\,\frac{\lambda^*}{\lambda_1} + \frac{8}{9}\sqrt{\frac{2}{1-\nu^2}}\,\frac{\sqrt{1+\theta^4}}{\sqrt{9\,S + 2\,\theta^4 - 1}}\left(1 - \frac{\lambda^*}{\lambda_1}\right)^{3/2} = 0. \tag{A 64}$$

Some numerical results are presented in sec. 4 (fig 6).

The formula for the overall compressive strain may be obtained by an extension of the theory of ref. 8 by taking into account those terms which are linear in the initial imperfections and quadratic in the additional displacements $au_1 + \bar{u}$. Alternatively this compressive strain may be obtained in a more direct way by observing that the *average* value of the axial (compressive) strain component of the middle surface should equal the average compressive stress divided by YOUNG's modulus, i.e.

$$\varepsilon - \frac{R}{l}\,\frac{1}{\beta_0}\int_0^{l/R} d\alpha \int_0^{\beta_0} d\beta\,\frac{1}{2\,R^2}[(w_0' + w')^2 - w_0'^2] = \lambda. \tag{A 65}$$

Because $\bar{w}$ is small compared to aw_1 we may replace this equation by

$$\varepsilon = \lambda + \frac{R}{l}\,\frac{1}{\beta_0}\int_0^{l/R} d\alpha \int_0^{\beta_0} d\beta\,\frac{1}{2\,R^2}[(w_0' + aw_1')^2 - w_0'^2]. \tag{A 66}$$

By substituting (A 10) and (A 60) into (A 66) we obtain

$$\varepsilon = \lambda + \frac{q^2}{8\,R^2}(2\,\mu h a + a^2). \tag{A 67}$$

This relation may be rewritten by remembering $q = \pi/\beta_0$, (A 9) and (A 17). Our final result is

$$\frac{\varepsilon}{\varepsilon_1} = \frac{\lambda}{\lambda_1} + \frac{3(1-\nu^2)}{8(1+\theta^4)}\left(2\,\mu\frac{a}{h} + \frac{a^2}{h^2}\right). \tag{A 68}$$

Some numerical results are again discussed in sec. 4 (figs. 4 and 5).

APPENDIX B.

Flexural strain energy in the stiffeners, due to tangential bending.

The flexural strain energy in the stiffeners due to tangential bending is per unit length of a stiffener with flexural rigidity B

$$\frac{1}{4}\,\frac{B}{R^4}\,\frac{p^4q^2[(2+\nu)p^2+q^2]^2}{(p^2+q^2)^4}=\frac{(3+\nu)^2\pi^2}{64\,\beta_0{}^2R^4}\,B, \tag{B 1}$$

on account of $p=q=\pi/\beta_0$ in the critical buckling mode for a narrow panel.

Denoting derivatives with respect to α by primes and derivatives with respect to β by dots, the extensional strain energy per unit length of a panel in the buckling mode (2.2) with $p=q=\pi/\beta_0$ is given by (cf. ref 8, eq. (72,6))

$$\frac{1}{l}\,\frac{Gh}{1-\nu}\int_0^{l/R}d\alpha\int_0^{\beta_0}d\beta\,\{\,u_1'^2+(\dot{v}_1+w_1)^2+2\,\nu u_1'(\dot{v}_1+w_1)+\frac{1}{2}(1-\nu)(\dot{u}_1+v_1')^2\,\}=\frac{1}{32}\,\frac{Ebh}{R^2}. \tag{B 2}$$

The ratio of (B 1) to (B 2) is therefore

$$\frac{1}{2}(3+\nu)^2\pi^2\,\frac{B}{Eb^3h}. \tag{B 3}$$

In many conventional structures this ratio is small compared to unity, and neglection of the flexural strain energy in the stiffeners due to tangential bending is then justified.